Technical Report Documentation Page

1. Report No.	2. Government Accession No.	3. Recipient's Catalog No.
FHWA/TX-07/0-4611-1		

4. Title and Subtitle	5. Report Date
THE DEVELOPMENT OF NON-PROPRIETARY UNDERGROUND STORMWATER QUALITY STRUCTURES	October 2006 Published: June 2007
	6. Performing Organization Code

7. Author(s)	8. Performing Organization Report No.
Harlow C. Landphair, Ming-Han Li, Jett McFalls, Aditya B. Raut Desai, Masatsugu Takamatsu, Michael E. Barrett, and Randall J. Charbeneau	Report 0-4611-1

9. Performing Organization Name and Address	10. Work Unit No. (TRAIS)
Texas Transportation Institute The Texas A&M University System College Station, Texas 77843-3135 Center for Transportation Research The University of Texas at Austin 3208 Red River, Suite 200 Austin, Texas 78705-2650	11. Contract or Grant No. Project 0-4611

12. Sponsoring Agency Name and Address	13. Type of Report and Period Covered
Texas Department of Transportation Research and Technology Implementation Office P. O. Box 5080 Austin, Texas 78763-5080	Technical Report: September 2005-August 2006
	14. Sponsoring Agency Code

15. Supplementary Notes

Project performed in cooperation with the Texas Department of Transportation and the Federal Highway Administration.
Project Title: Non-Proprietary, Small Footprint Stormwater Quality Structures for Use in Urban Areas

16. Abstract

Permanent stormwater quality structures in developed urban areas require the use of smaller footprints and underground structures. This project was undertaken to see if an underground treatment structure composed of off-the-shelf precast concrete sections would have adequate performance and require minimum maintenance. The project consisted of a literature review of small footprint and underground stormwater treatment devices, their cost, performance, and maintenance considerations; a physical model study to test the principles to be employed and construction of a full-scale prototype for proving the concepts. The project clearly demonstrated that extended detention can be an effective tool in removing suspended solids from stormwater compared to other proprietary devices. It also shows that less frequent maintenance will be needed to maintain the overall level of performance. While the efficiency of the structure is around 75 percent removal, approximately 17 percent of the solids discharged can be attributed to resuspension. Several refinements show promise in significantly reducing the resuspension loading which could increase the overall efficiency to over 80 percent with maintenance intervals in excess of twelve months. For this reason the project is being extended another year to further refine the performance and develop better design guidance.

17. Key Words	18. Distribution Statement
Stormwater, Highway Right-of-way, Runoff, Sediment Removal	No restrictions. This document is available to the public through NTIS: National Technical Information Service Springfield, Virginia 22161 http://www.ntis.gov

19. Security Classif.(of this report)	20. Security Classif.(of this page)	21. No. of Pages	22. Price
Unclassified	Unclassified	136	

Form DOT F 1700.7 (8-72) **Reproduction of completed page authorized**

THE DEVELOPMENT OF NON-PROPRIETARY UNDERGROUND STORMWATER QUALITY STRUCTURES

by

Harlow C. Landphair
Senior Research Scientist
Texas Transportation Institute

Ming-Han Li, P.E.
Assistant Research Engineer
Texas Transportation Institute

Jett McFalls
Assistant Research Scientist
Texas Transportation Institute

Aditya B. Raut Desai
Graduate Assistant Researcher
Texas A&M University

Masatsugu Takamatsu
Graduate Research Assistant
University of Texas at Austin

Michael E. Barrett
Research Professor
University of Texas at Austin

and

Randall J. Charbeneau
Professor
University of Texas at Austin

Report 0-4611-1
Project 0-4611
Project Title: Non-Proprietary, Small Footprint Stormwater Quality Structures for Use in Urban Areas

Performed in Cooperation with the
Texas Department of Transportation
and the
Federal Highway Administration

October 2006
Published: June 2007

TEXAS TRANSPORTATION INSTITUTE
The Texas A&M University System
College Station, Texas 77843-3135

DISCLAIMER

The contents of this report reflect the views of the authors, who are responsible for the facts and the accuracy of the data presented herein. The contents do not necessarily reflect the official view or policies of the Federal Highway Administration (FHWA) or the Texas Department of Transportation (TxDOT). This report does not constitute a standard, specification, or regulation. Mention of trade names or commercial products does not constitute an endorsement or recommendation for use. The researcher in charge of the project was Dr. Harlow Landphair, RLA, Texas, #1996.

ACKNOWLEDGMENTS

The authors acknowledge individuals who contributed to and assisted with the research and preparation of this report. The authors would like to thank David Zwernemann, TxDOT, who served as the project director. A special thanks also to members of the Project Monitoring Committee: George R. Herrmann, TxDOT; Amy Ronnfeldt, TxDOT; David Stolpa, TxDOT; and James Bice, Texas Commission on Environmental Quality (TCEQ), who actively participated in the direction of the project. Numerous other TxDOT personnel also took time to provide insights and information that assisted in the completion of the project, and we sincerely appreciate their help.

Texas Transportation Institute staff, especially Derrold Foster, Rodney Jackson, and Alex Ferrazas, deserve recognition for their hard work in the installation of tests, assistance with data collection, and project support.

This project was conducted in cooperation with TxDOT and FWHA.

TABLE OF CONTENTS

Page

List of Figures ix

List of Tables xi

Chapter 1: Introduction 1
Background 1
Objectives 1
Approach 2

Chapter 2: Design Consideration 3
Sediment Characteristics 3
Design Inflow 4
Sedimentation Basin Geometry 4
Detention Time 4

Chapter 3: Model Testing 5
Conceptual Model 5
- Model Description 5
- Hydraulics of the Basin 7
- Critical Settling Velocity 9
- Overall Removal Ratio of Particles 11

Model Characteristics 13
- Sediment Delivery 14
- Inlet Configuration 15
- Sedimentation Basin (Reduced-Scale Physical Model) 16
- Outlet Configuration 17

Data Acquisition 18
- Water Level 18
- Total Suspended Solids (TSS) Concentration 18

Data Processing 19
- Inflow and Outflow Rate Estimation 20
- Event Mean Concentration 22
- TSS Removal Ratio 23

Chapter 4: Prototype Testing 25
Prototype Characteristics 25
- Sediment Delivery 25
- Inlet Configuration 26
- Sedimentation Basin 27
- Outlet Configuration 28

Data Acquisition 28
- Water Level 28
- TSS Concentration 29

Data Processing 29
- Inflow and Outflow Rate Estimation 29

Event Mean Concentration 30
TSS Removal Ratio 30

Chapter 5: Results and Conclusions 31
Conceptual Model Results 31
Water Level Change 31
Outflow SSC Change 32
Removal Ratio 34
Scaling 36
Model Results 37
Inflow Conditions 38
Inflow SSC 38
Outflow SSC 40
Removal Efficiency 41
Prototype Results 45
Outflow Conditions 45
Total Suspended Solids 46
Mass Loading 49
Event Mean Concentration 52
TSS Removal Ratio 54
Discussion and Conclusions 55
Conclusions from Model Results 55
Conclusions from Prototype Results 59
Filling the Gap between Model and Prototype Testing 64
Resuspension Tests with Different Inlet Setups 67
Resuspension Tests with and without Accumulated Sediment 69

Chapter 6: Recommendations 71
Recommendations from Model Results 71
Recommendations from Prototype Results 71

Chapter 7: Work Plan 2006-2007 73
Proposed Scope of Work 74
Estimated Budget 74

References 75

Appendix A: TABULATED DATA 77

Appendix B: CONCEPTUAL MODEL PROGRAM IN MATLAB 95

Appendix C: CONCEPTUAL MODEL APPLICATION 105

LIST OF FIGURES

Page

Figure 2.1. Particle Size Distribution of SIL-CO-SIL®49 as Provided by Manufacturer. 3
Figure 3.1. Diagram of the Rectangular Stormwater Detention Basin. 6
Figure 3.2. Trajectory of Water Molecules and a Particle with Critical Settling Velocity in an Ideal Horizontal Flow Reactor (above) and Rectangular Stormwater Detention Basin during Filling (below). 7
Figure 3.3. Local Convectional Velocity at Storm Runoff Period. 8
Figure 3.4. Trajectory of a Particle with Lower Settling Velocity than Critical Settling Velocity and the Particle Ratio of Captured and Escaped. 12
Figure 3.5. Particle Delivery System (Left) and Inside of the Mixing Bucket (Right). 14
Figure 3.6. Piping Network for the Physical Model. 16
Figure 3.7. Sedimentation Basin with a View Window 17
Figure 3.8. Setups around Outlet Orifice (Left: View from Top, and Right: Orifice Hole). 18
Figure 3.9. $\sqrt{h}$ (Square Root of Water Level) Change with Time. 21
Figure 3.10. Measured and Calculated Water Level Change. 22
Figure 3.11. Conceptual Figure of Measured Outflow SSC Data (Discrete) and Estimated Outflow Rate (Continuous). 23
Figure 4.1. A. Hydroseeder for Making Slurry. B. Point of Injection into Main Line. 26
Figure 4.2. A. Energy Dissipation at Inlet. B. Mixing Tank 27
Figure 4.3. A. View from Upstream. B. View from Downstream. 27
Figure 4.4. A. Fixed and Floating Outlet. B. Independent Valves outside the Tank. 28
Figure 5.1. Measured and Calculated Water Level Change. 31
Figure 5.1. Measured and Calculated Water Level Change (continued). 32
Figure 5.2. Measured and Calculated Outflow SSC. 33
Figure 5.3. Measured and Calculated (Using Conceptual Model) Removal Efficiencies. 35
Figure 5.4. Time Series Inflow SSCs for all Eight Runs. 39
Figure 5.5. Measured Inflow and Outflow SSC Change. 41
Figure 5.6. Excel Spreadsheet to Calculate Removal Efficiency. 42
Figure 5.7. Relationship between Removal Efficiency and Theoretical Overflow Rate. 44
Figure 5.8. Outflow Rates v/s Time for Floating and Fixed Outlet. 46
Figure 5.9. TSS for Fixed Outlet with 50 lb Loading. 47
Figure 5.10. TSS for Floating Outlet with 25 lb Loading. 47
Figure 5.11. TSS for Floating Outlet with 50 lb Loading. 48
Figure 5.12. TSS for Floating Outlet with 100 lb Loading. 48
Figure 5.13. Mass Out for Fixed Outlet with 50 lb Loading. 49
Figure 5.14. Mass Out for Floating Outlet with 25 lb Loading. 49
Figure 5.15. Mass Out for Floating Outlet with 50 lb Loading. 50
Figure 5.16. Mass Out for Floating Outlet with 100 lb Loading. 51
Figure 5.17. Cumulative Mass Out for All Outlets and Loadings. 52
Figure 5.18. Average Event Mean Concentration in mg/l. 53
Figure 5.19. Removal Ratio. 55
Figure 5.20. Removal Ratio Change with Different Theoretical Overflow Rates and Different Runoff Volumes. 56

Figure 5.21. Removal Ratio Change with Different Effective Orifice Sizes..... 58
Figure 5.22. Removal Ratio Change with Different Particle Densities..... 59
Figure 5.23. Effect of Resuspension in Fixed Outlet with 50 lb Loading. 61
Figure 5.24. Effect of Resuspension in Floating Outlet with 25 lb Loading. 61
Figure 5.25. Effect of Resuspension in Floating Outlet with 50 lb Loading. 62
Figure 5.26. Effect of Resuspension in Floating Outlet with 100 lb Loading. 62
Figure 5.27. Outflow SSC for the Filling Period. 65
Figure 5.28. Accumulated Particles after Running a Run for the "No Energy Dissipator" Case (Left-Top), "with an Energy Dissipator" Case (Left-Bottom), and "with Flow Straightener" Case (Right-Top). 67
Figure 5.29. Outflow SSC for Three Different Inlet Setups. 68
Figure 5.30. Scouring Pattern around the Energy Dissipator Due to High Flow Rates. 69
Figure 5.31. Outflow SSC with and without Accumulated Sediment Right behind the Inlet. 70
Figure C.1. Relationship between Particle Diameter and Settling Velocity. 108
Figure C.2. Particle Size Distribution of SIL-CO-SIL®49 (Manufacturer Provided), Inflow Sample Measured by Coulter Counter, and the Best Fit Lognormal Distribution..... 109
Figure C.3. PDF of Mass Base Particle Size Distribution (Top-Left), CDF of Mass Base Particle Size Distribution (Bottom-Left), PDF of Theoretical Settling Velocity (Top-Right), and CDF of Theoretical Settling Velocity (Bottom-Right). 110
Figure C.4. (A) Calculated Water Level Change in the Sedimentation Basin and (B) Inflow and Outflow Rate. 112
Figure C.5. Theoretical Detention Time of Water Columns with Respect to their Inflow Time. 113
Figure C.6. Critical Particle Size Change with Respect to Inflow Time. 114
Figure C.7. Particle Size Distribution of Inflow Suspended Solid and the Fraction Removed.. 115
Figure C.8. Time Series Removal Ratio of Particles. 116
Figure C.9. Time Series Inflow SSC and Calculated Outflow SSC. 117
Figure C.10. SCS Triangular Hydrograph. 118
Figure C.11. Calculated Inflow and Outflow Rate Change. 119
Figure C.12. Calculated Time Series Outflow SSC. 119
Figure C.13. Inflow Hydrographs of Three Tested Examples. 120
Figure C.14. Timeseries Outlet Concentrations for the Three Different Hydrographs. 121
Figure C.15. Triangular and Flat Inflow Hydrograph. 122
Figure C.16. Outflow SSC for Triangular and Flat Hydrograph. 123

LIST OF TABLES

Page

Table 5.1. Gradient and Calculated Inflow SSC Difference between the Start and the End of Runoff Duration. 34
Table 5.2. Measured and Calculated Removal Efficiencies. 34
Table 5.3. Scaling Ratio of Each Variable. 37
Table 5.4. Dimensions and Inflow Conditions of Prototype to Have the Same Particle Removal Efficiency of Run A in Model Scale. 37
Table 5.5. Setup Conditions and Inflow Hydraulic Conditions. 38
Table 5.6. Inflow Experimental Conditions. 40
Table 5.7. Removal Efficiency and EMC of Each Run. 43
Table 5.8. Event Mean Concentrations in mg/l. 53
Table 5.9. TSS Removal Ratios. 54
Table 5.10. Particle Removal Ratio and Corresponding Maximum Water Level for Different Flow Rate and Different Orifice Sizes. 57
Table 5.11. Effect of Resuspension on the Performance of the Small Footprint BMP. 63
Table 5.12. Particle Removal Efficiency of the Six Hydraulically Identical Runoffs. 64
Table A.1. Data from Prototype Run FX050-1 79
Table A.2. Data from Prototype Run FX050-2 80
Table A.3. Data from Prototype Run FX050-3 81
Table A.4. Data from Prototype Run FX050-4 82
Table A.5. Data from Prototype Run FL025-1. 83
Table A.6. Data from Prototype Run FL025-2. 84
Table A.7. Data from Prototype Run FL025-3. 85
Table A.8. Data from Prototype Run FL050-1. 86
Table A.9. Data from Prototype Run FL050-2. 87
Table A.10. Data from Prototype Run FL050-3. 88
Table A.11. Data from Prototype Run FL050-4. 89
Table A.12. Data from Prototype Run FL050-5. 90
Table A.13. Data from Prototype Run FL050-6. 91
Table A.14. Data from Prototype Run FL100-1. 92
Table A.15. Data from Prototype Run FL100-2. 93
Table A.16. Data from Prototype Run FL100-3. 94
Table C.1. Input Parameters, their Units, and Values for the Model Application. 107
Table C.2. Inflow Condition and Calculated Removal Ratio. 120
Table C.3. Inflow Conditions and Resulting Particle Removal Ratios for Flat Hydrographs (A', B', and C') and Particle Removal Ratio of Corresponding Triangular Hydrograph (A, B, and C). 121

CHAPTER 1:
INTRODUCTION

BACKGROUND

The National Pollutant Discharge Elimination System (NPDES) regulations increasingly require permanent stormwater quality structures to mitigate stormwater impacts of transportation construction projects. For new construction in rural areas, it is usually possible to acquire sufficient right-of-way (ROW) to treat runoff in grass swales or to construct earthen structures to meet stormwater requirements. However, in urban areas where ROWs are extremely limited or land prices are prohibitive, stormwater structures must have minimal footprints and be placed underground. There are a number of proprietary devices based on centrifugal separators, or filtration, which can be employed in these situations. While these devices do provide some protection, they require frequent maintenance with specialized parts and equipment. Previous stormwater quality research conducted by the Texas Department of Transportation (TxDOT) at the Center for Transportation Research (CTR), Texas Tech University (TTU), and the Texas Transportation Institute (TTI) suggested that extended detention was one of the simplest and most effective means of removing most stormwater-borne particles. This project was initiated to develop and experimentally evaluate a structure based on off-the-shelf materials that could be used to treat stormwater in limited ROW conditions.

OBJECTIVES

The objectives of the project are as follows:

- Develop a physical model to test the viability of using extended off-the-shelf precast concrete sections as a stormwater quality structure.
- Develop a prototype based on the physical model to prove the effectiveness of the concept.
- Develop design criteria and specifications for structures.
- Develop maintenance guidelines.

APPROACH

Researchers conducted the project in three phases over a period of three years.

1. Phase one consisted of an extensive literature review documenting small footprint technologies being used for stormwater quality treatment. This phase was completed in 2005.
2. Phase two ran concurrent with phase one and involved the development of a $1/5^{th}$ scale physical model to test the potential effectiveness of a simple detention structure for stormwater treatment.
3. Phase three was the development of a prototype structure to verify the results of the physical modeling phase.

CHAPTER 2:
DESIGN CONSIDERATION

Researchers conceptualized the essential features of the small footprint stormwater sedimentation basin. A physical model was designed based on the design of a prototype scale rectangular stormwater detention basin. Initial performance testing was carried out on the physical model, followed by testing on the prototype to validate the results and get an estimate of the performance capabilities and limitations. The following sections describe the salient features of the prototype and model and the design considerations involved therein.

SEDIMENT CHARACTERISTICS

Commercial synthetic sediment, having a known and uniform particle size distribution, was used as the suspended solids for the testing instead of using real suspended solids from the natural environment. This substitution considerably reduced the variability in the experimental process.

SIL-CO-SIL®49, a product of US Silica Company, was used as the sediment in this experiment. The density of the product provided by the manufacturer was 2.65 g/cm^3. The particle size distribution was also provided by the manufacturer, as shown in Figure 2.1, and shows that the silica was well-graded. The particle size distribution graph indicates that almost all the particles were smaller than 50 micron. The particles used in the prototype study were considerably smaller than typical suspended solid particles found in stormwater (1-200 μm). This selection of particles with smaller size would consider a worst case scenario, and the actual removal efficiency would be much higher than that indicated by the model and prototype study.

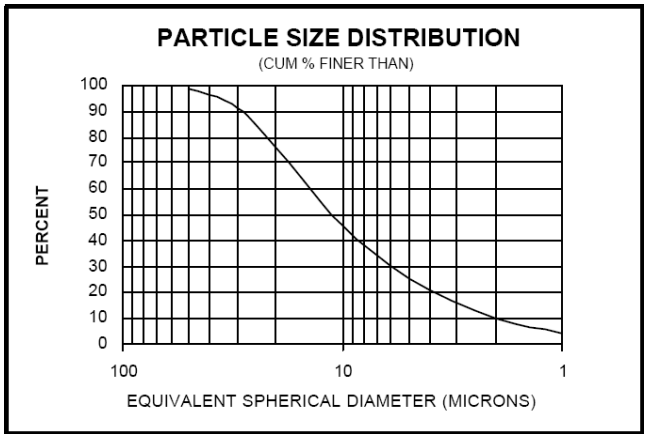

Figure 2.1. Particle Size Distribution of SIL-CO-SIL®49 as Provided by Manufacturer.

DESIGN INFLOW

Researchers designed the prototype to receive stormwater runoff from a watershed having a stormwater quality treatment volume of 1 acre/inch. The volume was based on the fact that the 90th percentile storm for small watersheds typical of the highway environment is on the order of 1 acre/inch. One acre-inch is equal to 3630 ft^3. An inflow rate of about 1 cfs, which required approximately 1 hr to fill the prototype tank, was used for the test program. This rate was considered average for a long, narrow watershed, which is most typical for highways.

SEDIMENTATION BASIN GEOMETRY

Based on the runoff volume, the total volume of the prototype would have to be equal to 3630 ft^3. The prototype dimensions were established as 80 ft long, 10 ft wide, 6 ft high, and having a 4.5 ft high weir wall at the outlet end providing an overall volume of 3600 ft^3 to the prototype sedimentation tank. The dimensions were set to fit in the right-of-way area along a highway. The weir wall was provided as an overflow release mechanism in case the runoff exceeded 1 acre/inch. A length scaling ratio L_R of 1:5 was considered while building the model. The corresponding model dimensions were 22.8 ft long by 2 ft wide. There was no weir for overflow in the physical model since that factor would not affect the hydraulic performance. The overall volume of the model sedimentation basin was 720 ft^3.

DETENTION TIME

The drainage time for the prototype was assumed to be approximately 24 hours. The corresponding drainage time for the model was set at approximately 5 hours.

$$Q = \frac{\forall}{\theta} = \frac{3630\,ft^3}{24hr} \times \frac{1hr}{3600\,\text{sec}} \approx 0.042cfs$$

CHAPTER 3:
MODEL TESTING

CONCEPTUAL MODEL

The removal efficiency of particles with a known settling velocity in a primary settling basin can be simply calculated by ideal horizontal flow reactor theory. Researchers developed a conceptual model to calculate particle removal efficiency in the same manner of the ideal horizontal flow reactor theory by employing similar assumptions. This chapter describes how the conceptual model was developed to calculate removal efficiency of particles. In addition, two example problems and their solutions using the developed conceptual model are shown in Appendix C to demonstrate how the conceptual model can be applied. The first one is a simple example that has a constant inflow rate and suspended sediment (SS) concentration (SSC) so that it can be reproduced using the physical model. The second example employs a triangular hydrograph as inflow, which makes the inflow condition more realistic than the first example.

Model Description

This section describes how a rectangular detention basin was modeled and how the modeling process was similar and/or different from the ideal horizontal flow reactor theory. Figure 3.1 shows a diagram of the detention basin. Stormwater runoff from a roadway surface flows into the basin through inlet pipes and drains out of the basin through the outlet orifice. Water level increases when the inflow rate is larger than the outflow rate and decreases when the opposite occurs. The flow process here is very different from a primary settling tank in the following two points: first, inflow and outflow rates are not always constant, and they are not equal; second, water level varies depending on the inflow rate and volume of water in the basin.

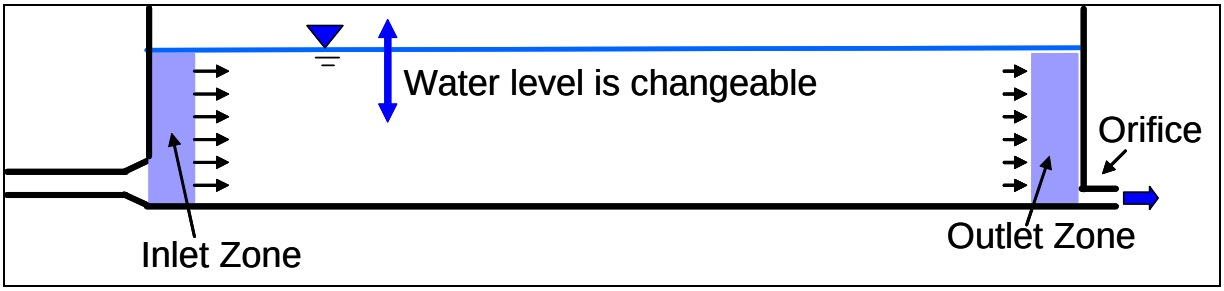

Figure 3.1. Diagram of the Rectangular Stormwater Detention Basin.

The conceptual model was based on the following assumptions:

- zero water level when runoff starts,
- well distributed inflow over the submerged depth of the basin,
- plug flow condition in the basin, and
- no sediment resuspension.

Outflow rate was controlled by an orifice set at the bottom of the end wall. Particles that did not reach the outlet zone would be retained in the detention basin. Water was allowed to overflow in the case that runoff volume was larger than the basin capacity. However, the overflow condition was not considered in this study.

Critical settling velocity is the velocity where all the particles with higher settling velocities will settle out in a reactor. In the ideal horizontal flow reactor, critical settling velocity is simply the overflow velocity, which is a constant flow rate divided by the surface area. However, in this rectangular detention basin, calculating critical settling velocity was not that simple because of an unsteady inflow and outflow rate and variable water level. Figure 3.2 shows the trajectory of water molecules and a particle that has a critical settling velocity in both an ideal horizontal flow reactor and the rectangular detention basin. Trajectories of a water molecule and a particle are curved in the rectangular detention basin, while the trajectory of a particle in an ideal horizontal flow reactor is straight. During this stage, methodologies to calculate the curved particle trajectory and critical settling velocity for a rectangular detention basin are developed within the stated model assumptions.

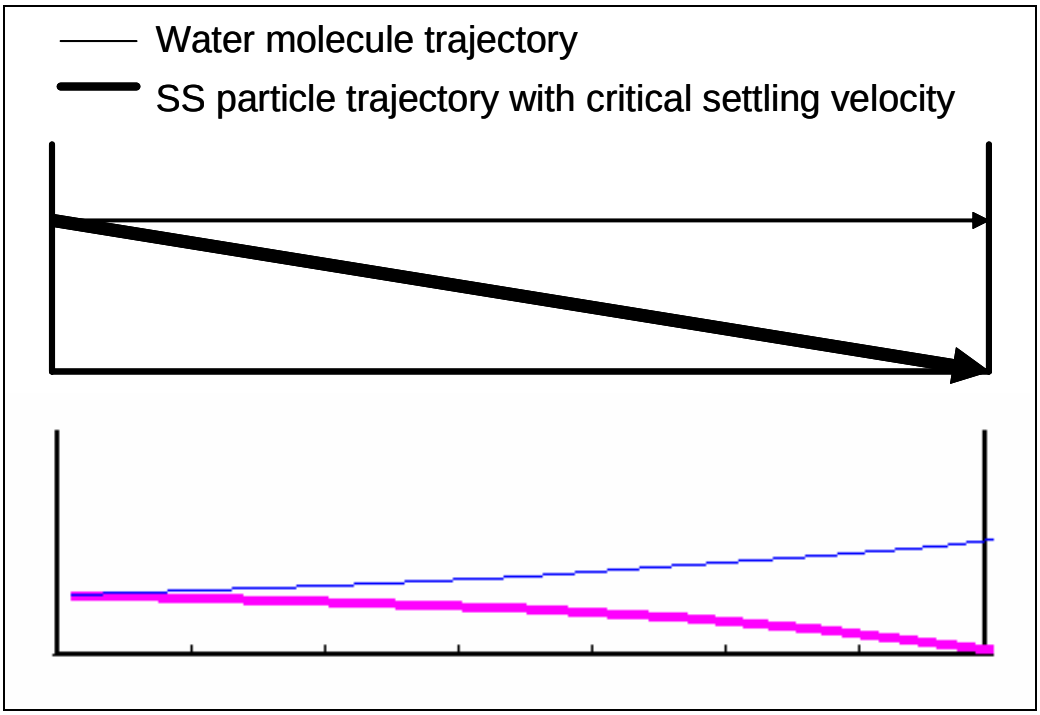

Figure 3.2. Trajectory of Water Molecules and a Particle with Critical Settling Velocity in an Ideal Horizontal Flow Reactor (above) and Rectangular Stormwater Detention Basin during Filling (below).

Hydraulics of the Basin

Water level is constantly changing from the start of runoff to the end of drainage, which makes the system unsteady. Water level change can be determined as follows from mass balance if both the inflow rate, $Q_{in}(t)$, and outflow rate, $Q_{out}(t)$, are known. The water level as a function of time is $h(t)$, B is width, L is the length of the basin, and t represents time.

$$\frac{dh(t)}{dt} = \frac{1}{B \cdot L}\left(Q_{in}(t) - Q_{out}(t)\right) \qquad (3.1)$$

We assumed that there is no horizontal or vertical mixing in the sedimentation basin. Numerical simulation would be required if mixing is significant. This assumption implies that longitudinal velocity is uniform over the vertical cross section, and vertical velocity is uniform over the horizontal cross section.

Mass balance was considered in a control volume at the right side of the detention basin, including the outlet orifice, as shown in Figure 3.3. The local flow rate at *x* and *t*, *Q(x,t)*, is equal to the sum of the outflow rate, $Q_{out}(t)$, and upflow rate (or downflow rate when the tank is emptying) within the control volume, as shown in Equation 3.2.

$$Q(x,t) = (L - x) \cdot B \cdot \frac{dh(t)}{dt} + Q_{out}(t) \qquad (3.2)$$

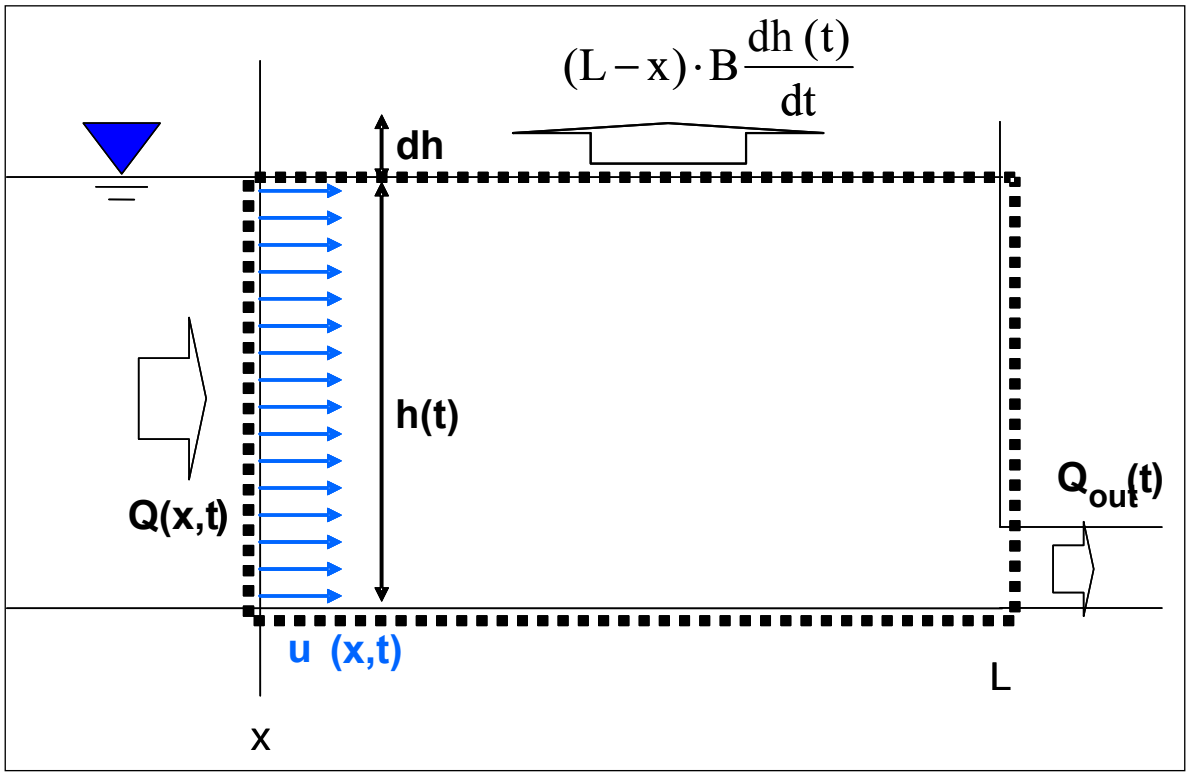

Figure 3.3. Local Convectional Velocity at Storm Runoff Period.

The corresponding local horizontal flow velocity at *x* and *t*, *u(x,t)*, is *Q(x,t)* divided by the submerged cross sectional area at *t*, as shown in Equation 3.3.

$$u(x,t) = \frac{Q(x,t)}{B \cdot h(t)} \qquad (3.3)$$

Vertical flow velocity at the water surface is the velocity of water level change, $\frac{dh(t)}{dt}$, and 0 at bottom. Vertical velocity in between, *v(z,t)*, is linearly distributed over depth:

$$v(z,t) = \frac{dz}{dt} = \frac{dh(t)}{dt} \cdot \frac{z}{h(t)} \qquad (3.4)$$

Critical Settling Velocity

As mentioned in the model description section, the particle path is not straight as seen in the ideal horizontal flow reactor, but is instead curved. Therefore, trajectories of particles should be calculated first in order to calculate critical settling velocity. Researchers calculated trajectories, or pathlines, of particles from the velocity field. A pathline is a line that is traced out in time by a given fluid particle as it flows; while a streamline is an instantaneous line whose tangents are everywhere parallel to the velocity vector (Currie, 1974). A pathline is calculated using Equation 3.5:

$$\frac{dx}{dt} = u(x,t)$$
$$\frac{dz}{dt} = v(z,t) \qquad (3.5)$$

The benefit of using the pathline concept in this study is that the position of a particle can be traced with time. This section describes both water molecules and particle pathlines. Pathlines for a water molecule can be derived in Equation 3.6 from local flow rate (Equation 3.2), local flow velocity (Equation 3.3), and pathline (Equation 3.5) as follows:

$$\frac{dx_w}{dt} = \frac{(L - x_w)}{h(t)} \cdot \frac{dh}{dt} + \frac{Q_{out}(t)}{B \cdot h(t)} \qquad (3.6)$$

where x_w means the position of the traced water molecules. Equation 3.6 was analytically solved with the initial condition that the longitudinal position of a water molecule at time t_{in}, $x_w(t_{in}; t_{in})$, is *0*. Then, $x_w(t; t_{in})$ stands for the longitudinal position at time t of a traced water molecule that flowed into the tank at time t_{in}. Equation 3.7 is the solution of 3.6.

$$x_w(t; t_{in}) = \frac{1}{B \cdot h(t)} \int_{t_{in}}^{t} Q_{in}(t)dt \qquad (3.7)$$

The vertical position of water molecules can be determined by the integration of Equation 3.4 from t_{in} to t and $h(t_{in})$ to $h(t)$ as follows (Equation 3.8) depending on initial height, $z(t_{in}; t_{in})$:

$$z_w(t; t_{in}) = \frac{h(t)}{H(t_{in})} z_w(t_{in}; t_{in}) \qquad (3.8)$$

The combination of Equations 3.7 and 3.8 shows the position of water molecules.

Next, the researchers found the pathline of a particle. The velocity vector of a particle can be determined as follows using the velocity vector of water. Settling velocity was assumed to be independent of the ambient flow field.

$$\begin{aligned} u_p(t;t_{in}) &= u(t;t_{in}) \\ v_p(t;t_{in}) &= v(t;t_{in}) - v_s \end{aligned} \qquad (3.9)$$

where $u_p(t;t_{in})$ is the x component of particle velocity, $v_p(t;t_{in})$ is the z component of particle velocity, and v_s is the settling velocity of the particle. Longitudinal position of a suspended solid particle at t with given t_{in}, $x_p(t;t_{in})$, is the same as the position of water particle, $x_w(t;t_{in})$ since longitudinal velocity of water molecules and particles are assumed to be the same.

$$x_p(t;t_{in}) = \frac{1}{B \cdot h(t)} \int_{t_{in}}^{t} Q_{in}(t)dt \qquad (3.10)$$

Substitution of the vertical flow velocity (Equations 3.4 and 3.9) for the pathline (Equation 3.5) yields the vertical velocity vector equation of a particle.

$$\frac{dz_p(t;t_{in})}{dt} = \frac{z_p(t;t_{in})}{H(t)} \cdot \frac{dh(t)}{dt} - v_s \qquad (3.11)$$

Equation (3.11) was analytically solved with the initial position of the particle at $t=t_{in}$, which is $z_p(t;t_{in})=z_p(t_{in};t_{in})$.

$$z_p(t;t_{in}) = H(t)\left\{ -v_s \int_{t_{in}}^{t} \frac{1}{h(t)} dt + \frac{z_p(t_{in};t_{in})}{h(t_{in})} \right\} \qquad (3.12)$$

Finally, detention time of the particle is calculated here. Since the position of the suspended solid particle, $(x_p(t;t_{in}), z_p(t;t_{in}))$, is known, time to reach the end of the tank, t_{out}, for the particle can be calculated by substituting $x_p(t;t_{in})=L$ in Equation 3.10 and solving for t. Detention time of a particle can be simply calculated from t_{out}- t_{in}. As shown in Figure 3.2, a particle with critical settling velocity, which enters the basin at the very top of the water column, will settle to the bottom on the right-hand side when reaching the outlet. Therefore, the focus was on a particle released from the water surface at the inlet. Initial vertical position of such a particle is the same as the water level at t_{in}, or simply $h(t_{in})$. Therefore, vertical position of the particle is

shown in Equation 3.13 by substituting $z_p(t_{in};t_{in})=h(t_{in})$ in Equation 3.12, the pathline equation of a particle.

$$z_{p,top}(t;t_{in}) = h(t)\left\{-v_s \cdot \int_{t_{in}}^{t} \frac{1}{h(t)}dt + 1\right\} \qquad (3.13)$$

Then, the minimum particle that meets $z_{p,top}(t_{out};t_{in}) > 0$ establishes the critical settling velocity, $v_{s,c}(t_{in})$ as shown in Equation 3.14.

$$v_{s,c}(t_{in}) = \frac{1}{\int_{t}^{tout} \frac{1}{h(t)}dt} \qquad (3.14)$$

Overall Removal Ratio of Particles

If the settling velocity of a particle is smaller than critical velocity, then it may or may not settle out depending on its starting position. Figure 3.4 shows the trajectories of a particle with lower settling velocities. The figure shows a particle released from the water surface that did not settle out, but the other particle released from the middle of the water level just settled out at the outlet. This situation implies that particles with a higher initial position than this particle will all escape, and those with lower initial position will all settle out. The ratio of settling can be calculated as described below.

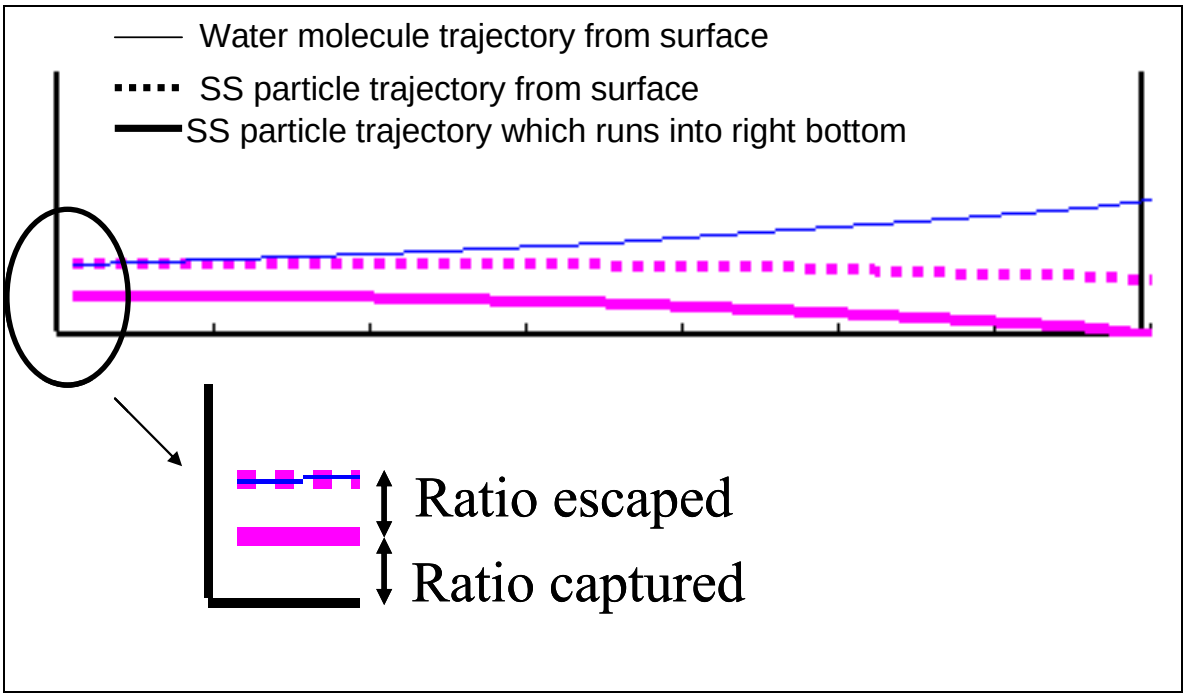

Figure 3.4. Trajectory of a Particle with Lower Settling Velocity than Critical Settling Velocity and the Particle Ratio of Captured and Escaped.

First, the pathline equation can be calculated for a particle that exactly runs into the bottom orifice by putting $(t,z_p)=(t_{out},0)$ into the particle pathline Equation 3.12. The settling ratio can then be calculated by solving $\frac{z_p(t_{in};t_{in})}{h(t_{in})}$, since $z_p(t_{in};t_{in})$ is the maximum initial height for particles to settle. The captured mass ratio, which is the captured number ratio with the same size particles, can be simplified as the ratio of settling velocity to the critical settling velocity.

$$\frac{z_p(t_{in};t_{in})}{h(t_{in})} = v_s \cdot \int_{t_{in}}^{t_{out}} \frac{1}{h(t)}\,dt = \frac{v_s}{v_{s,c}(t_{in})} \qquad (3.15)$$

The captured mass ratio, also known as reactor settling potential function is shown in Equation 3.16. This equation suggests that all particles with settling velocity larger than critical

settling velocity will settle out, and the fraction $\frac{v_s}{v_{s,c}(t_{in})}$ will settle out for particles with settling velocity smaller than critical settling velocity.

$$F(v_s, t_{in}) = \begin{cases} 1 \text{ for } v_s > v_{s,c}(t_{in}) \\ \frac{v_s}{v_{s,c}(t_{in})} \text{ for } v_s < v_{s,c}(t_{in}) \end{cases} \quad (3.16)$$

Assuming that the settling velocity of inflow particles has its own probability density function, $e(v_s)$, then, the mass removal ratio can be calculated as a function of inflow time.

$$\begin{aligned} R_{out}(t_{in}) &= \int_0^\infty F(v_s) \cdot e(v_s) dv_s \\ &= \int_{vs,c(tin)}^\infty 1 \cdot e(v_s) dv_s + \int_0^{vs,c(t_{in})} \frac{v_s}{v_{s,c}(t_{in})} \cdot e(v_s) dv_s \end{aligned} \quad (3.17)$$

The overall mass removal ratio of suspended solids can be calculated by the total mass of particles flowing out divided by the total mass of particles flowing in the basin as follows:

$$R = \frac{\int_0^{Ts} Q(t_{in}) \cdot C(t_{in}) \cdot R_{out}(t_{in}) dt_{in}}{\int_0^{Ts} Q(t_{in}) \cdot C(t_{in}) dt_{in}} \quad (3.18)$$

where T_s represents duration of storm runoff.

Time series outflow SSC can be estimated by Equation 3.19.

$$C(t_{out}; t_{in}) = C(t_{in}) \cdot (1 - R_{out}(t_{in})) \quad (3.19)$$

MODEL CHARACTERISTICS

Researchers built and tested a 20 ft long model of the sedimentation basin with inlet and outlet controls at Center for Research in Water Resources (CRWR) . The sedimentation basin was made of ¾-inch plywood. Prior to construction, nine cutout boards, three each for both sides and bottom, were painted with a polycrylic waterproofing medium, followed by primer paint and a tinted water-based latex paint. The nine boards were carefully connected to each other with screws and placed on cinder blocks. Pieces of wood boards were attached to support connections

between longitudinally connected boards, and 1 × 1 inch boards surround several cross sections of the basin to firmly support the hydraulic pressure. The seams were then sealed with silicone caulking. To complete the waterproofing of the model basin, resin was applied in a multiple-coat thickness throughout the whole inside surface of the model basin. This resulted in excellent waterproofing.

Sediment Delivery

The duration and flow rate of a model runoff were ascertained, and the inflow SSC was determined to be approximately 200 mg/L. Accordingly, concentrated slurry of the SSC was prepared in a 22 L bucket and mixed by a submersible pump that drew water from the bottom and pushed water out through a 1-inch diameter opening.

The concentrate slurry was delivered to the pipe network using a peristaltic pump (Manostat Vera, 1-3400 mL/s) with a constant flow rate. A dial adjusted the speed of the pump, so the relationship between the pump speed and the flow rate was calibrated beforehand to control inlet SSC. Researchers introduced sediment to the pipe network right before the inlet opening of the model basin. The whole sediment delivery system and a picture of the mixing box are shown in Figure 3.5. A uniformity coefficient parameter was computed to determine whether inflow SSC was kept constant enough.

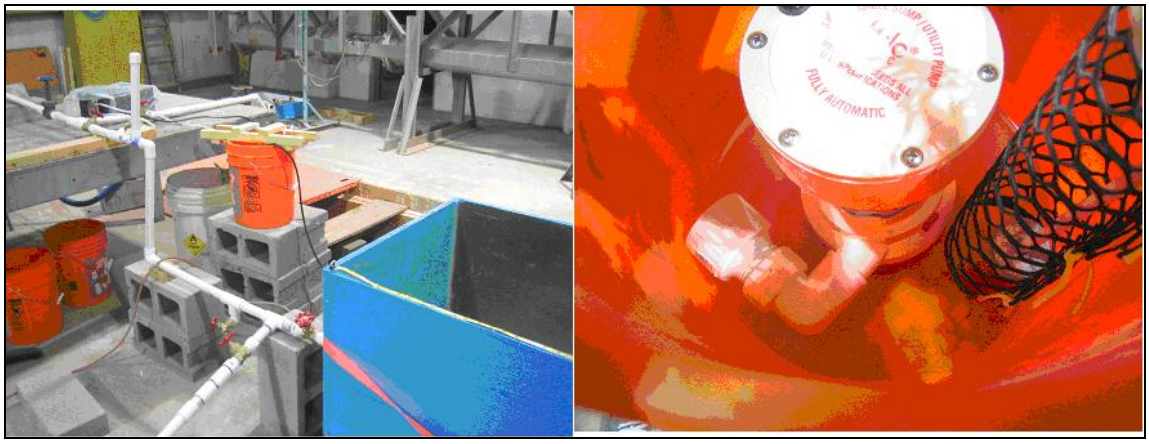

Figure 3.5. Particle Delivery System (Left) and Inside of the Mixing Bucket (Right).

Inlet Configuration

A 1-inch pipe was attached near the center at the bottom of the end piece of the sedimentation basin as the inflow opening. This opening was much smaller than the 3-inch pipe required by the 1/5 scaling of an 18-inch pipe, which is the minimum diameter of stormwater pipes. This smaller pipe diameter was considered because the flow velocity with the 3-inch pipe was small, which could cause particle accumulation in the pipe.

Inflow to the model basin was taken either from the indoor reservoir via a pump system or from tap water. Figure 3.6 shows the schematic of the pipe network used for the physical model. Tap water was preferred to pump water because the reservoir water contains a few mg/L of SSC, and this might affect the particle size distribution of inflow particles. Therefore, the pump system was used only when tap water couldn't achieve the required flow rate. Water, taken either from pump or tap water, was circulated back to the indoor reservoir when the water was clean, and it was drained out when the water contained a certain SSC. Once the pump was switched on, the flow rate was regulated by valve V_B, while valve V_C was open for bypass and valve V_D was closed, blocking inflow to the model basin. V_A was always widely open when water was taken from the indoor reservoir during an experimental run to prevent pump impairment, because the required inflow to the model basin is very small relative to the pump capacity, and too little flow through a large pump can easily impair the pump.

The flow rate was roughly measured at the outfall, following valve V_C, by measuring the time needed to fill a bucket of known volume. When multiple measurements showed the flow rate to be steady, researchers noted this rate, and then V_C was closed and V_D was opened. Flow was led to the bypass through V_E by closing V_F until the silica slurry was prepared in the mixing tank, delivered via the peristaltic pump to the pipe system, and stabilized. Finally, runoff with a certain SSC was led to the model basin.

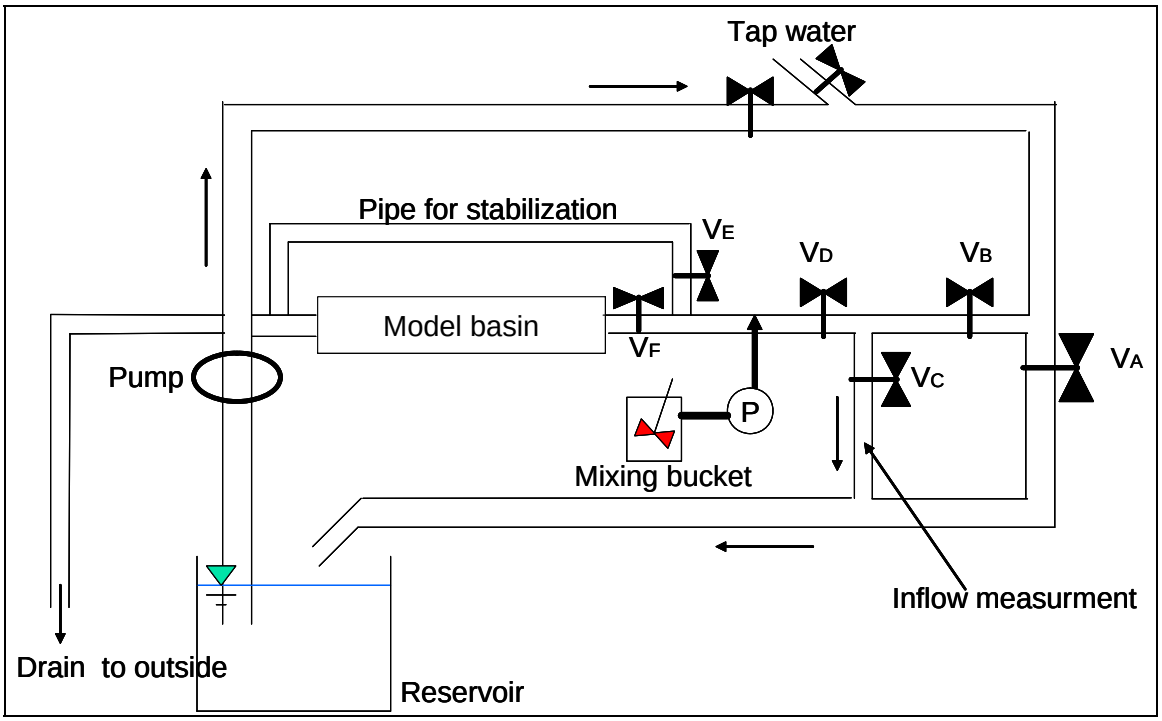

Figure 3.6. Piping Network for the Physical Model.

A small wooden block with a 3.5 × 3.5 inch (9 cm × 9 cm) square face and streamline tail was attached to the bottom, 5.1 inch (13 cm) behind the inlet opening as an energy dissipater. The purpose of the energy dissipater is to disperse the strong momentum of the inflow jet and prevent the resuspension of sediment around the inlet area. The position and shape of the energy dissipater determined the effect it would have on the flow and sedimentation pattern around it. These effects were not studied intensively in this research because they do not strongly affect particle removal efficiency in the model.

Sedimentation Basin (Reduced-Scale Physical Model)

The sedimentation basin has the length of 22.8 ft (6.96 m) and width of 2.0 ft (0.62 m). The bottom of the basin was painted dark blue and the side was painted gray. At the middle of the basin, a Plexiglas window was attached to watch sedimentation pattern or flow pattern using dye. Figure 3.7 shows the sedimentation basin with Plexiglas window. To simulate conditions similar to a real detention basin the particles precipitated from previous runs in the sedimentation

basin (model) were retained for successive runs. Therefore, each experimental result has some extent of influences such as resuspension from previous runs. After several measurements were taken at the original length basin, researchers shortened the basin to two-thirds the length of the original.

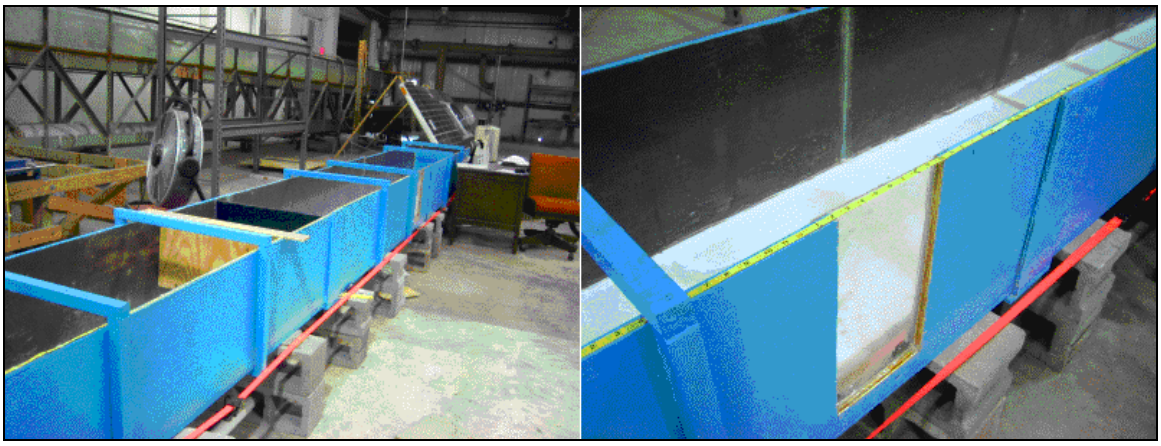

Figure 3.7. Sedimentation Basin with a View Window.

Outlet Configuration

At the far end of the sedimentation basin, plywood and a small section of metal sheeting made up a composite 1.2 ft (0.37 m) high overflow weir and outlet orifice (Figure 3.8). The effective area of the orifice necessary to completely drain the basin in 4.8 hours was calculated as 0.11 inch^2 (0.69 cm^2). To have this effective orifice area, the diameter of orifice was calculated as 0.43 inch (1.1 cm), assuming an orifice coefficient of 0.8. Then the circular orifice with the diameter was cut out from sheet metal by metal scissors.

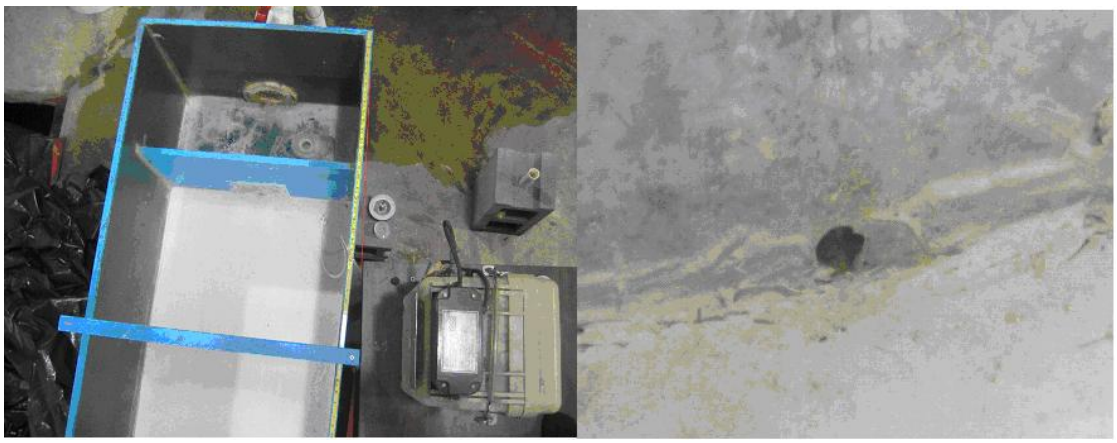

Figure 3.8. Setups around Outlet Orifice (Left: View from Top, and Right: Orifice Hole).

DATA ACQUISITION

Measurable parameters in the physical model are the water level of the sedimentation basin and SSC. Inflow and outflow rate, event mean concentration (EMC), and removal ratio are the parameters to be calculated. How values of these parameters were acquired and calculated and how a set of experiments was conducted are explained here.

Water Level

Water level in the model basin was measured by an automatic bubbler flow meter (ISCO 3230). A flexible polyurethane tube is fixed to the model basin bottom and then connects to the bubbler flow meter, which sends a slow air stream through the tube allowing the release of air bubbles from the bottom of the model basin. The bubble meter continuously measures the hydrostatic pressure due to the depth of water above the bubbling end of the tube. The meter automatically transfers the pressure into a water height reading. The measurement interval was set for 1 minute for this research.

Total Suspended Solids (TSS) Concentration

Water samples were taken periodically from the inlet and outlet. Inlet samples were taken through a nozzle attached in front of the sedimentation basin, and outlet samples were taken directly from a cascade installed at the bottom of the outlet area. Inflow samples were taken around

5-10 seconds after opening the nozzle to prevent taking particles accumulated in the nozzle.

Occasionally, samples were taken from the lengthwise midpoint of the sedimentation basin when necessary. Turkey basters were used to take samples instead of actual pipets since this method is much quicker in taking a sample of approximately 200 (mL).

Here is the experimental procedure that took place at each run:

- Target inflow rate, runoff duration, and inflow SSC were determined prior to each run. Inflow was bypassed to drainage, and inflow rate was roughly measured using a stopwatch and bucket of known volume.
- Detemine SSC in the mixing bucket, C_{slurry}, and the speed of peristaltic pump, Q_{slurry}.
- Inflow runoff with a given SSC was introduced to the sedimentation basin and maintained for a predetermined duration.
- Samples were taken periodically from the inlet and outlet by using 250 mL polyethylene bottles. Inflow samples were taken periodically so that at least four or five samples could be taken. Outflow samples were taken periodically (5 to 10 minute intervals) from the time runoff started until 10 to 20 minutes after the runoff stopped. After that, intervals of taking samples became longer, up to 30 minutes, since the SSC change was small.
- Water level in the basin was recorded every minute for the entire runoff and drain process using a bubble flow meter (ISCO 3230). Acquired data were used to calculate inflow and outflow rates.
- SSC of each sample was measured by the filtration method after the entire process was finished.

DATA PROCESSING

The variable water level and resulting outflow change made the system unsteady, even though the inflow rate and inflow SSC were kept constant. However, the hydraulics part concerning the water level and both inflow and outflow rates are fairly easy to estimate, which is a big advantage in consideration of this unsteady system.

Inflow and Outflow Rate Estimation

Effective Orifice Area

Prior to calculating the inflow and outflow rate, the effective orifice area was calculated using water level change. Equation 3.20 shows that water level change is only a function of time for the emptying period, and $\sqrt{h}$ is a linear function of time. Figure 3.9 shows the $\sqrt{h}$ change with time for two different orifices that were actually used in experiments. Effective orifice area can be calculated from the gradient of the graph of $\sqrt{h}$ with respect to time.

$$\begin{aligned}\sqrt{h_1} &= \sqrt{h_{max}} - \sqrt{\frac{g}{2}}\frac{A_e}{BL}(t_1 - T_s)\\ \sqrt{h_2} &= \sqrt{h_{max}} - \sqrt{\frac{g}{2}}\frac{A_e}{BL}(t_2 - T_s)\\ A_e &= -\frac{\sqrt{h_2} - \sqrt{h_1}}{t_2 - t_1}\frac{BL}{\sqrt{g/2}}\end{aligned} \qquad (3.20)$$

where (t_1, h_1) and (t_2, h_2) are two combinations of a time during the emptying period and the corresponding measured water level.

With appropriate units,

$$A_e(cm^2) = -\frac{\sqrt{h_2(m)} - \sqrt{h_1(m)}}{(t_2(min) - t_1(min)) * 60(s/min)} \cdot \frac{BL(m^2)}{\sqrt{g(m/s^2)/2}} \cdot 10^4 \qquad (3.21)$$

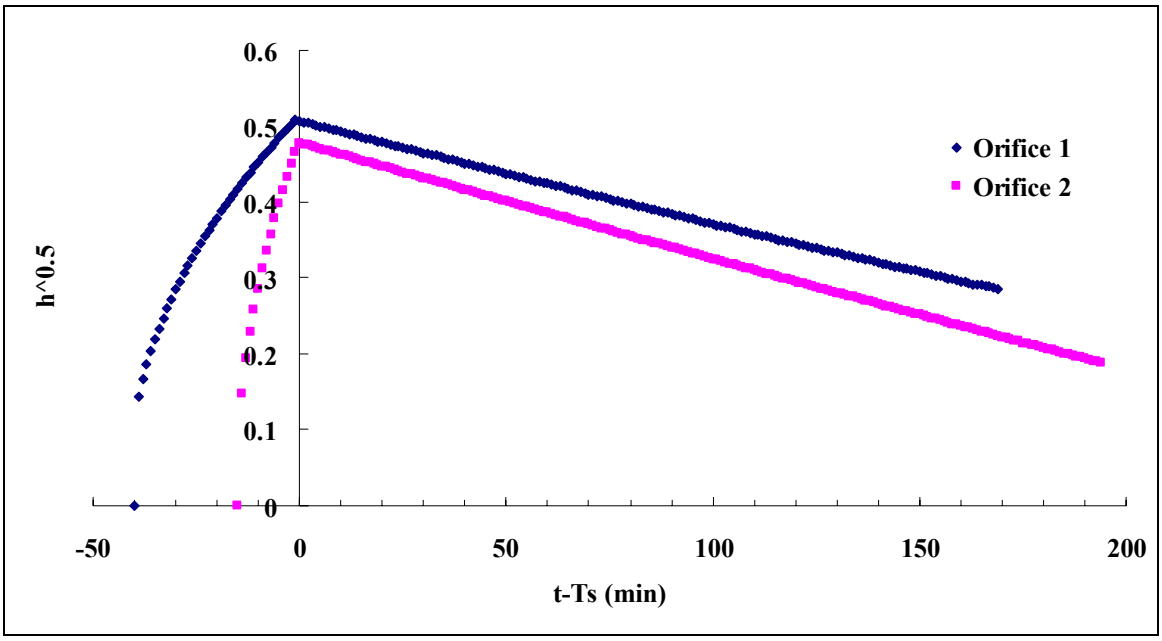

Figure 3.9. $\sqrt{h}$ (Square Root of Water Level) Change with Time.

In the experiment two different size orifices were used, and their effective areas were calculated using the following equation (3.22) as 0.07 inch^2 (0.43 cm^2) for orifice 1 and 0.08 inch^2 (0.49 cm^2) for orifice 2.

Outflow Rate

Outflow rate was calculated by the orifice equation with the calculated effective orifice sizes as follows:

$$Q_{out}(t) = A_e\sqrt{2gh(t)} \qquad (3.22)$$

Inflow Rate

Since the mass balance equation for the filling period is non-linear the inflow rate was adjusted by trial and error until the numerically calculated water level change, fitted with the measured water level change. Figure 3.10 shows an example of water level change comparison between measured and calculated. The figure shows a good fit although there are still some errors equal to or less than a half inch between these two. The errors are mainly due to the water level being measured near the outlet and travel time not being considered.

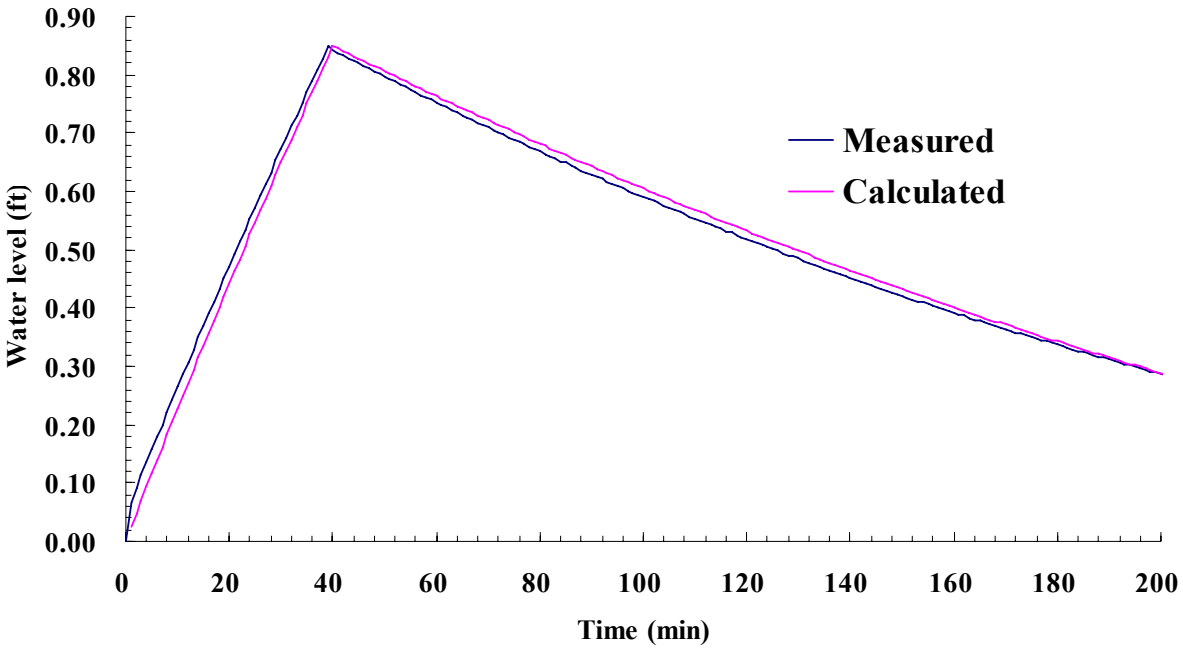

Figure 3.10. Measured and Calculated Water Level Change.

Event Mean Concentration

Samples for measuring SSC can be taken during a storm runoff event for only limited times. The interval of taking samples may not be the same through each storm runoff. Specifically, samples should be taken more frequently during a high-flow period than during a low-flow period because the mass flow rate of particles is greater during a high-flow period due to both high-flow rate and high-particle concentration. The discharged mass of particles can be estimated by the measured outflow SSC and the estimated outflow rate, as described in the previous section. Figure 3.11 shows a conceptual figure of measured discrete outflow SSC data and continuous estimated outflow data.

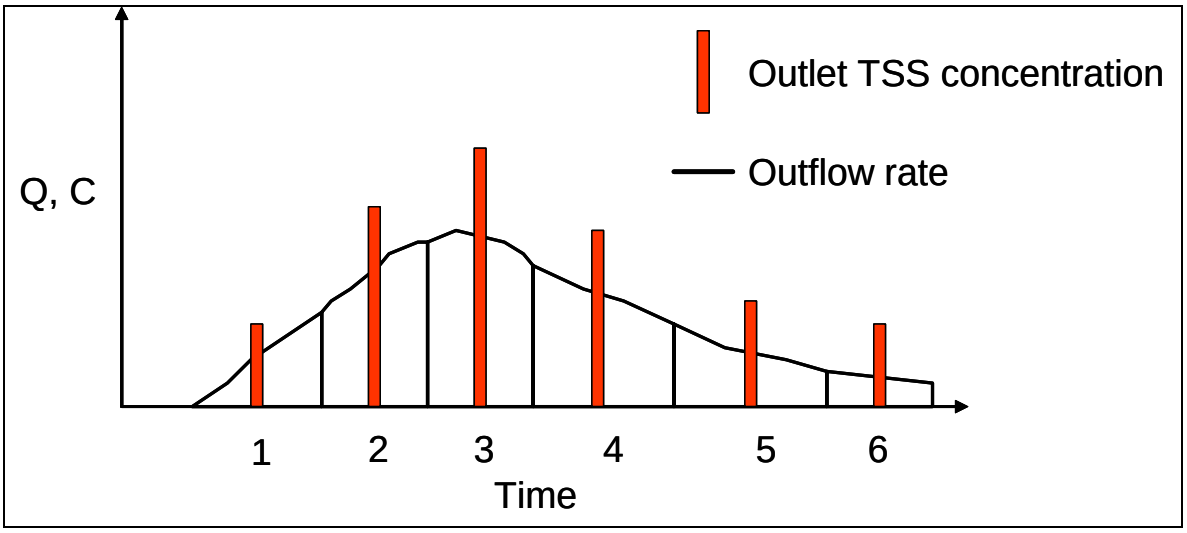

Figure 3.11. Conceptual Figure of Measured Outflow SSC Data (Discrete) and Estimated Outflow Rate (Continuous).

EMC is defined in the following Equation 3.23:

$$EMC = \frac{M_{out}}{V_{out}} = \frac{\int Q_{out} \cdot C_{out} dt}{\int Q_{out} dt} \tag{3.23}$$

In the case of discrete sampling, the kth value of outflow SSC taken at T_k minutes is the representative value of a group of time that is closer to T_k than T_{k-1} or T_{k+1}. Then, EMC should be estimated as follows:

$$EMC = \frac{\sum_{k=1}^{n} \left\{ C_{out}^{k} \cdot \int Q_{out}^{k} dt \right\}}{\int Q_{out}^{k} dt} \tag{3.24}$$

TSS Removal Ratio

Mass removal ratio of TSS, or simply particle removal ratio, can be defined as follows:

$$R = 1 - \frac{M_{out}}{M_{in}} = 1 - \frac{\int Q_{out} \cdot C_{out} dt}{\int Q_{in} \cdot C_{in} dt} \tag{3.25}$$

In this physical model study, total mass of inflow particles are simply defined as $Q_{in} C_{in} T_s$. Therefore, the mass removal ratio of particle can be estimated as follows:

$$R = 1 - \frac{\sum_{k=1}^{n} \left\{ C_{out}^{k} \cdot \int Q_{out}^{k} dt \right\}}{Q_{in} C_{in} T_s} \tag{3.26}$$

The relationship between EMC and removal ratio is shown in Equation 3.27:

$$\begin{aligned} M_{out} &= V_{in} \cdot EMC = M_{in}(1 - R) \\ \Rightarrow EMC &= \frac{M_{in}}{V_{in}}(1 - R) \end{aligned} \tag{3.27}$$

CHAPTER 4:
PROTOTYPE TESTING

PROTOTYPE CHARACTERISTICS

The prototype of the small footprint stormwater detention basin was designed to service the 1 acre (4047 m2) watershed. Based on this requirement, researchers designed and tested a conceptual model and a physical model at University of Texas, Austin. The scaling ratio, L_R, between the model and the prototype was 1:5. The tests on these models give an idea of the expected performance of the prototype.

Sediment Delivery

The SIL-CO-SIL®49 was first mixed in a hydroseeder (Figure 4.1) to form concentrated sediment slurry that was continuously agitated to maintain sediment homogeneity. The slurry contained 25 lb, 50 lb, or 100 lb of silica in 500 gallons of water to give slurries having concentrations of 5991, 11,983, or 23,965 mg/l, respectively. The slurry was injected into the main line feeding the sedimentation tank with water at a flow rate of about 0.0223 cfs. The main line pumped water into the tank at a flow rate of about 1.2 cfs. The resulting dilution ratio, as shown in the calculation below, is 0.0182, giving an inlet concentration of approximately 109 mg/l, 219 mg/l, and 437 mg/l for a mass loading of 25 lb, 50 lb, and 100 lb, respectively. The 50 lb loading leading to a 200 mg/l concentration is typical of urban highway runoffs (Li, et al. 2006).

$$C = \frac{Q_1 \times C_1 + Q_2 \times C_2}{Q_1 + Q_2} = \frac{Q_1}{Q_1 + Q_2} \times C_1 = \frac{0.0223}{1.2223} \times C_1 = 0.0182 \times C_1$$

$since\ C_2\ is \cong 0$

Figure 4.1. A. Hydroseeder for Making Slurry. B. Point of Injection into Main Line.

Inlet Configuration

The sedimentation tank had an 18-inch diameter inlet connected to a mixing tank from the outside (Figure 4.2). The simulated runoff water entered at the top of the mixing tank and dropped down in a free fall causing turbulence and preventing any sedimentation at the inlet. The mixing tank also simulated a more real life inflow regime. Seven concrete blocks were arranged in a staggered fashion in two rows approximately 1 ft from the inlet as energy dissipaters to disperse the momentum of the incoming water. The energy dissipation setup was intended to reduce the shear force exerted by the initial sheet of water and consequently reduce the resuspension of the particles settled in the previous runs.

Figure 4.2. A. Energy Dissipation at Inlet. B. Mixing Tank.

Sedimentation Basin

The small footprint tank was made of precast concrete assembled on the site. The sedimentation basin was 80 ft long, 10 ft wide, and 6 ft high with an overflow weir 4.5 ft high at the outlet end (Figure 4.3). The overall runoff holding volume of the sedimentation tank with dimensions was 4800 ft^3 (35,907 gallons).

Figure 4.3. A. View from Upstream. B. View from Downstream.

Outlet Configuration

Researchers drilled two 8-inch holes near the bottom of the weir wall: one in the center and one at the edge. The two types of outlets tested included a fixed outlet connected to the hole at the edge of the weir and a floating outlet connected to the hole at the center of the weir (Figure 4.4). The two outlets were controlled by two independent gate valves situated outside the tank.

Figure 4.4. A. Fixed and Floating Outlet. B. Independent Valves outside the Tank.

DATA ACQUISITION

Researchers used an ISCO (International Soil Conservation Organization) sampler to monitor the water level in the sedimentation basin and collect samples from the outlet end of the sedimentation tank. This section gives a brief explanation of the monitoring equipment and procedure.

Water Level

The ISCO bubbler recorded data that were transferred to the computer using a rapid transfer device. The data were accessed on the computer using FLOWLINK. Data included water level readings at every 15-second interval, as well as the time of the sample acquisition. This water level data could then be used to get an approximate value for the inflow and outflow rate.

TSS Concentration

Samples were collected manually every 10 minutes at the inlet during the first 1 hour interval when the sedimentation tank was filling up. The average of the TSS was reported as the input TSS concentration. Samples were collected at 1 hour intervals at the outlet end by the ISCO sampler. These samples were collected at the site and transported to the laboratory for TSS analysis.

The 1.5 μm particle retention size glass fiber filters (Glass Microfiber Filters 47mm, 934-AH, Whatman) were washed with three successive 20 ml portions of re-agent-grade water through a vacuum filtering apparatus. The washed filters were then placed in well labeled aluminum weighing dishes dried in an oven at 212°F The weighing dishes with the filters were removed from the oven and cooled in a desiccator, and their weights were recorded as A_i. The filters were then placed on the vacuum filtering device. The sampling bottles were shaken thoroughly, and a 100 ml portion representative of the samples was pipetted out onto the respective filters. The sample was forced through the filter under the influence of the vacuum. The filters were then placed in their respective aluminum dishes and placed in the oven for drying. On drying, the weighing dishes were removed from the oven, cooled in a desiccator, and weighed. The weights were recorded as B_i. Researchers calculated the total suspended solids using the following formula:

$$mg\ total\ suspended\ solids \Big/ liter = \frac{(B_i - A_i) \times 1000}{100}$$

DATA PROCESSING

The measured and analyzed data were then processed to interpret the significance of the testing results. The procedure involved in determining inflow/outflow rate, event mean concentration, and TSS removal ratio is described in detail in the following sub-sections.

Inflow and Outflow Rate Estimation

The consecutive water level readings at every 1 hour interval from the commencement of the test were subtracted to get the rise or fall in the water level. The first 1 hour was ignored as water was flowing into the sedimentation tank as well as flowing out of it. This fall in water level was then multiplied by the surface area of the tank to get the outflow rate:

$$Outflow\,Rate(cfs) = \frac{Fall\,in\,water\,level(\ ft)}{1(hr)} \times \frac{1(hr)}{3600(sec)} \times Surface\,area\,of\ tank(sq.ft.)$$

$$Outflow\,Rate(cfs) = \frac{Fall\,in\,water\,level(\ ft)}{1(hr)} \times \frac{1(hr)}{3600(sec)} \times 800(sq.ft.)$$

$$Outflow\,Rate(cfs) = 0.222 \times Fall\,in\,water\,level(\ ft)$$

Event Mean Concentration

Researchers used the flow and concentration measured for every 1 hour interval to calculate the EMC. The EMC can be used to characterize the quality of the water leaving the sedimentation basin in terms of suspended solids.

$$EMC = \frac{\sum_{i=1}^{24}(C_i \times Q_i)}{\sum_{i=1}^{24} Q_i}$$

TSS Removal Ratio

The TSS ratio, calculated according to the formula below, was an indicator of the performance of the sedimentation tank.

$$R = \frac{Mass_{in} - Mass_{out}}{Mass_{out}}$$

CHAPTER 5:
RESULTS AND CONCLUSIONS

CONCEPTUAL MODEL RESULTS

In this section, the developed conceptual model is examined by comparison with experimental results. Researchers compared the conceptual model results with experimental results using three parameters: change in water level, outflow SSC, and particle removal efficiency.

Water Level Change

Water level change is the most fundamental parameter in this detention basin since it was measured accurately every minute during the run. The value is very important for the conceptual model since the water level determines the cross sectional area of the plug flow model. Therefore, water level change should be very accurately calculated using the conceptual model. Water level was explicitly calculated numerically using mass balance for the entire period. Figure 5.1 shows experimental and calculated results of water level change. This figure shows that the water level was accurately calculated by the numerical calculation.

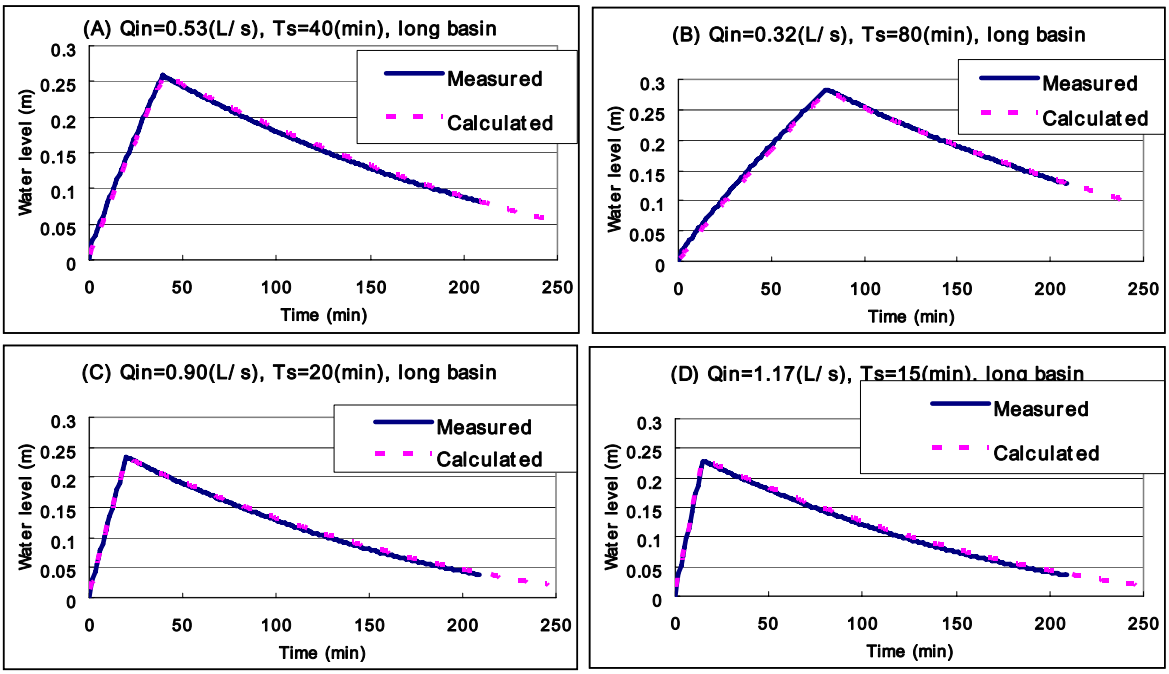

Figure 5.1. Measured and Calculated Water Level Change.

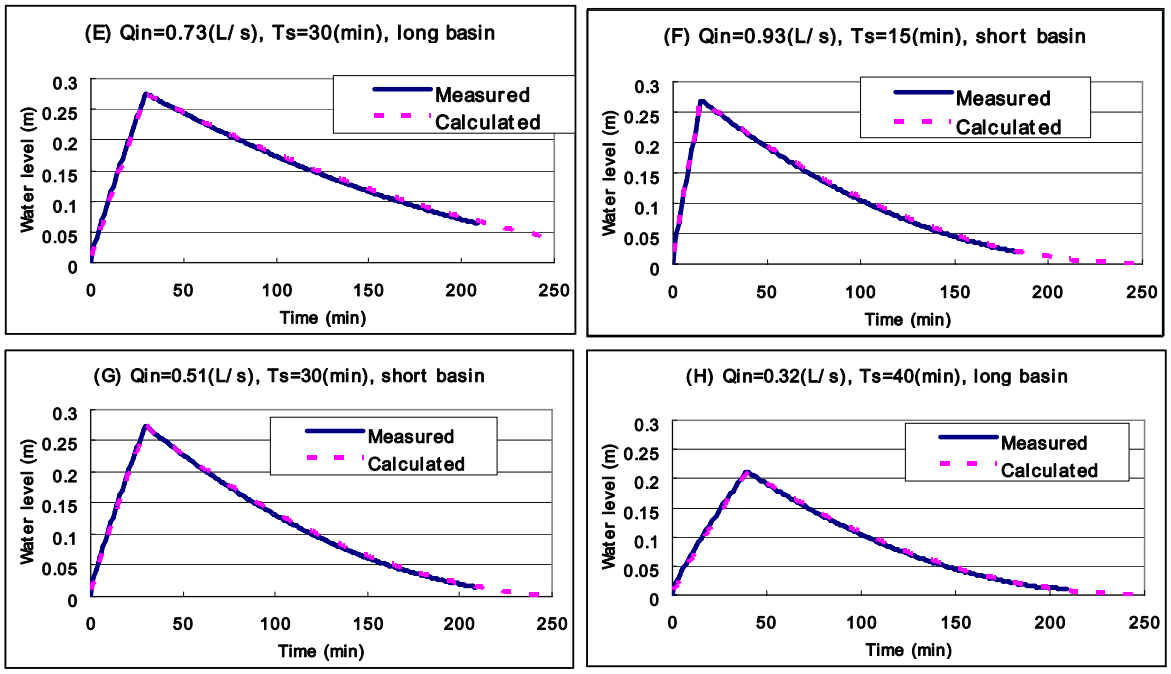

Figure 5.1. Measured and Calculated Water Level Change (continued).

Outflow SSC Change

Water level change was calculated very accurately in the model. Researchers determined the outflow SSC using the calculated water level change. Figure 5.2 shows the calculated and measured outflow SSC for all eight runs. Calculated results from all runs except runs B and G fit well with the measured outflow SSC results. The reason for the poor fit is not apparent since inflow conditions of runs B and G are quite different — run B has the longest duration and the slowest theoretical overflow rate, but run G has medium duration and medium overflow rate.

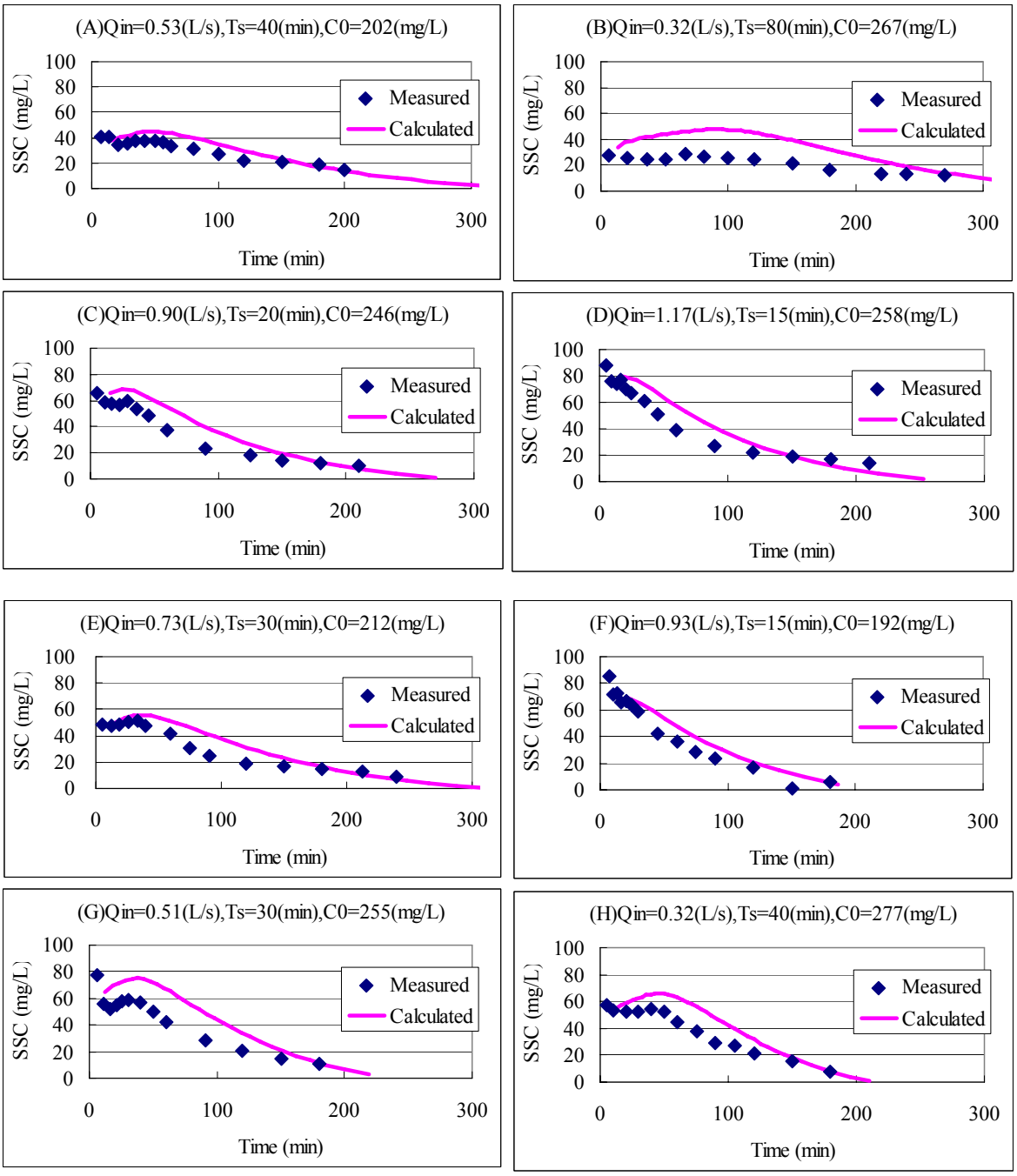

Figure 5.2. Measured and Calculated Outflow SSC.

One possible reason to identify why these two estimates are worse than the others is found in the outflow SSC graph (Figure 5.2). To determine if the SSC increases or decreases with time, a trend line was drawn for each run to see if the gradient was positive or negative. The gradient of the trend line, which has unit of mg/min, is shown in Table 5.1. Also, runoff duration was multiplied by the gradient in order to know how much the difference in SSC for each run is

for the entire duration period. Table 5.1 shows that runs B and G had the greatest inflow SSC differences, which could result in the large deviations of these two cases. Smaller inflow SSC at the initial stage would make the outflow SSC lower, and a greater inflow SSC at end of runoff would not reach the outlet until a later time when the basin is considered a plug flow reactor. If more accurate results are necessary, discrete SSC should be used for input data instead of using mean inflow SSC.

Table 5.1. Gradient and Calculated Inflow SSC Difference between the Start and the End of Runoff Duration.

Run	Gradient of inflow SSC (mg/min)	Calculated difference of inflow SSC between at the beginning and end of the runoff (mg)
A	0.2	8.1
B	1.0	77.4
C	1.4	27.1
D	-1.9	-28.3
E	1.1	34.0
F	-0.1	-1.9
G	2.4	71.5
H	1.2	47.2

Removal Ratio

Table 5.2 shows the calculated and measured particle removal efficiency, as well as the error which is the calculated minus measured removal efficiency for each run. Figure 5.3 shows the resulting and measured removal efficiencies. The figure shows that calculated results underestimated the removal efficiency by a few percentage points, but the trend is consistent.

Table 5.2. Measured and Calculated Removal Efficiencies.

Run	Calculated removal efficiency	Measured removal efficiency	Error (calculated-measured) (%)
A	0.88	0.89	-1.4
B	0.89	0.93	-4.6
C	0.86	0.89	-3.2
D	0.85	0.87	-1.8
E	0.85	0.88	-2.8
F	0.80	0.82	-2.4
G	0.81	0.87	-5.2
H	0.84	0.88	-3.6

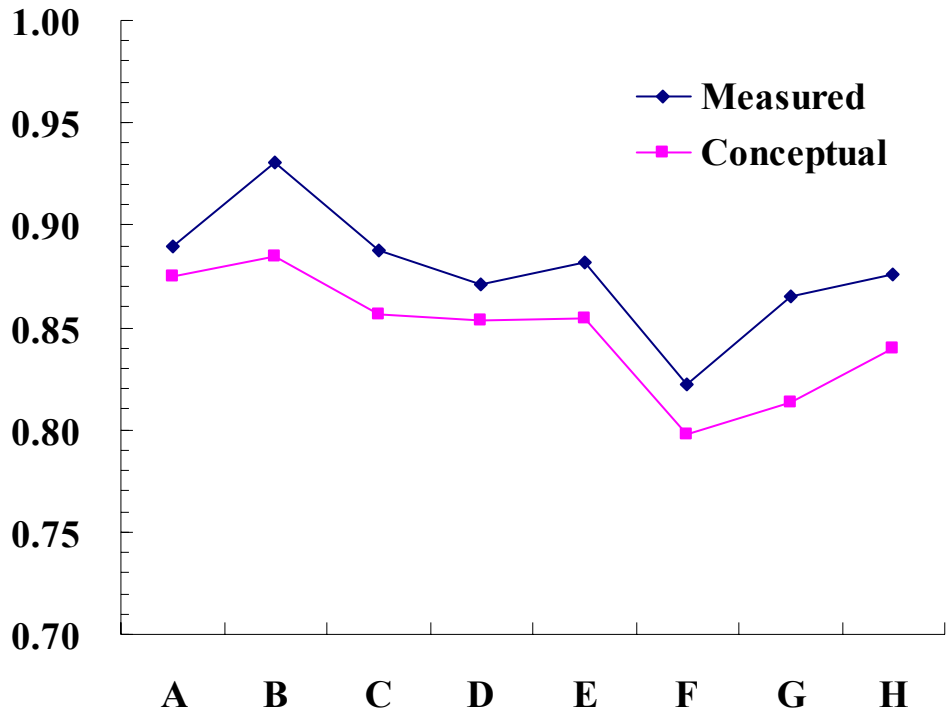

Figure 5.3. Measured and Calculated (Using Conceptual Model) Removal Efficiencies.

The conceptual model was developed to treat the sedimentation basin as a plug flow reactor since the basin has a long path and narrow cross sectional area, which is similar to channel flow. The model worked well to estimate time series outflow SSC, although the model always underestimated the removal efficiency by a few percentages. If a storm runoff is evaluated by only average inflow rate and SSC, the conceptual model may overestimate the removal efficiency because the high inflow SSC, called first flush, will result in higher outflow SSC and lower removal efficiency.

Actually, the conceptual model has two important characteristics. First, the model has no calibration parameter, which means the model results cannot be modified by experimental results. This is a desirable characteristic when designing because the conceptual model could show reasonably accurate results for any given conditions without conducting any experiments even though there may be a few percentage errors. The second characteristic is its complexity. The model requires numerical calculations with Matrix Laboratory (MATLAB), lognormal mean and lognormal standard deviation of inflow particle size. So far, the conceptual model is more

reliable than the empirical model developed from the experimental results. The conceptual model was developed on the basis of ideal horizontal tank theory, which is still widely used for designing, and the empirical model should be tested more by experiments with an actual prototype basin.

Scaling

The next objective is to see whether or not Hazen number scaling works to accomplish the same sedimentation performance between the physical model and the prototype. The conceptual model was used for analysis since the prototype experimental results were not available. As shown in the physical model design section, length ratio, L_p / L_m ; time ratio, t_p / t_m , and velocity ratio, $u_p(t_p) / u_m(t_m)$,were set to L_r, L_r, and *1*, respectively. The orifice size ratio, $A_{e,p} / A_{e,m}$, was $L_r^{3/2}$ to keep the water level change between the model and the prototype consistent with the time and the length scales. The maximum water level of the prototype should be L_r times larger than that of the model, and the time required to drain water from the maximum water level to zero for the prototype should be L_r times longer than that of the model. Sizes of particles should be the same between model and prototype so that settling velocity ratio can be kept at 1. This is very important because scaling up particle size means scaling up the whole particle size distribution, which is very difficult. Inflow SSCs are not necessary to scale up since the outflow SSC is always normalized to the inflow SSC, and the ratio is considered to be the same for any inflow SSC in the conceptual model. Table 5.3 summarizes the scaling ratio for parameters used for the physical model scaling.

Table 5.3. Scaling Ratio of Each Variable.

Variable	Description	Ratio X_p / X_m
L	Length of the detention basin	L_R
B	Width of the detention basin	L_R
h(t)	Height of the water level	L_R
Ts	Storm duration	L_R
v	Velocity	1
Q_{in} and $Q_{out}(t)$	Flow rate	$L_R^{\ 2}$
A_e	Effective area of orifice	$L_R^{\ 3/2}$
C_{in} and $C_{out}(t^*)$	Concentration	1
λ and ζ	Parameters of particle size distribution	1
Rd	Removal ratio	1

To verify the scaling assumptions, Run A, shown in the physical model section, was scaled up to the prototype with a length ratio, L_R, of 5. Inflow conditions for the model and prototype are shown in Table 5.4. The conceptual model was run for both the model and the prototype scale, and the time series outlet SSC and particle removal efficiency were calculated.

Table 5.4. Dimensions and Inflow Conditions of Prototype to Have the Same Particle Removal Efficiency of Run A in Model Scale.

	Inflow rate, Qin (cfs)	Runoff duration, Ts (min)	Effective area of orifice, Ae (inch^2)	Basin length, L (ft)	Basin width, B (ft)	Inflow mean SSC (mg/L)
Model	0.019	40	0.07	22.8	2.0	202
Prototype	0.094	200	0.75	114.2	10.2	202

MODEL RESULTS

Researchers developed the conceptual model to explain how sedimentation would occur in a rectangular detention basin under ideal conditions and to estimate removal efficiency of suspended solid particles. The physical model was built to measure the sedimentation performance of a scaled down basin. In this chapter, results from both the physical model and conceptual model are described and compared.

Inflow Conditions

Eight experimental runs were conducted with different inflow rates, runoff durations, and inflow SSCs. Table 5.5 shows the summary of inflow conditions including the experimental setup and given hydraulic conditions. Three combinations of setup conditions were tested. Two runs (A and B) were conducted with a smaller orifice area and full length of the basin. The next three (C, D, E) were conducted with a larger orifice area and full length of the basin. The remainder (F, G, H) were conducted with the larger orifice area and 2/3 length of the original sedimentation basin.

Inflow rate and runoff duration are also shown in Table 5.5. Among them, only the inflow rates were calculated values, which were fitted to the measured time series water level change. Theoretical overflow rate, $Q_{in}/(BL)$, was calculated, as seen in the table. Overflow rate, or storm intensity in other words, was chosen to have wider range (i.e., 0.27 to 1.16 m/hr) so that the physical model could test runoff with a wide range of properties.

Table 5.5. Setup Conditions and Inflow Hydraulic Conditions.

	Setup conditions		Inflow hydraulic conditions			Inflow SSC condtions	
	Effective area of orifice, A_e (inch^2)	Basin length, L (ft)	Inflow rate, Q_{in} (cfs)	Runoff duration, T_s (min)	Overflow rate, Q_{in}/BL (m/hr)	Mean inflow SSC (mg/L)	Uniformity coefficient, CU
A	0.067	22.8	0.019	40	0.44	257	0.97
B	0.067	22.8	0.011	80	0.27	410	0.85
C	0.074	22.8	0.032	20	0.75	266	0.97
D	0.074	22.8	0.041	15	0.98	271	0.97
E	0.074	22.8	0.026	30	0.61	279	0.95
F	0.074	15.2	0.033	15	1.16	161	0.97
G	0.074	15.2	0.018	30	0.64	234	0.91
H	0.074	15.2	0.011	40	0.40	213	0.89

Inflow SSC

To calculate the mean inflow SSC and check whether or not the inflow particle concentration was uniform enough for each run, five to eight inflow samples were taken from the inlet pipe through the nozzle, and SSCs were measured. Figure 5.4 shows measured SSC data with respect to sampling time. The graph shows that all of the SSC inflows are greater than 150 mg/L and less than approximately 350 mg/L. This inflow SSC range is reasonable since the event mean concentration, which refers to a mass based mean SSC in a storm event, of

stormwater runoff is approximately 140-220 mg/L, and it usually varies from a few mg/L to over 1000 mg/L.

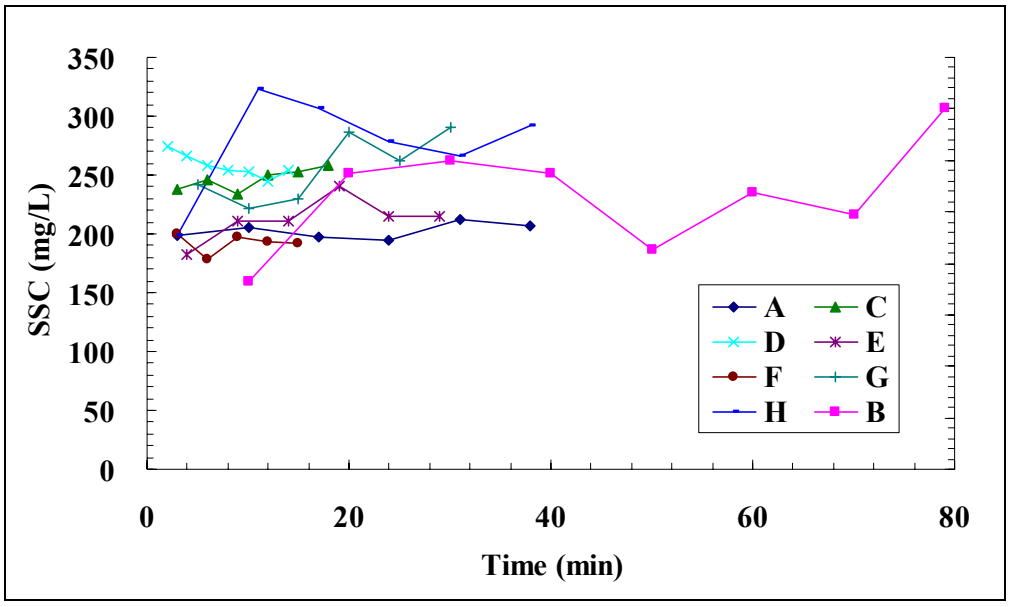

Figure 5.4. Time Series Inflow SSCs for all Eight Runs.

Researchers calculated the mean inflow SSC for each run by taking an arithmetic average of all the data points because inflow SSC is designed to be constant, and samples were taken uniformly over time. Then to check the uniformity of inflow SSCs, a uniformity coefficient was calculated. Table 5.6 shows mean SSC, total mass of inflow particles, and uniformity coefficient of each run in addition to inflow rate and runoff duration. Overall, uniformity coefficient values are very high, and all of them are much greater than 0.8, which was set as the criteria. Any strong trend, such as long-term increase or decrease, cannot be found from the graph. The table implies that it is difficult to hold inflow SSC uniform when the inflow is very low (e.g., B and H) or duration is very long (e.g., B). Actually, it was very difficult to conduct run B in terms of the uniformity since the flow rate of the peristaltic pump was very low in order to maintain a certain SSC value for a long time. This might have resulted in sedimentation in the tube.

Table 5.6. Inflow Experimental Conditions.

	Inflow rate, Q_{in} (L/s)	duration, T_s (min)	Mean inflow SSC, C_{in} (mg/L)	Total inflow mass, M_{in} (g)	Uniformity coefficient, CU (-)
A	0.53	40	202	257	0.97
B	0.32	80	267	410	0.85
C	0.9	20	246	266	0.97
D	1.17	15	258	271	0.97
E	0.73	30	212	279	0.95
F	0.93	15	192	161	0.97
G	0.51	30	255	234	0.91
H	0.32	40	277	213	0.89

Outflow SSC

Outflow samples were taken periodically for both the filling and emptying periods, and their SSCs were measured. Figure 5.5 shows time series SSC change of both inflow and outflow for all eight runs. Actually, these time series data are difficult to compare since multiple inflow parameters, such as inflow rate, runoff duration, and initial SSC, are different between runs. Therefore, comparison of time series outflow SSC is done in the next section using the nondimensionalized technique. However, one thing to be noted from the graph is that outflow SSC changes are all very smooth, even when the inflow SSC fluctuates significantly such as for runs B, G, and H, which implies that the system has the effect of equalization to eliminate the fluctuation of inflow SSC.

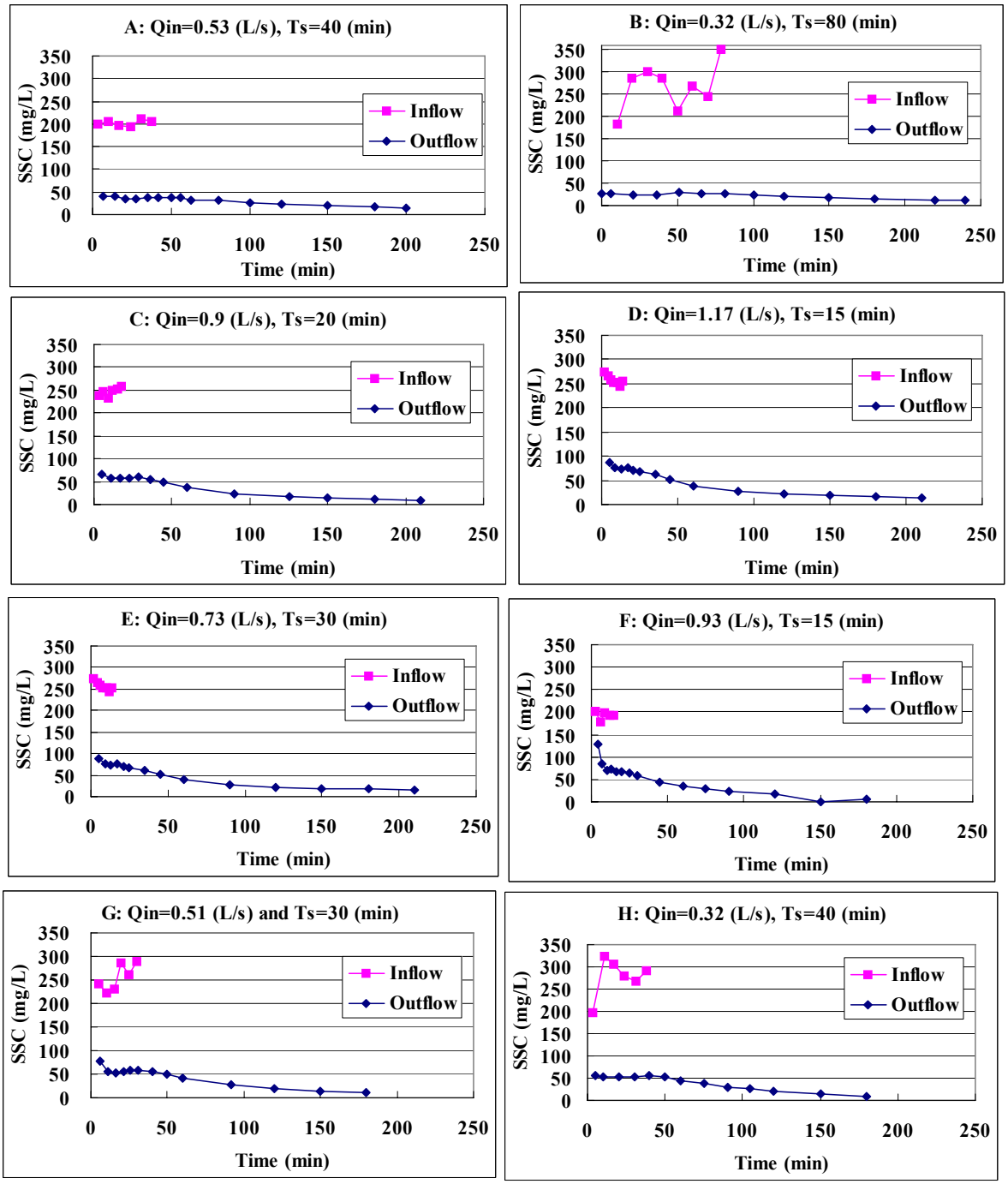

Figure 5.5. Measured Inflow and Outflow SSC Change.

Removal Efficiency

The calculation method for removal efficiency was conceptually shown in Chapter 3. Here, the calculation for removal efficiency of each run is shown. Figure 5.6 is a screen shot of the Excel spreadsheet used in the process of removal efficiency calculation for run A.

	A	B	C	D	E	F	G	H	I	J	K
1	Inflow condition (A)	t (min)	h (m)	Q_{out} (L/s)	C_{out} (mg/L)	from (min)	to (min)	v_{out} (L)	m_{out} (g)	Summary	
2	Ts(min)	7	0.06	0.05	40.3	0.0	10.5	29.6	1.2	V_{in} (L)	1272
3	40	14	0.11	0.06	40.3	10.5	17.5	26.1	1.1	V_{out} (L)	932
4	Cin(mg/L)	21	0.15	0.07	34.7	17.5	24.5	31.0	1.1	$V_{residual}$ (L)	340
5	202	28	0.19	0.08	35.8	24.5	31.5	35.1	1.3	M_{in} (g)	257
6	Qin(L/s)	35	0.24	0.09	37.2	31.5	38.5	38.8	1.4	Min M_{out} (g)	26
7	0.53	42	0.25	0.10	37.7	38.5	46.0	43.2	1.6	Max M_{out} (g)	31
8		50	0.24	0.09	37.2	46.0	53.0	39.4	1.5	Max R_{out}	0.90
9		56	0.23	0.09	36.4	53.0	59.5	36.0	1.3	Min R_{out}	0.88
10		63	0.23	0.09	33.0	59.5	71.5	65.1	2.1	Average R_{out}	0.89
11		80	0.20	0.09	31.1	71.5	90.0	95.4	3.0		
12		100	0.18	0.08	26.7	90.0	110.0	97.0	2.6		
13		120	0.16	0.08	21.9	110.0	135.0	113.5	2.5		
14		150	0.13	0.07	21.1	135.0	165.0	122.8	2.6		
15		180	0.10	0.06	18.8	165.0	190.0	91.6	1.7		
16		200	0.09	0.06	14.8	190.0	210.0	67.6	1.0		

Figure 5.6. Excel Spreadsheet to Calculate Removal Efficiency.

Column A: The inflow conditions consisting of runoff duration, Ts (min), mean inflow SSC, Cin (mg/L), and inflow rate, and Qin (L/s) are listed here.

Column B: Time of each sampling (min).

Column C: Measured water level (m) at the time of sampling.

Column D: Calculated outflow rate (L/s) at the time of sampling using the orifice equation.

Column E: Measured SSC (mg/L) at the time of sampling.

Columns F and G:

Start time (min) and end time (min) during the sampling period. The sampling time is assumed to be in the middle of the range.

Column H: Volume (L) of water discharged from time F to time G, which is calculated by D*(G-F)*60.

Column I: Mass (g) of particles discharged from time F to time G, which is calculated by E*H/1000.

Cell (K2): Total volume of inflow water (L), calculated by A3*A7*60.

Cell (K3): Total outflow volume from the beginning of runoff to the end time represented by the last sampling, calculated by the sum of column H.

Cell (K4): Volume of water that remained in the tank after the end of the last sampling, calculated by Cell (K3)-Cell (K2).

Cell (K5): Total mass of inflow particles (g), calculated by total inflow volume multiplied by mean inflow SSC.

Cell (K6): Minimum mass of discharged particles (g), calculated by the sum of column I.

Cell (K7): Maximum mass of discharged particles (g) assuming all the residual water drained out with the SSC at the last sampling, calculated by Cell(K6)+Cell(K4)*Cell(E15)/1000.

Cell (K8): Minimum removal ratio, calculated by 1-Cell(K6)/Cell(K5).

Cell (K9): Maximum removal ratio, calculated by 1-Cell(K7)/Cell(K5).

Cell(K10): Removal ratio, average value of Cell(K8) and Cell(K9).

Minimum and maximum calculated values of total discharged particle mass, M_{in}, removal efficiency, and EMC are shown in Table 5.7 with the inflow mean SSC, C_{in}, and the total inflow mass, M_{in}. For practical reasons, the average minimum and maximum removal efficiencies are considered as the removal efficiency of each run, which was calculated in Cell (K20). This is because maximum and minimum values of removal efficiencies are all very close to each other. The table shows that removal efficiencies are over 86 percent except in run F, which was conducted with the highest theoretical overflow rate (1.16 m/hr see Table 5.5 and had the removal ratio of only 82 percent. Figure 5.7 shows the relationship between removal ratio and theoretical overflow rate. This figure shows that the larger the overflow rate is, the worse the removal efficiency is, but it is not a very strong relationship. These data are further analyzed in the next section with the assistance of nondimensionalization.

Table 5.7. Removal Efficiency and EMC of Each Run.

	Inflow mean SSC, C_{in} (mg/L)	Total mass of inflow particle, M_{in} (g)	Total mass of discharged particle, M_{out} (g)		Removal efficiency		EMC (mg/L)	
			Min	Max	Max	Min	Min	Max
A	202	257	26	31	0.90	0.88	20	24
B	267	410	27	30	0.93	0.93	17	19
C	246	266	29	30	0.89	0.89	27	28
D	258	271	34	36	0.87	0.87	33	34
E	212	279	32	34	0.88	0.88	25	26
F	192	161	28	29	0.82	0.82	34	35
G	255	234	31	32	0.87	0.86	34	35
H	277	213	26	27	0.88	0.88	34	35

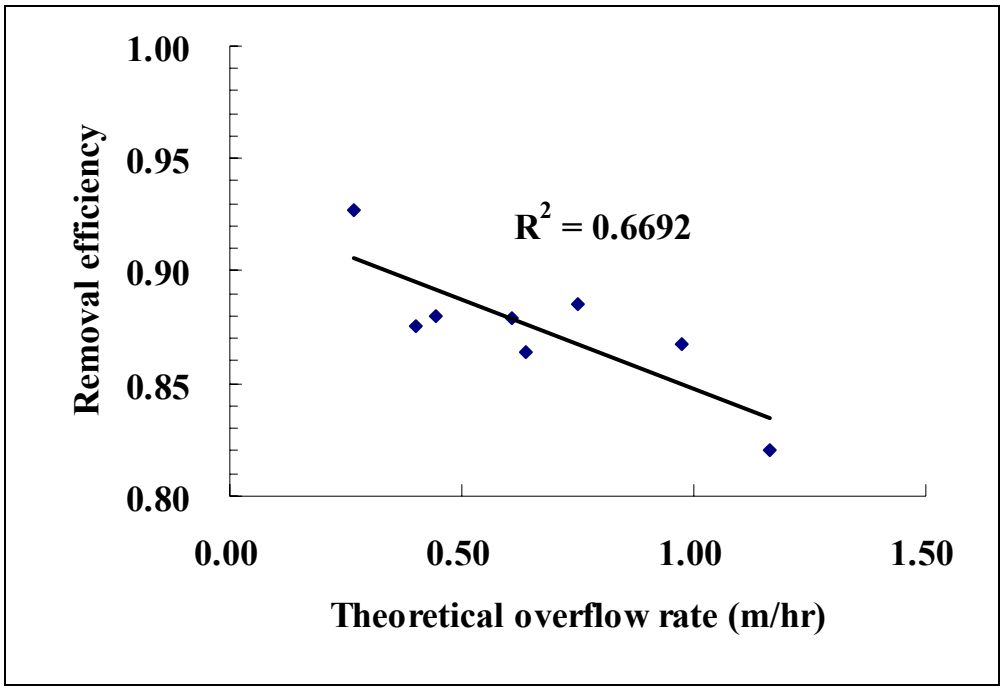

Figure 5.7. Relationship between Removal Efficiency and Theoretical Overflow Rate.

PROTOTYPE RESULTS

The tests conducted on the small footprint Best Management Practices (BMP) prototype included:

- four repetitions of the test using fixed outlet and 50 lb loading (FX050).
- three repetitions of the test using floating outlet and 25 lb loading (FL025).
- six repetitions of the test using floating outlet and 50 lb loading (FL050).
- three repetitions of the test using floating outlet and 100 lb loading (FL100).

The statistical comparison conducted on the data included:

- Outlet Comparison
  - FX050 v/s FL050
- Loading Comparison
  - FL025 v/s FL050
  - FL050 v/s FL100
  - FL025 v/s FL100

The details of the prototype testing results are discussed in the following sections.

Outflow Conditions

Two outflow conditions existed depending on the outlet type. The outflow rate from the sedimentation basin was maintained at approximately 0.04 cfs for most of the test duration in the case of floating outlet, while in the case of fixed outlet, the outflow rate dropped linearly from ~ 0.095 cfs to ~ 0 cfs. Figure 5.8 shows the variation of outflow rate with time for the two outlet types. The floating outlet had a considerably lower outflow rate than the fixed outlet for the initial 10 hrs when the concentration of suspended solids was high. The lower initial outflow rate resulted in a lower mass of suspended solids escaping from the sedimentation basin.

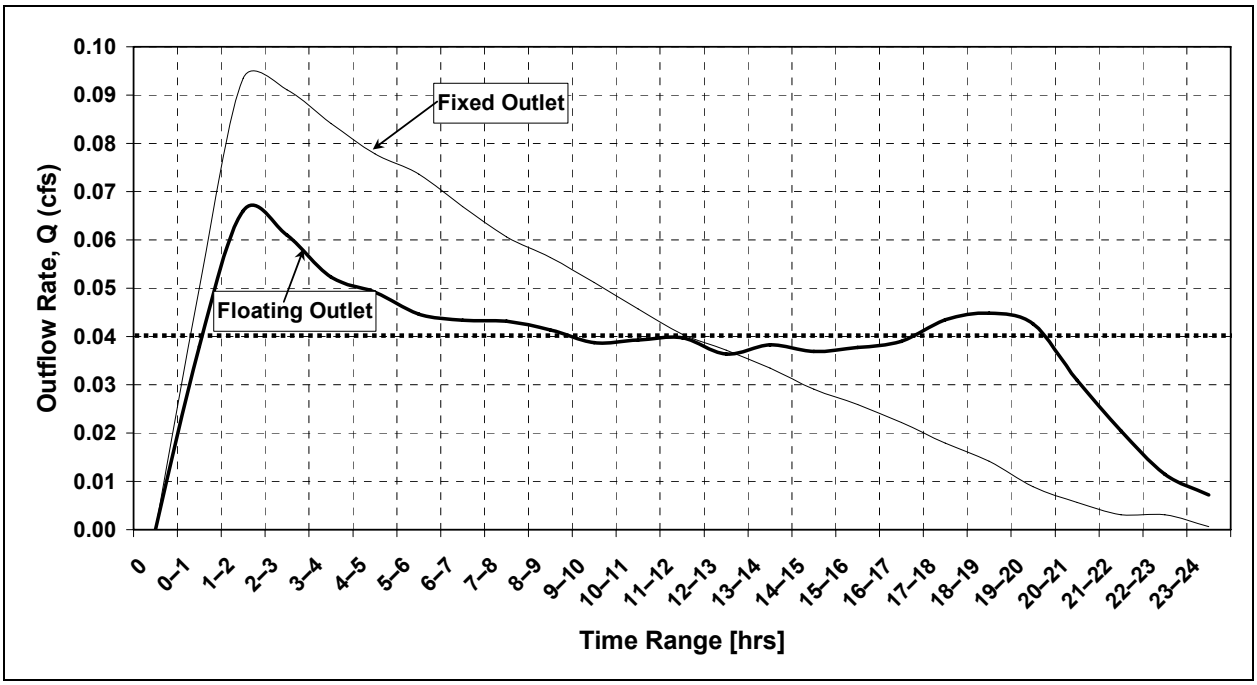

Figure 5.8. Outflow Rates v/s Time for Floating and Fixed Outlet.

Total Suspended Solids

The box-plots of total suspended solids for each hour of the test for FX050, FL025, FL050, and FL100 are shown in Figures 5.9, 5.10, 5.11, and 5.12, respectively. As we can see from the figures, the suspended solids concentration is high initially but drops down rapidly over the first 6 hours. The TSS concentration drops negligibly over the rest of the testing duration.

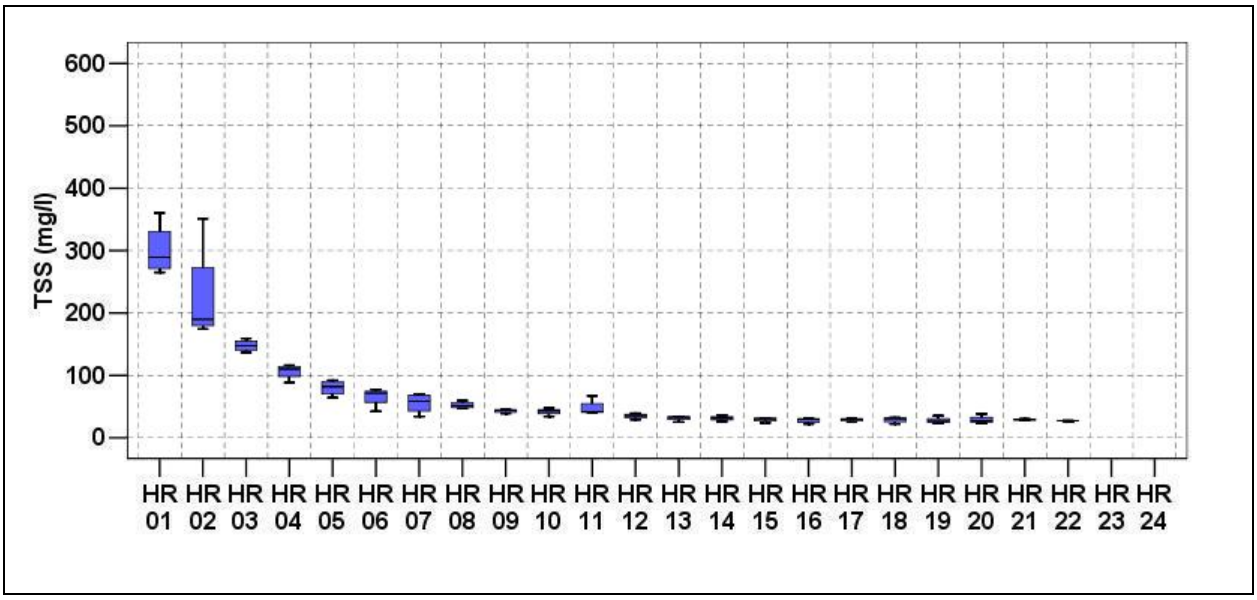

Figure 5.9. TSS for Fixed Outlet with 50 lb Loading.

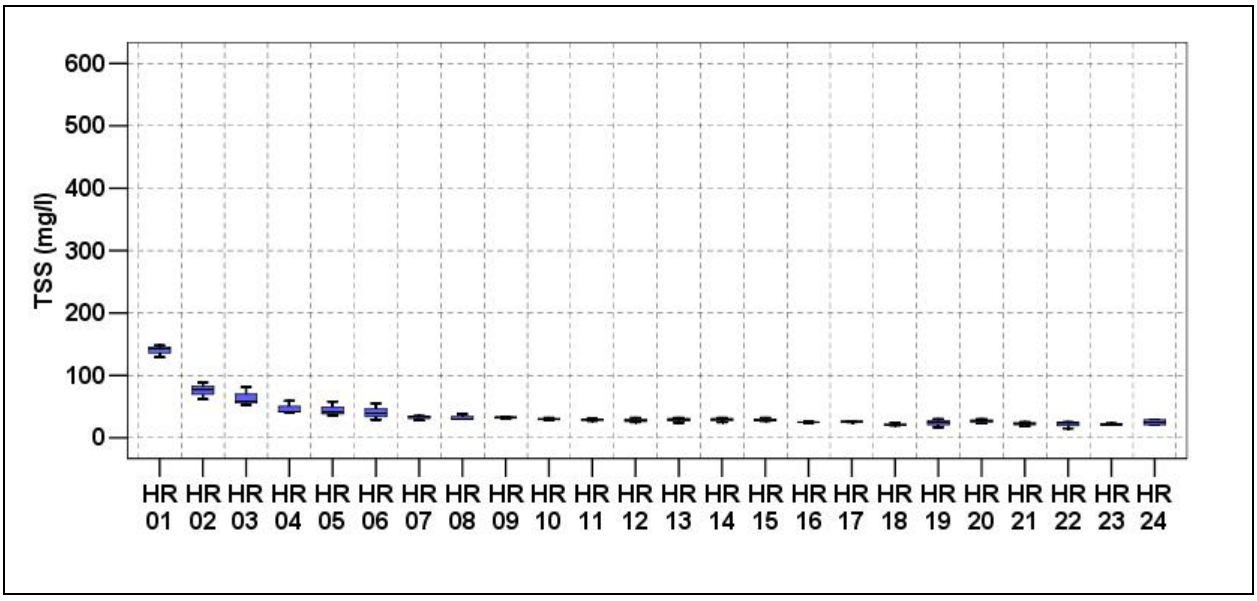

Figure 5.10. TSS for Floating Outlet with 25 lb Loading.

The researchers also observed that the lowest concentration of TSS in the water leaving the sedimentation basin rarely dropped below 30 mg/l. Another interesting observation was that the lowest achievable concentration in the sediment basin effluent was a function of the input

mass loading. The higher the input mass loading, the higher was the lowest achievable TSS concentration at the outlet of the basin.

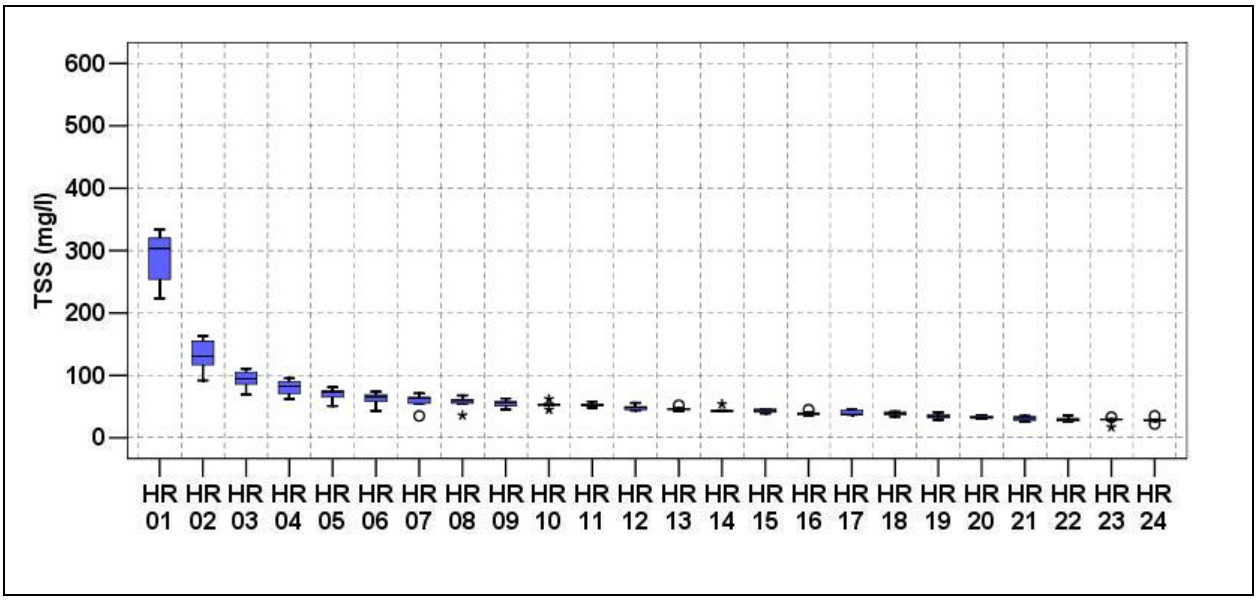

Figure 5.11. TSS for Floating Outlet with 50 lb Loading.

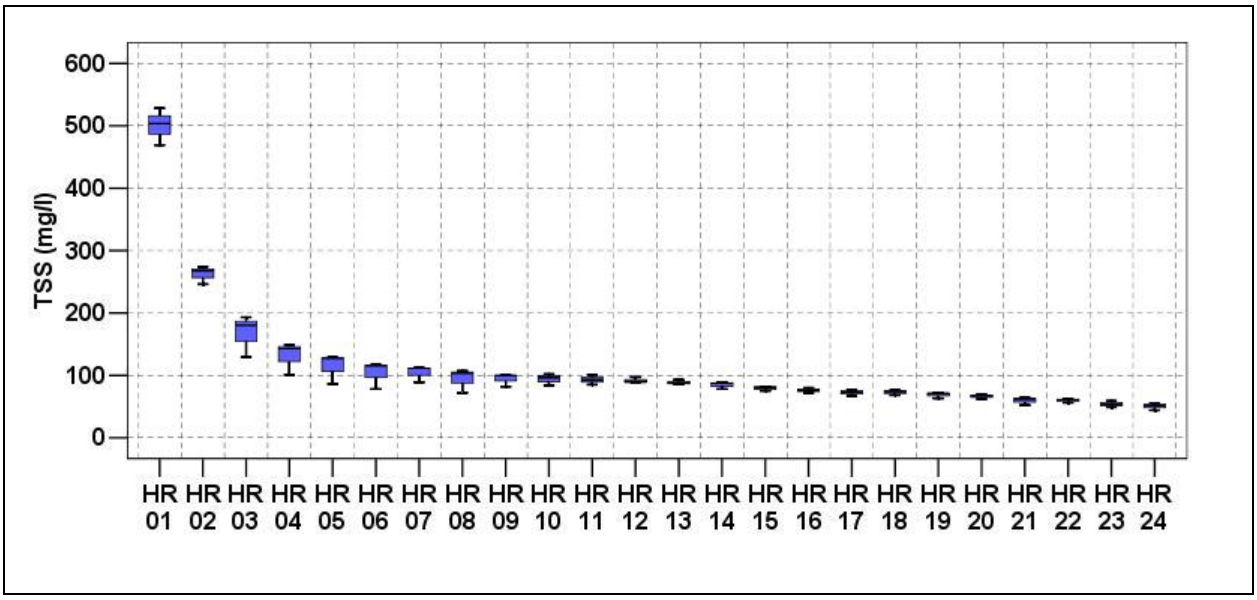

Figure 5.12. TSS for Floating Outlet with 100 lb Loading.

Mass Loading

The mass in pounds exiting the sedimentation basin every hour of the test duration is presented in Figures 5.13, 5.14, 5.15, and 5.16 for FX050, FL025, FL050, and FL100, respectively.

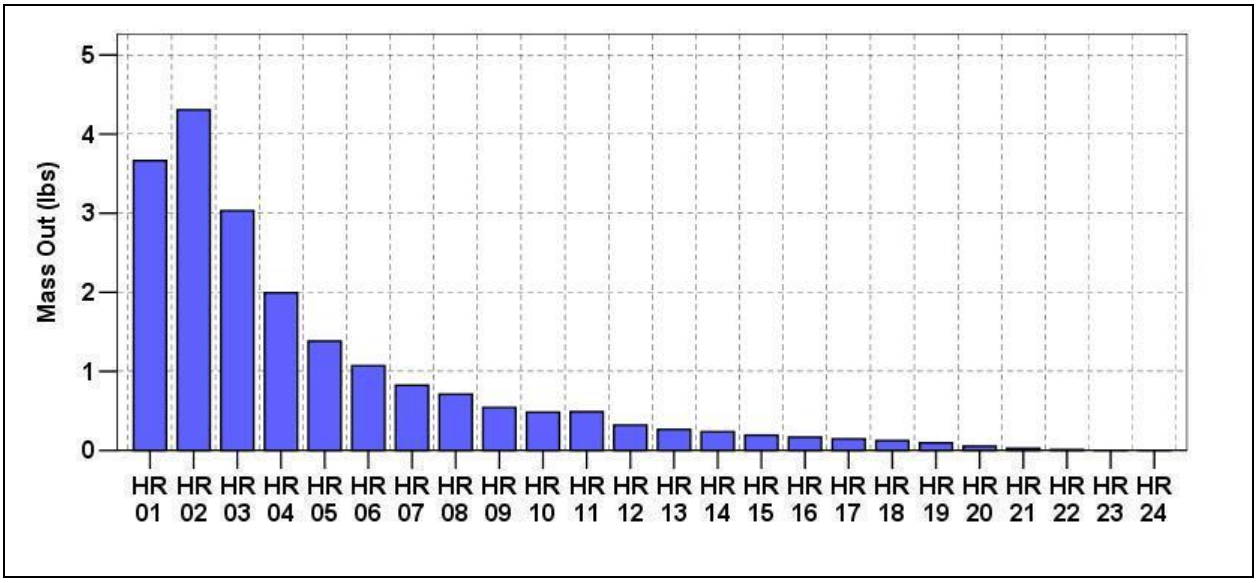

Figure 5.13. Mass Out for Fixed Outlet with 50 lb Loading.

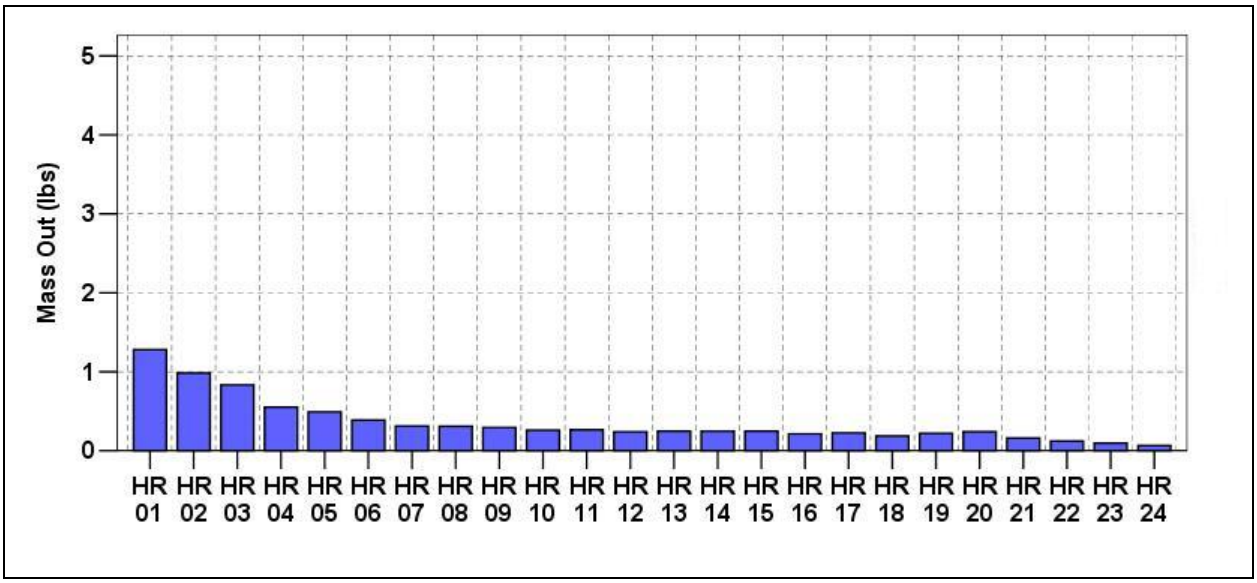

Figure 5.14. Mass Out for Floating Outlet with 25 lb Loading.

The figures show that substantial amounts of suspended solids leave the sediment basin in the initial phase of the test duration. The mass leaving the sedimentation basin during the initial 6 hours, in the case of the fixed outlet, is significantly higher than that for the floating outlet. This mass loss could be attributed to the higher initial flow rate outfall from the sedimentation basin for the fixed outlet.

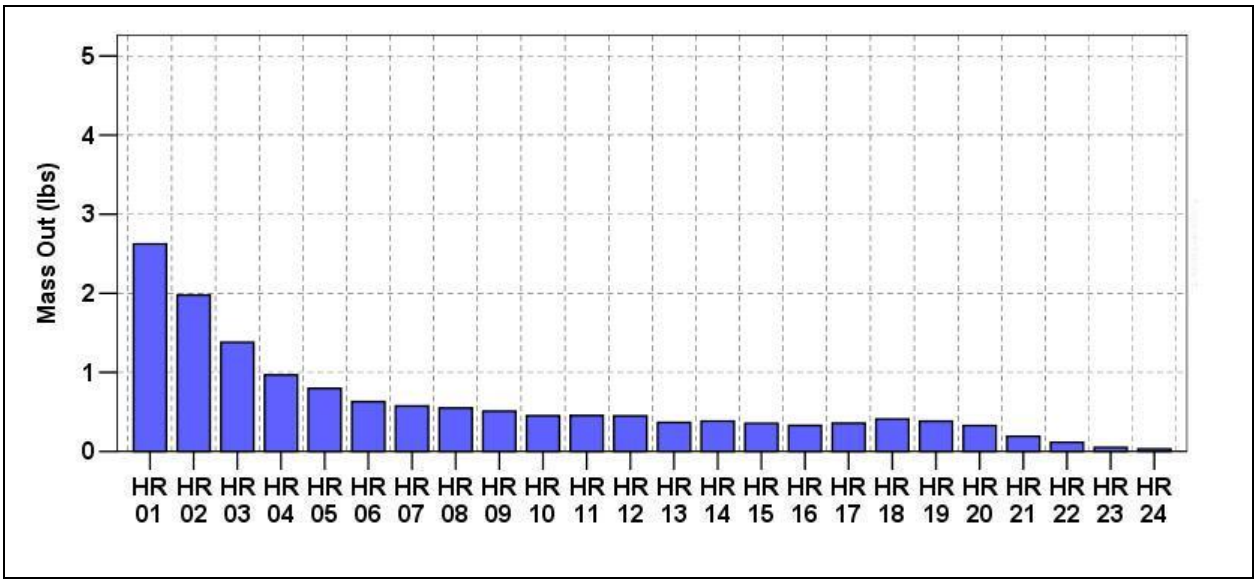

Figure 5.15. Mass Out for Floating Outlet with 50 lb Loading.

Statistical contrast between the fixed and floating outlet for the 50 lb loading revealed that the total mass leaving the sedimentation basin was significantly higher ($p=0.005$) in the case of fixed outlet.

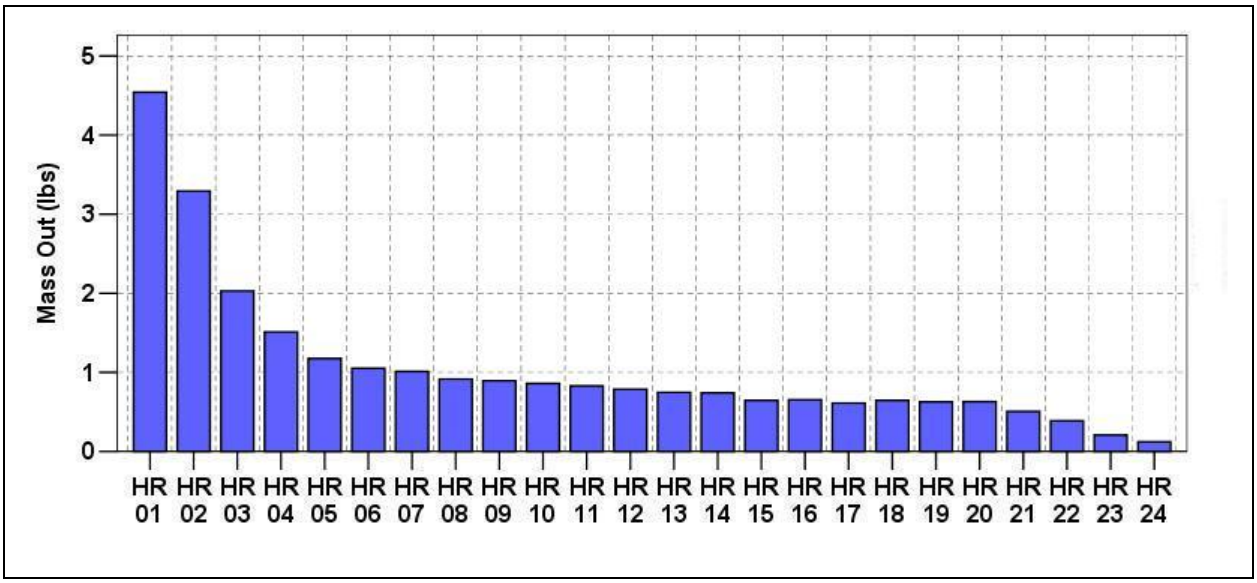

Figure 5.16. Mass Out for Floating Outlet with 100 lb Loading.

Figure 5.17 shows the cumulative mass loss per hour for FX050, FL025, FL050, and FL100. The figure shows that the mass loss fraction in the first 6 hours of the test duration is 0.75 and 0.5 for the fixed and floating outlet, respectively. The cumulative mass out increases logarithmically with time. The curves for the floating outlet are clustered close together, indicating that the trend of mass loss over time is dependent on the outlet type and is independent of the mass loading.

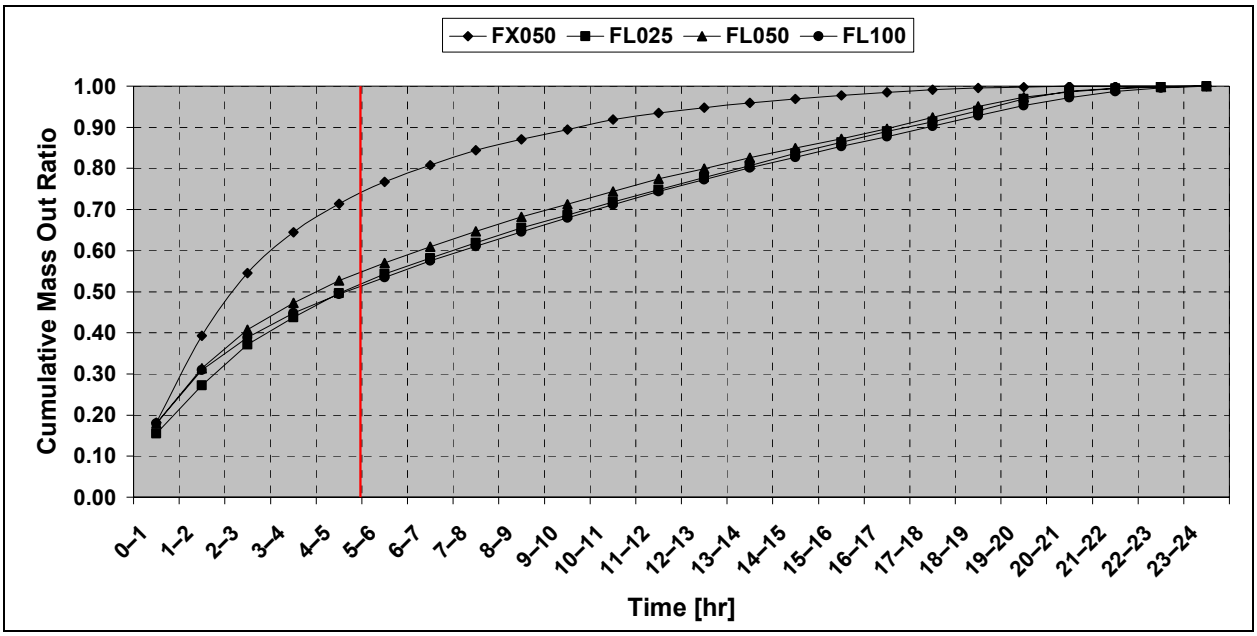

Figure 5.17. Cumulative Mass Out for All Outlets and Loadings.

Event Mean Concentration

Researchers calculated the event mean concentration, and the Analysis of Variance (ANOVA) coupled with linear contrast was conducted on the data. The linear contrast comparing the mean of the EMCs revealed that EMC for the fixed outlet was significantly higher ($p=0.010$) than that of the floating outlet with 50 lb loading. When the floating outlet with 25 lb, 50 lb, and 100 lb loading were compared for the EMC, the results indicated that there was significant difference, with the 100 lb having the highest EMC and 25 lb having the lowest EMC. All of the average event mean concentrations are presented in Figure 5.18. Detailed calculations of the average event mean concentrations are presented in Table 5.8.

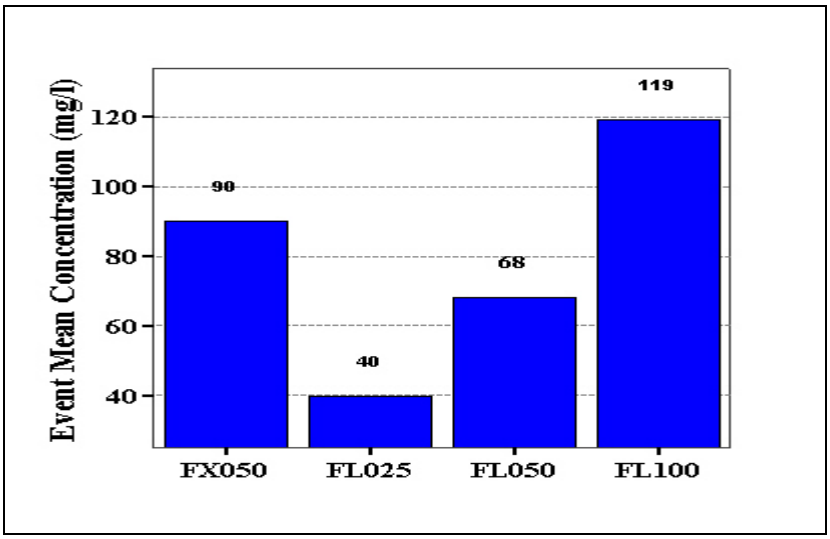

Figure 5.18. Average Event Mean Concentration in mg/l.

Table 5.8. Event Mean Concentrations in mg/l.

RUN	OUTLET TYPE	$\sum C_i \times Q_i$	$\sum Q_i$	EMC	MEAN EMC
FX050–1	Fixed	18.84	1.096	85.22	90.53
FX050–2	Fixed	22.95	0.996	103.67	
FX050–3	Fixed	19.49	0.990	87.70	
FX050–4	Fixed	19.09	0.997	85.53	
FL025–1	Floating	9.27	0.949	43.46	40.43
FL025–2	Floating	8.55	0.973	39.09	
FL025–3	Floating	7.60	0.918	38.75	
FL050–1	Floating	15.37	0.974	70.14	68.06
FL050–2	Floating	13.93	0.938	65.96	
FL050–3	Floating	13.69	0.965	62.83	
FL050–4	Floating	14.44	0.961	66.75	
FL050–5	Floating	13.80	0.963	63.68	
FL050–6	Floating	16.66	0.938	79.01	
FL100–1	Floating	23.05	0.956	107.03	119.12
FL100–2	Floating	26.05	0.939	123.18	
FL100–3	Floating	27.08	0.946	127.15	

TSS Removal Ratio

The TSS removal ratio results are presented in Table 5.9 and Figure 5.19. Results show that the floating outlet performed significantly better than the fixed outlet (p=0.005). Results also indicate that the mass loading had a significant impact on the removal ratios. The results could be misconstrued to indicate that the FL100 performed better as compared to the FL025 run. This result needs to be interpreted with caution because the final equilibrium concentration in the case of the FL025 run was ~20 mg/l compared to ~ 60 mg/l in the case of FL100. It would be easier to clean water that is dirty but difficult to clean water that is relatively cleaner. A more accurate interpretation of the performance of the sedimentation tank would be the event mean concentration discussed in the previous section.

Table 5.9. TSS Removal Ratios.

RUN	OUTLET TYPE	$MASS_{IN}$	$MASS_{OUT}$	REMOVAL RATIO	MEAN REMOVAL RATIO
FX050–1	Fixed	50	18.84	0.6232	0.5981
FX050–2	Fixed	50	22.95	0.5409	
FX050–3	Fixed	50	19.49	0.6101	
FX050–4	Fixed	50	19.09	0.6181	
FL025–1	Floating	25	9.27	0.6290	0.6610
FL025–2	Floating	25	8.55	0.6578	
FL025–3	Floating	25	7.60	0.6961	
FL050–1	Floating	50	15.37	0.6926	0.7070
FL050–2	Floating	50	13.93	0.7214	
FL050–3	Floating	50	13.69	0.7263	
FL050–4	Floating	50	14.44	0.7111	
FL050–5	Floating	50	13.80	0.7239	
FL050–6	Floating	50	16.66	0.6667	
FL100–1	Floating	100	23.05	0.7695	0.7461
FL100–2	Floating	100	26.05	0.7395	
FL100–3	Floating	100	27.08	0.7292	

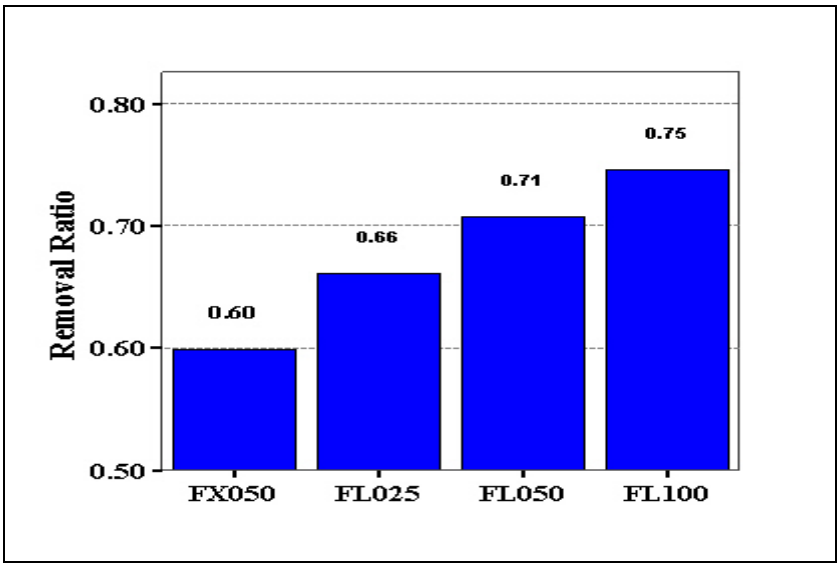

Figure 5.19. Removal Ratio.

DISCUSSION AND CONCLUSIONS

Conclusions from Model Results

Several simulations were conducted to see how overflow rate change affects particle removal efficiency. Figure 5.20 shows the relationship between removal efficiency and theoretical overflow rates for three different storm volumes (0.82, 0.41, and 0.20 of the basin volume). As shown in the graph, storms with larger runoff volumes have lower suspended solid removal efficiency, although 80 percent removal was calculated even for the worst case. This graph suggests that intense storms would result in a lower removal ratio than less intense storms. The removal efficiency does not drop significantly when the theoretical overflow rate is very strong. It is because no matter how large the storm is, the detention basin will have almost the same drainage time for the emptying period.

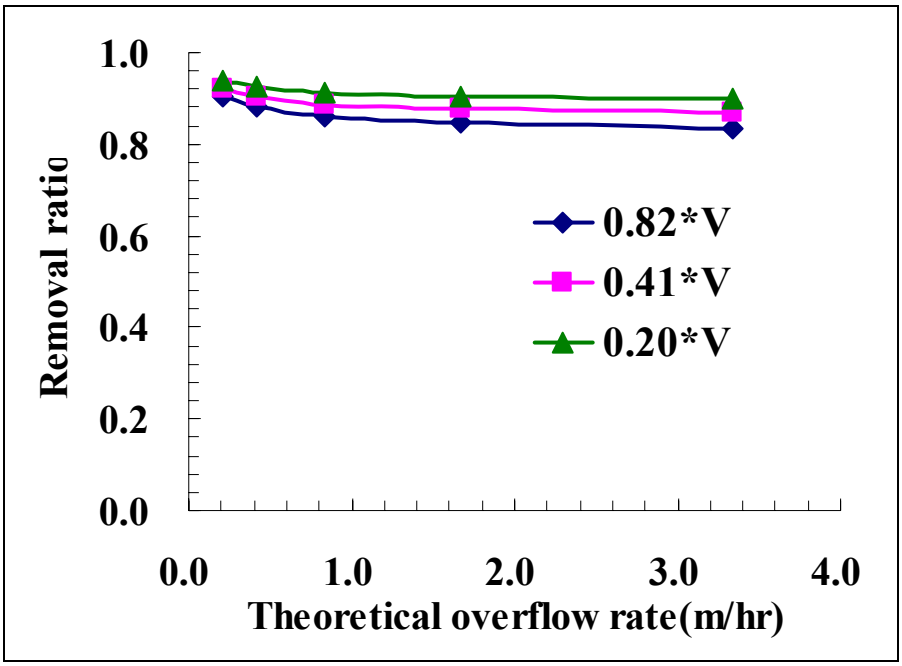

Figure 5.20. Removal Ratio Change with Different Theoretical Overflow Rates and Different Runoff Volumes.

In the conceptual model, which employs the plug flow concept, the calculated removal efficiency did not change when only length/width ratio (L/B) changed. This is because a narrower basin results in a faster advection velocity. However, this may not be true in an extreme case, such as for an L/B ratio less than 1. For this case, plug flow cannot exist, and the short cutting and large dead space may result in lower removal efficiency.

The process to determine the drainage time is equivalent to the process used to determine the outflow orifice size. The theoretical drainage time, t_d (hr), is defined as the time to drain all the water from full [h=H(m)] to empty.

$$\sqrt{h} = \frac{A_e}{B \cdot L}\sqrt{\frac{g}{2}} \cdot t_d$$

$$A_e = \frac{B \cdot L}{t_d}\sqrt{\frac{2h}{g}}$$

$$A_e\left(cm^2\right) = \frac{B(m) \cdot L(m) \cdot 10^4 (cm^2/m^2)}{3600(s/hr) \cdot t_d(hr)}\sqrt{\frac{2h(m)}{g(m/s^2)}} \qquad (5.1)$$

$$A_e\left(cm^2\right) = \frac{0.62 * 6.96 * 10^4}{3600} * \sqrt{\frac{2 * 0.34}{9.81}} \cdot \frac{1}{t_d(hr)} = \frac{3.16}{t_d(hr)}$$

Then, removal efficiency of suspended solid was calculated for four different orifice sizes [0.41, 0.82, 1.23, and 1.64 (cm^2)], which correspond to theoretical drainage times of 7.7, 3.9, 2.6, and 1.9 hours (according to equation 5.1) for three different flow rates [Q_{in}=0.5, 1.0, and 2.0 (L/s)]. However, the runoff volume is the same for all cases. The calculation results are shown in Figure 5.21. Removal efficiency decreased significantly with increasing orifice size when compared to the increasing flow rate. Table 5.10 shows the maximum water level and removal efficiency.

Table 5.10. Particle Removal Ratio and Corresponding Maximum Water Level for Different Flow Rate and Different Orifice Sizes.

	Effective area of orifice (cm^2)	0.41	0.82	1.23	1.64
Q_{in}=0.5 (L/s)	Particle removal efficiency	0.88	0.82	0.78	0.76
	Maximum water level (m)	0.25	0.21	0.19	0.16
Q_{in}=1.0 (L/s)	Particle removal efficiency	0.86	0.79	0.75	0.71
	Maximum water level (m)	0.26	0.25	0.23	0.21
Q_{in}=2.0 (L/s)	Particle removal efficiency	0.85	0.77	0.72	0.68
	Maximum water level (m)	0.27	0.26	0.25	0.25

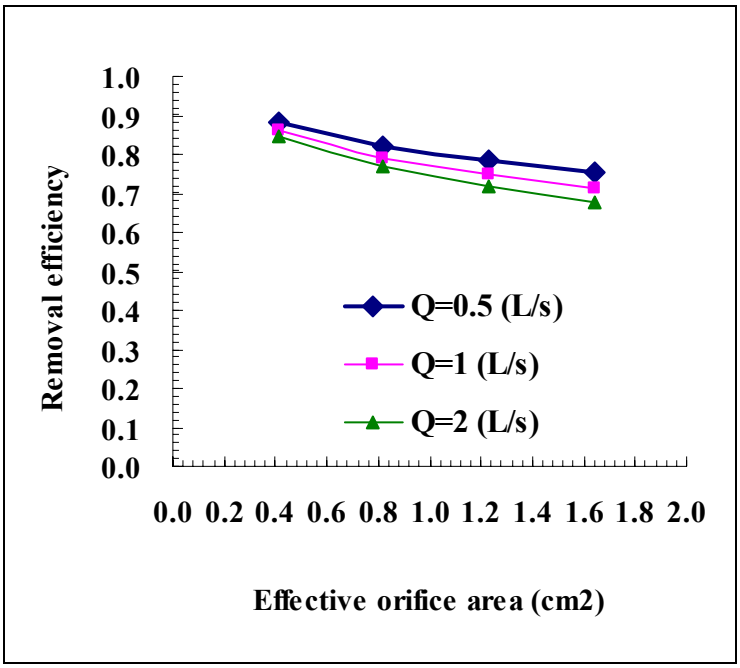

Figure 5.21. Removal Ratio Change with Different Effective Orifice Sizes.

According to the table, a smaller orifice works much better than a larger orifice since the maximum water level is almost the same for a short but strong storm. However, for a weak but long storm, the difference in removal efficiency for different orifice sizes is not as big as the difference for a short but strong storm. For a flow rate of 0.5 L/s, the maximum water level was 16 cm, or 47 percent of the overflow weir height, for an orifice area of 1.64 cm^2. However, for the same storm event (0.5 L/s), the maximum water level was 25 cm, or 74 percent of the overflow weir height, for the orifice area of 0.41 cm^2. Therefore, a smaller orifice opening is preferred if the design is intended for an intense short duration storm. However, a larger orifice opening can be effective when the design is made for less intense storms since the volume increases that can be captured by the basin before overflow will occur.

The particle removal efficiency was calculated for particles with different densities, and simulations with different flow rates were compared while keeping the runoff volume the same. Of primary interest are particles with densities less than 2.65 g/cm^3. Figure 5.22 shows the removal efficiency of suspended solids for particles with densities ranging from 1.2 to

2.65 g/cm^3, using the assumption that density is uniform for all the particle sizes. Removal efficiency is lower if density is lower, and the decrease is more significant for lighter particles. The density of smaller particles in stormwater runoff can range from 1.1 g/cm^3 (Cristina et al., 2002) for typical highway organic soil to around 3.0 g/cm^3 for larger particles (Zanders, 2005). Karamalegos (2006) measured the density of particles smaller than 75 μ m for 13 storm runoff samples in Austin, Texas. The measured density ranges from 0.81 to 2.80 mg/L, and the mean value was approximately 1.5 g/cm^3. When combined with the influence of density on removal efficiency, these results suggest that characteristics of particle density should be considered in analysis and the design of stormwater treatment systems.

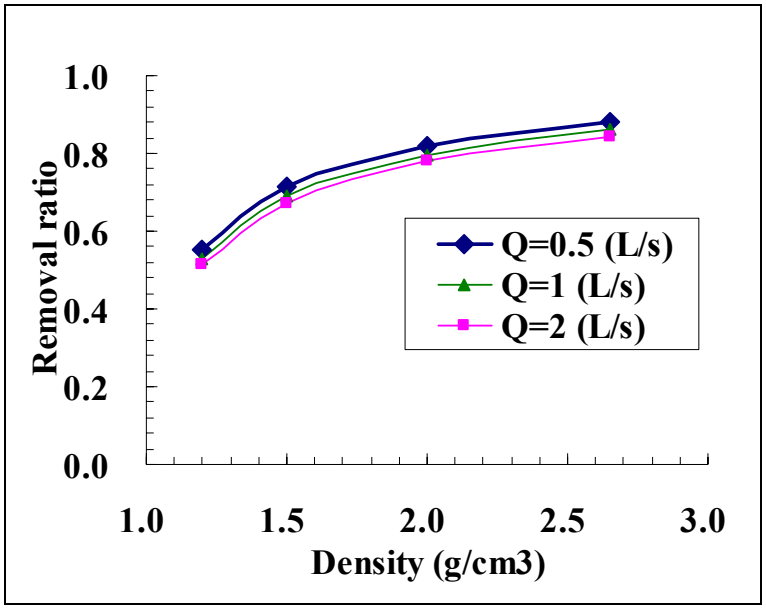

Figure 5.22. Removal Ratio Change with Different Particle Densities.

Conclusions from Prototype Results

From the results of prototype testing, we can see that the first 6 hours are critical in terms of sediment trapping and removal efficiency. The first 6 hours, much turbulence and re-suspension is observed in the tank that can negatively impact the performance characteristics. After this initial 6 hours, quiescent conditions develop in the tank, and little re-suspension is observed. These quiescent conditions facilitate the unabated settling of the sediments. We can conclude that the floating outlet displays potential in terms of performance due to its control of

the outflow rate during the first 6 hours. Another factor that could have contributed to the performance of the floating outlet was the fact that the floating outlet was actually skimming water from the surface of the tank, where the concentration of the sediment is found to be the lowest.

The inlet mass loading had reasonable impact on the sedimentation tank performance. However, these results can be easily misinterpreted and should be considered carefully. If the removal ratio is considered, then the results seem to indicate that it is better to have high inlet loading, which is counterintuitive. The study needs to concentrate on event mean concentrations and final achievable concentration at the outlet as an indicator of the performance of the sedimentation tank.

Another important factor was the resuspension effect that resulted in reducing the sediment removal performance of the sedimentation tank. To get a rough estimate of the amount of resuspension, a simple calculation was carried out on the existing data. The mean of the outlet concentrations for the floating outlet with 400 mg/l, 200 mg/l, and 100 mg/l inflow TSS concentration, as well as the fixed outlet with 200 mg/l TSS loading, were plotted separately. The concentrations were adjusted to get a smooth concentration drop profile at the outlet. It is safe to assume that the outlet concentration at the beginning would be equal to the inlet concentration in the absence of resuspension. Next, tangential curves were plotted to these curves starting with 400 mg/l, 200 mg/l, or 100 mg/l depending upon the loading. The graphical results of the procedure are presented in Figures 5.23, 5.24, 5.25, and 5.26. The shaded area between the curves shown in the figures can be considered as the potential TSS reduction in outflow once resuspension is mitigated. The reduction is much more significant on the fixed outlet, as shown in Figure 5.23. The contribution of resuspension to the outlet was calculated and summarized in Table 5.11. As observed from the results, it would be beneficial to reduce the resuspension by curbing the initial shear due to sheet flow as well as turbulence.

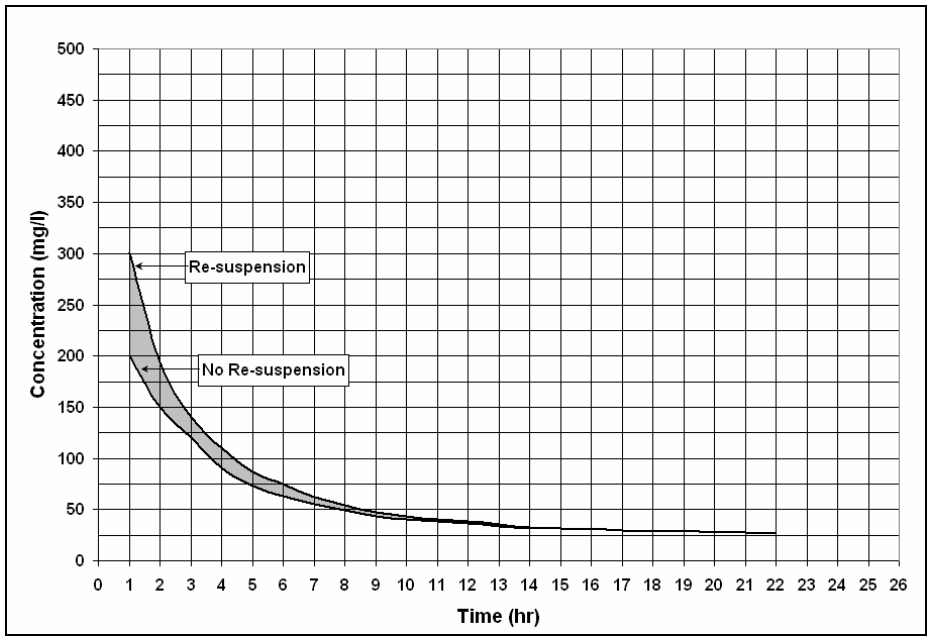

Figure 5.23. Effect of Resuspension in Fixed Outlet with 50 lb Loading.

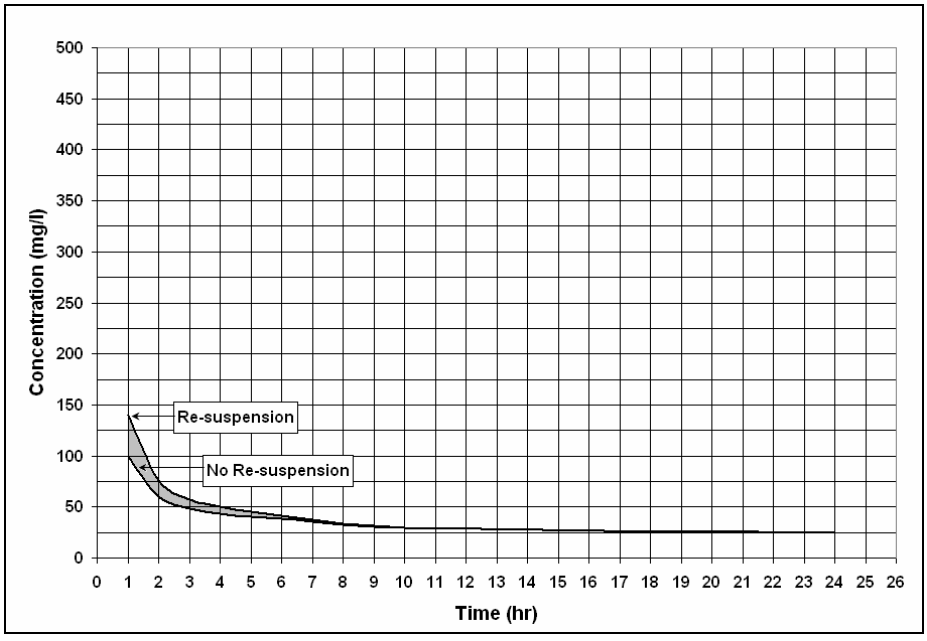

Figure 5.24. Effect of Resuspension in Floating Outlet with 25 lb Loading.

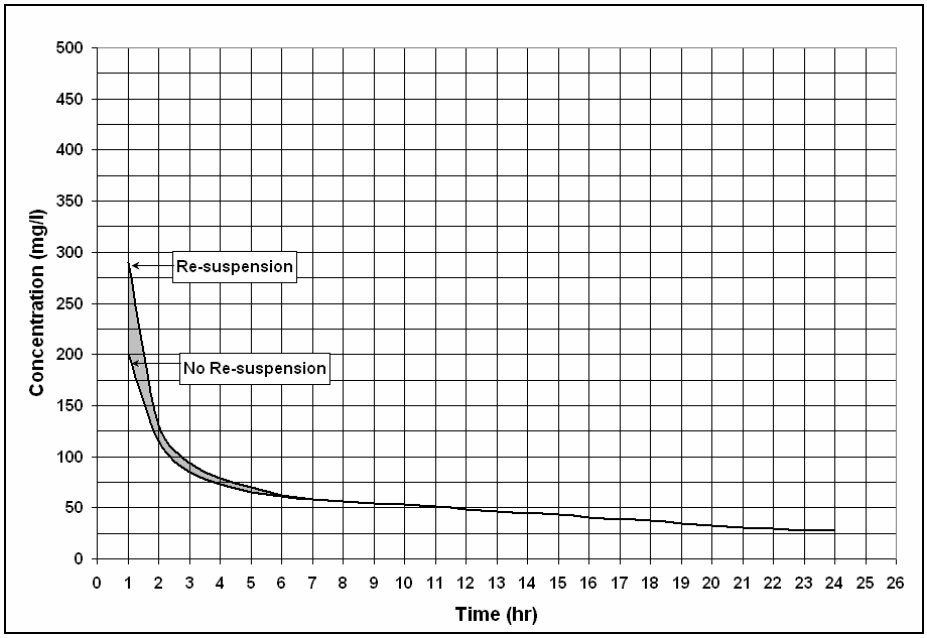

Figure 5.25. Effect of Resuspension in Floating Outlet with 50 lb Loading.

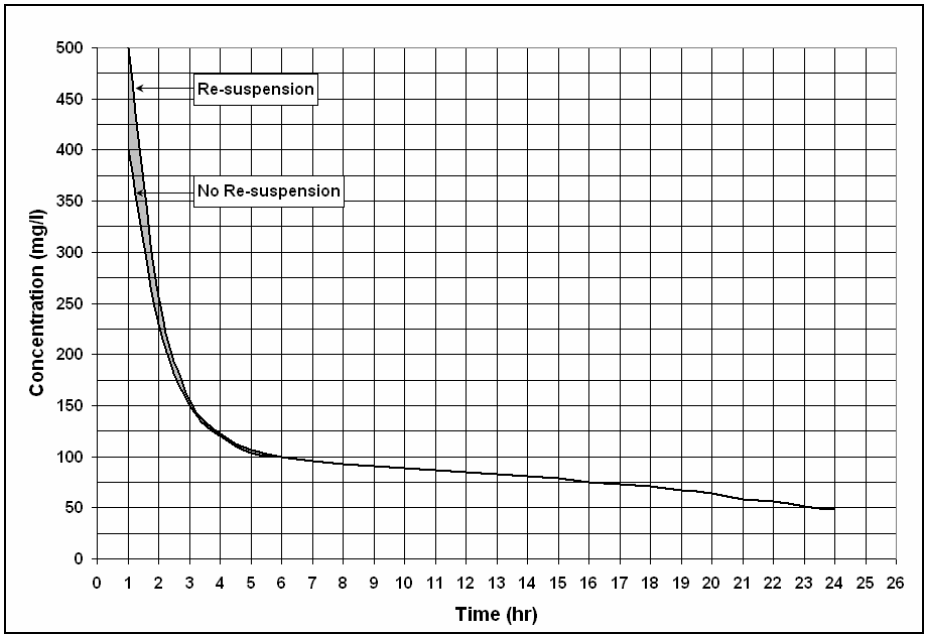

Figure 5.26. Effect of Resuspension in Floating Outlet with 100 lb Loading.

Table 5.11. Effect of Resuspension on the Performance of the Small Footprint BMP.

Outlet Type/ Loading	Outlet Mass Loading (lb)		Contribution of Resuspension (%)	Removal Performance (%)	
	With Resuspension	Without Resuspension		With Resuspension	Without Resuspension
Fixed/ 50 lb ≈ 200 mg/l	18.83	15.57	17.31	62	69
Floating/ 25 lb ≈ 100 mg/l	8.47	7.80	9.80	66	69
Floating/ 50 lb ≈ 200 mg/l	14.65	13.13	8.67	71	74
Floating/ 100 lb ≈ 400 mg/l	25.39	23.77	5.36	75	76

Filling the Gap between Model and Prototype Testing

The focus and approach for the project were quite different between model scale and prototype scale, especially in experiments. In model scale, inflow conditions were determined to have a variety of runoff conditions such as inflow intensity and duration, but tried to have inflow SSC approximately 200 mg/L for all runs. In prototype scale, however, several inflow SSCs were tested, but inflow conditions such as inflow rate and duration were kept constant for all runs. It is quite reasonable for the prototype to keep inflow hydraulic conditions the same and simple because it is much harder to conduct a run in prototype than doing the corresponding run in model scale. Actually, to do a run in prototype takes five times longer and requires 125 times more water and sediments than a run in the model scale. Based on an understanding of this difference, the significance and the limitation for the model scale study are discussed here.

The Importance of Overflow Rate

The significance of the model scale study is the experimental result with various inflow conditions since they are difficult to conduct in prototype. Researchers conducted six runs to see how removal efficiencies are different in the same runoff rate and duration but different inflow SSCs. Those six runs have approximately 0.46 (L/s) of inflow rate and 28 minutes of runoff durations. Table 5.12 shows the mean inflow SSC, maximum water level, normalized outflow SSC at filling period using the mean inflow SSC, and removal efficiency.

Table 5.12. Particle Removal Efficiency of the Six Hydraulically Identical Runoffs.

Run	Mean Inflow SSC, C_{in} (mg/L)	Maximum Water Level (ft)	Outflow SSC at filling normalized by inflow SSC, C_{out} for filling / C_{in}	Removal Efficiency
A	381	0.219	0.136	0.90
B	266	0.218	0.135	0.91
C	190	0.216	0.165	0.89
D	150	0.221	0.176	0.88
E	93	0.218	0.190	0.88
F	57	0.219	0.193	0.86

The table shows that the removal efficiency is better for runs that have a higher inflow SSC. This might be the effect of coagulation inside the tank (i.e, collision and condensation process between particles happen more frequently for higher SSCs).

Previous experimental results show that normalized outflow SSC for the filling period is linear to the overflow rate. In Figure 5.27, the six new results show that outflow SSC for the filling vary with inflow SSC, and the value range contains the regression line. However, the value range for these six runs is not as wide as the value range for the original eight runs with various overflow rates. This implies that overflow rate is a very important factor to influence the removal efficiency of the detention basin.

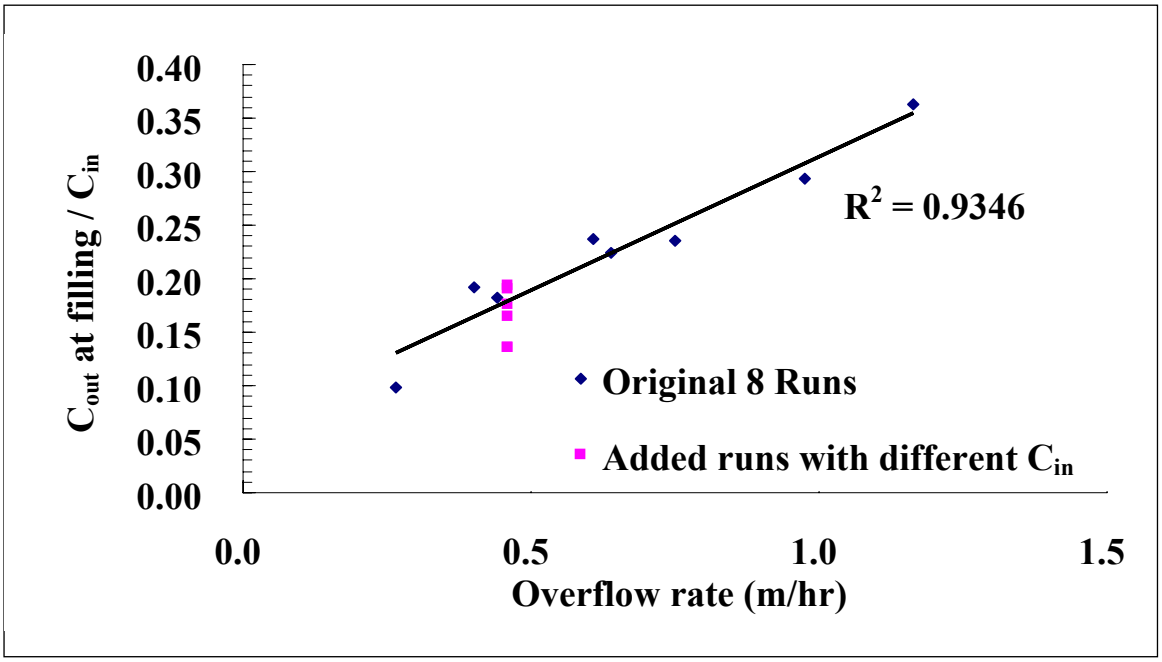

Figure 5.27. Outflow SSC for the Filling Period.

Measured particle removal efficiencies were between 82 to 93 percent (see Tables 5.7 and 5.12). The minimum value of 82 percent, regardless of its highest overflow rate condition, is very high compared to the removal efficiency of approximately 60 to 70 percent in the prototype. The difference may occur because resuspension effects were not properly scaled in the physical model basin. In addition, lake water that contained of algae was used in prototype testing. The algae in lake water may be responsible for the minimum TSS discharge in outflows. Therefore,

prototype scale testing with different overflow rates or development of a mathematical model with the capability of modeling resuspension effects should be considered to discuss the effect of overflow rate in prototype scale.

Resuspension Effect

Considering a single storm runoff event, one might notice that particles in the outflow have two major sources. The first source is the current inflow runoff, and the other source is the resuspension of accumulated particles in the basin due to previous runoffs. The developed conceptual model can calculate the removal efficiency of particles from current runoff, and it fits well with the model scale experimental results since the resuspension of accumulated particles is not significant. However, experimental results in the model scale, which are 82 percent in the worst case, were very different from the results in prototype scale, which are approximately 60 percent even though scaling was done properly with Hazen number scaling (i.e., overflow rate in model and prototype are identical).

One of the speculations for the reason of this difference in removal efficiency is that the resuspension effect is much higher for the prototype than the model. Actually, mean longitudinal velocity and particle size are identical between the model and the prototype. Therefore, the scouring effects should be similar even though local flow velocity might be a little different between this model and prototype. However, what is different is the depth of accumulated particles. In a single run, the volume of inflow water and the mass of inflow particle is 125 times larger for the prototype than that for the model since the length ratio is five. Assume all the particles will settle down here. Then the accumulated particle depth in the prototype after water is drained is five times deeper than that of the model because the water column with particles in the prototype is five times higher than that in the model. After multiple runs, the accumulated sediment depth for the prototype would become much higher than the depth for the model. This difference in accumulated sediment depth in the basin might lead to significant difference in resuspension effect between the model and the prototype. Several resuspension tests were conducted to study how resuspension makes the difference when a large amount of sediments are prepared right behind the inlet pipe.

Resuspension Tests with Different Inlet Setups

Three tests were conducted with identical flow conditions. The first run was done without energy dissipater; the second was done with the current energy dissipater, and the third was done with turbulent damper, or flow straightener, which creates uniform flow. Tap water was used as inflow, and no particles were added to see only the resuspension effects. Prior to each run, 2 kg of SIL-CO-SIL®49 particles were uniformly distributed onto a 4 ft long, 2 ft wide wooden board that was installed right behind the inlet. Flow rate was approximately 0.46 (L/s), and runoff duration was 28 minutes for all three cases. Figure 5.28 shows pictures of the particles accumulated on the board taken after each run. These pictures show that the area of scouring for the "no energy dissipator" case was much larger than those for the other two cases. Almost no scouring was observed for the "with flow straightener" case, and some scouring was observed for the "with an energy dissipator" case in front and side of the energy dissipator.

Figure 5.28. Accumulated Particles after Running a Run for the "No Energy Dissipator" Case (Left-Top), "with an Energy Dissipator" Case (Left-Bottom), and "with Flow Straightener" Case (Right-Top).

Outflow SSC was also measured. The particles in outflow come from only accumulated particles in the basin since inflow SSC was zero using clear tap water. Figure 5.29 shows the outflow SSC for these three different setups. The outflow SSC for the "no energy dissipator" case is much higher than the other two cases for all the times, and the SSC never dropped to 20 mg/L until 150 minutes. However, there is no significant SSC difference between "with an energy dissipater" and "with flow straighteners" cases except the peak concentration at 4 minutes for "with an energy dissipater" is approximately 100 mg/L higher than that for "with flow straighteners." However, that difference does not matter much for removal efficiency since the outflow rate is very low at four minutes. Therefore, the simple single energy dissipater works fine with these low flow rates. The observed resuspension in these two cases is not due to the strong momentum from the inflow jet, but the dislodging of sediment while water is running through the basin for the earlier part of the filling period.

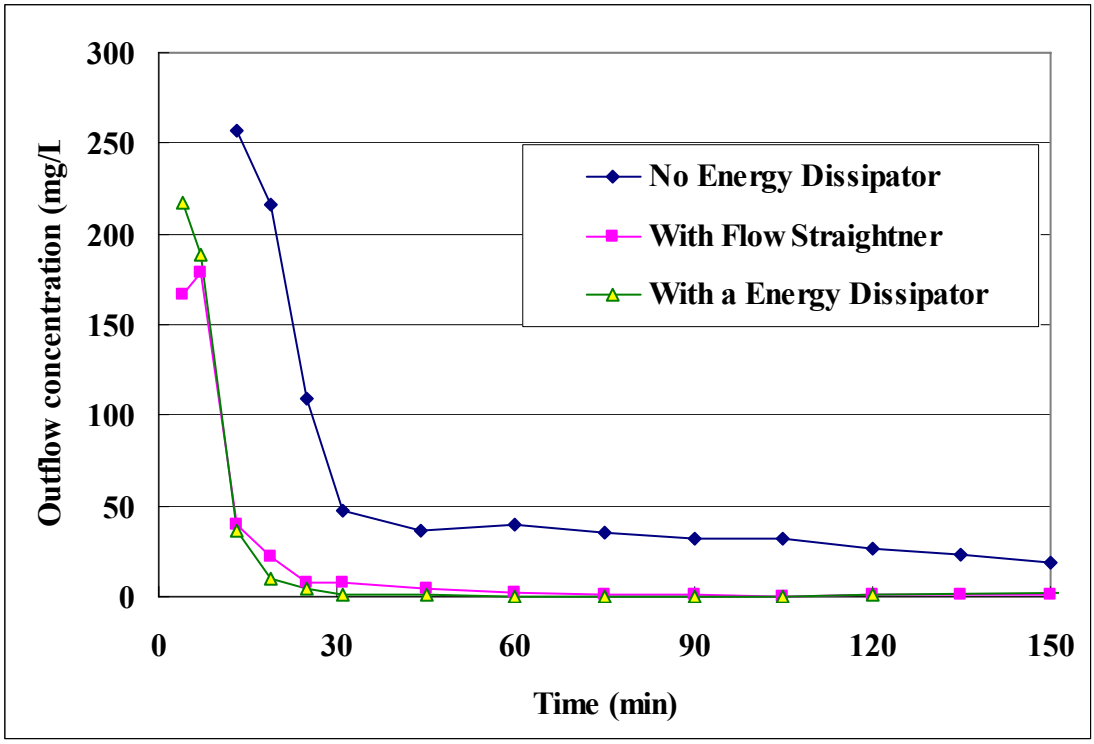

Figure 5.29. Outflow SSC for Three Different Inlet Setups.

Resuspension Tests with and without Accumulated Sediment

Resuspension tests were also conducted with clear inflow water in a high flow rate. Two tests with very similar runoffs were conducted with approximately 1.1 L/s flow rates and 12 minutes duration. These tests were conducted to separate the outflow SSC caused by the scouring of accumulated sediment right behind the inlet from the outflow SSC due to the trapping of accumulated sediment from the rest of the basin. Two setups were prepared to make it happen. To do the run without accumulated sediment, the 2 ft x 4 ft board with the energy dissipator was cleaned prior to the run. For the run with accumulated sediment, 1 kg of SIL-CO-SIL®49 particle was uniformly distributed in the front half of the board (i.e., 2 ft x 2 ft area for sediment). Figure 5.30 shows the scouring pattern of the accumulated sediment around the inlet. The area of scouring was much bigger than the pattern with the energy dissipator in Figure 5.30.

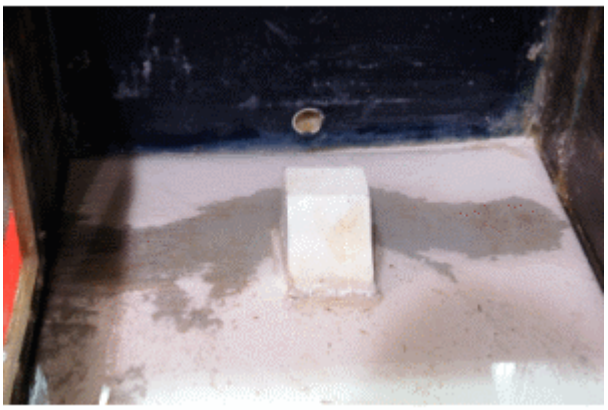

Figure 5.30. Scouring Pattern around the Energy Dissipator Due to High Flow Rates.

Figure 5.31 shows the outflow SSC for these two cases. Outflow SSCs are almost the same after 20 minutes, despite being very different during the runoff duration. The outflow SSC difference between the line with diamond-shape dots and the line with square-shape dots can be controlled using an alternate energy dissipator or diffuser at the end of the inlet. However, the result without sediment accumulation around inlet also shows very high SSC until runoff ends. This buildup means that the resuspension of sediments occurs not only around the inlet but also around the whole basin during an intense storm, which might be difficult to control.

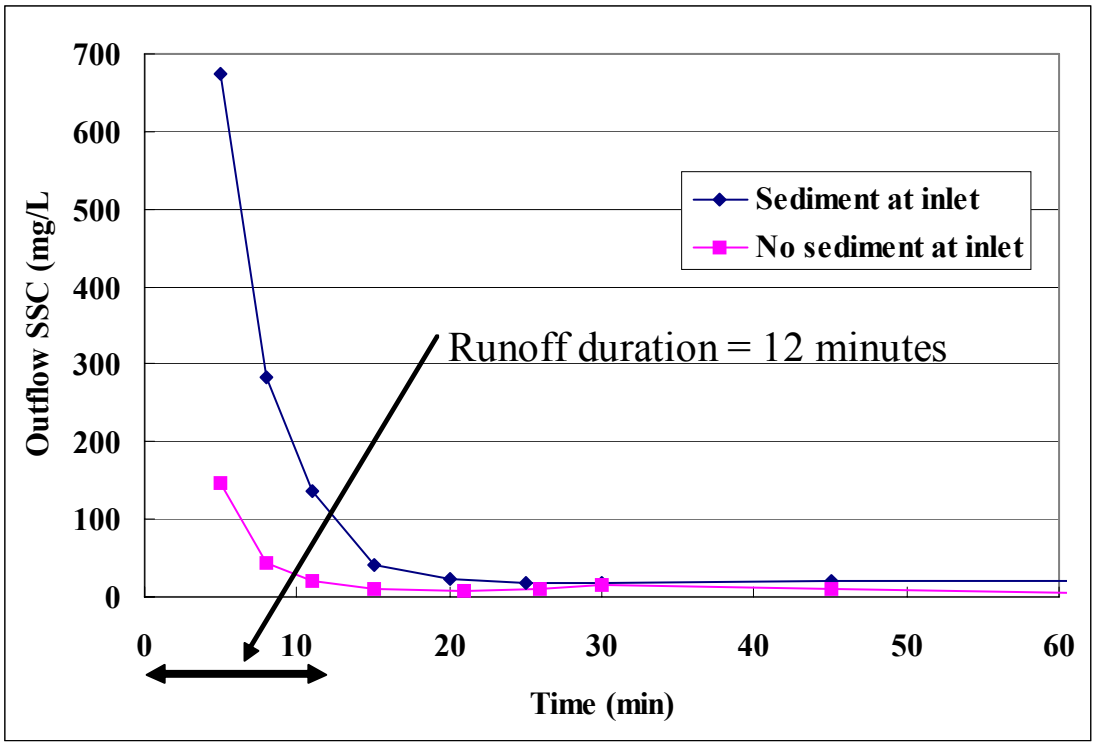

Figure 5.31. Outflow SSC with and without Accumulated Sediment Right behind the Inlet.

CHAPTER 6:
RECOMMENDATIONS

RECOMMENDATIONS FROM MODEL RESULTS

1. A conceptual model was built to estimate and understand how sedimentation occurs in the detention basin. The simulation results using the conceptual model show a good accordance with the time-series outflow SSC and sediment removal efficiency. However, the conceptual model does not deal with the resuspension effect, which was especially significant in the prototype. Therefore, resuspension effects should be modeled in the prototype.

2. A significant finding from the model scale study is that the sediment removal performance is strongly dependent on the overflow rate, which is the velocity of water height increase during the filling period. The outflow SSC at the end of the filling period has a strong linearity with the overflow rate. This makes developing an empirical model much easier since peak concentration is one of the most important variables to be estimated.

3. Findings from the analyses using the conceptual model are the following: 1) Particle removal efficiency will decrease as overflow rate increases. However, the decrease will be limited because the same amount of detention time can be taken no matter how strong storm runoff flows in. 2) Particle removal efficiency will decrease linearly as the effective orifice area increases. 3) Particle settling velocity will significantly decrease, especially if particle density is smaller than 2.0 mg/L. This incident will worsen particle removal efficiency.

RECOMMENDATIONS FROM PROTOTYPE RESULTS

Resuspension is dependent on several factors, such as the amount of sediment previously deposited in the prototype, amount of water present in the tank prior to the commencement of the test, type of outlet, etc. To address the problem of resuspension, it is necessary to identify how much sediment was resuspended. Ways to abate the resuspension and improve the performance of the sedimentation tank should be tried and tested.

CHAPTER 7:
WORK PLAN 2006-2007

Based on these findings, the Project Advisory Committee agreed that it would be valuable to continue the project because potentially high performance could be achieved through some design adjustment on the prototype. Some key findings are summarized below:

1. Overall, the simple detention structure is a cost effective stormwater treatment option.

2. The sediment removal performance of particles in the range of 49 μ is between 62 and 75 percent, depending on the inflow TSS concentration and the outlet type, fixed or floating. This performance is considered very reasonable when comparing it to national data for other devices.

3. The floating outlet appears to offer better and more consistent performance than the fixed outlet.

4. The performance of the prototype in the first 5-6 hours is significantly impacted by TSS resuspension. Approximately 17 percent of the total solids discharged from the prototype can be attributed to this initial resuspension spike if a fixed outlet is used.

Since the prototype (approximately 80 ft long, 10 ft wide and 5 ft deep) is located on TTI's Riverside Campus, it would seem that we could maximize the benefit of the current investment by running further tests with control techniques to reduce the resuspension spike. If this could be accomplished, the overall performance would be significantly improved.

PROPOSED SCOPE OF WORK

In the fiscal year of 2007, the researchers propose the following tasks for consideration:

- Investigation of techniques to control the resuspension of sediment during the filling time. Possible techniques may include (1) a pilot channel to divert flow, (2) relocation of an outlet opening to be away from sediment-concentrated areas during the filling time, (3) baffles near the mid-point of the tank, or (4) an automated valve that closes the outlet during the filling time and begins to discharge after the desired detention time is reached.

- Prototype runs where the device still contains water from a previous event to study how that affects sediment removal performance. Depending on the successful techniques that control the resuspension, the conditions may include (1) shallow sheer of water in which the sediment is saturated, and (2) depth that the inlet pipe is completely submerged.

- Fine tuning on the floating outlet for stability and maintenance issues.

- Criteria to control the maintenance schedule per the acceptable technique suggested.

ESTIMATED BUDGET

Because the prototype and most of the apparatus for testing are already in place, the expense would be substantially less than what was budgeted for FY04-06. This proposed scope of work will need a full-time engineering Ph.D. student and some professional staff time. Since the Ph.D. student, Aditya Raut Desai, has been involved with the project for three years and will still be available in FY07, proposed work can proceed immediately without further training needed. Some supply fee will be needed for modifying the prototype design. The total budget is estimated to be no more than $40,000 for the proposed work in FY07.

REFERENCES

1. Andral, M.C., Roger, S., Montrejaud-Vignoles, M., and Herremans, L. (1999). "Particle size distribution and hydrodynamic characteristics of solid matter carried by runoff from motorways." *Water Environment Research*, 71 (4), 398-407.
2. Buchan, G.D. (1989). Applicability of the simple lognormal model to particle-size distribution in soils. *Soil Science*. 147:155–161.
3. Campbell, G.S. (1985). Soil physics with BASIC: Transport models for soil-plant systems. Elsevier, Amsterdam.
4. Cristina, C., Tramonte, J., Sansalone, J. (2002) "A granulometry-based selection methodology for separation of traffic-generated particles in urban highway snowmelt runoff." *J. Water, Air, and Soil Pollution*, 136: 33-53, 2002.
5. Currie, I.G. 1974. "Fundamental Mechanics of Fluids." McGraw-Hill, Inc, New York, 38-39.
6. Hwang, N. H.C., and Houghtalen, J.R. (1996). "Fundamentals of hydraulic engineering system." Prentice-Hall Inc., 308.
7. Karamalegos, A.M., Barrett, M.E., Lawler, D.F., Malina, J.F., Jr. (2005). "Particle size distribution of highway runoff and modification through stormwater treatment." Online Report 05-10, Center for Research in Water Resources, University of Texas at Austin, Austin, Texas.
8. Minton, G. (2002). "Stormwater treatment." Amica International Inc.
9. Takamatsu, M., Barrett, M.E., Charbeneau, R.J. (2006). "Physical and conceptual modeling of sedimentation characteristics in stormwater detention basin." Online Report 06-05. Center for Research in Water Resources, University of Texas at Austin, Austin, Texas.
10. Young, G.K., Stein, S., Cole, P., Kammer, T., Graziano, F., and Bank, F. (1996). "*Evaluation and Management of Highway Runoff Water Quality.*" Publication No. FHWA-PD-96-032, U.S. Department of Transportation, Federal Highway Administration, Office of Environment and Planning.
11. Zanders, J.M. (2005). "Road sediment: Characterization and implications for the performance or vegetated strips for treating road run-off." *J. Science of Total Environment* 339, 41-47.
12. Li, Y.X., Lau, S.L., Kayhanian, M., and Stenstrom, M.K. (2006). "Dynamic characteristics of particle size distribution in highway runoff: Implications for settling tank design." *Journal of Environmental Engineering-ASCE*, 132(8), 852-861.

APPENDIX A:
TABULATED DATA

Table A.1. Data from Prototype Run FX050-1.

Time Interval [hr]	Level Drop [ft]	Flow Rate Q_i [cfs]	TSS C_i [mg/L]	$Mass_{OUT}$ $C_i \times Q_i$ [lb]	Mass Fraction $\frac{C_i \times Q_i}{\sum C_i \times Q_i}$	Mass Fraction Cumulative
0–1	---[1]	0.050[2]	277	3.32	0.18	0.18
1–2	0.462	0.110	174	4.02	0.21	0.39
2–3	0.469	0.104	159	3.72	0.20	0.59
3–4	0.424	0.094	88	1.86	0.10	0.69
4–5	0.393	0.087	64	1.26	0.07	0.75
5–6	0.368	0.082	42	0.77	0.04	0.79
6–7	0.318	0.071	34	0.54	0.03	0.82
7–8	0.282	0.063	59	0.83	0.04	0.87
8–9	0.263	0.058	39	0.51	0.03	0.89
9–10	0.226	0.050	34	0.38	0.02	0.91
10–11	0.203	0.045	67	0.68	0.04	0.95
11–12	0.164	0.036	29	0.24	0.01	0.96
12–13	0.145	0.032	25	0.18	0.01	0.97
13–14	0.128	0.028	26	0.17	0.01	0.98
14–15	0.111	0.025	24	0.13	0.01	0.99
15–16	0.079	0.018	22	0.09	0.00	0.99
16–17	0.069	0.015	25	0.09	0.00	1.00
17–18	0.033	0.007	22	0.04	0.00	1.00
18–19	0.010	0.002	23	0.01	0.00	1.00
19–20	0.013	0.003	---[3]	0.00	0.00	1.00
20–21	0.010	0.002	---[3]	0.00	0.00	1.00
21–22	0.003	0.001	---[3]	0.00	0.00	1.00
22–23	0.013	0.003	---[3]	0.00	0.00	1.00
23–24	0.105	0.110	---[3]	0.00	0.00	1.00
	$\sum Q_i$ =	1.096	$\sum C_i \times Q_i$ =	18.84		

1 ***Could not be assessed due to tank filling***

2 ***Estimated average***

3 ***No sample collected due to low/no outflow***

Table A.2. Data from Prototype Run FX050-2.

Time Interval [hr]	Level Drop [ft]	Flow Rate Q_i [cfs]	TSS C_i [mg/L]	$Mass_{OUT}$ $C_i \times Q_i$ [lb]	Mass Fraction $\frac{C_i \times Q_i}{\sum C_i \times Q_i}$	Mass Fraction Cumulative
0–1	---[1]	0.050[2]	360	4.38	0.19	0.19
1–2	0.367	0.089	351	6.43	0.28	0.47
2–3	0.410	0.091	136	2.79	0.12	0.59
3–4	0.381	0.085	112	2.13	0.09	0.69
4–5	0.361	0.080	76	1.37	0.06	0.75
5–6	0.328	0.073	72	1.18	0.05	0.80
6–7	0.308	0.068	51	0.78	0.03	0.83
7–8	0.285	0.063	47	0.67	0.03	0.86
8–9	0.260	0.058	45	0.58	0.03	0.89
9–10	0.236	0.052	43	0.51	0.02	0.91
10–11	0.210	0.047	42	0.44	0.02	0.93
11–12	0.193	0.043	39	0.38	0.02	0.94
12–13	0.164	0.036	34	0.28	0.01	0.96
13–14	0.158	0.035	31	0.24	0.01	0.97
14–15	0.141	0.031	31	0.22	0.01	0.98
15–16	0.118	0.026	28	0.17	0.01	0.98
16–17	0.095	0.021	31	0.15	0.01	0.99
17–18	0.079	0.018	29	0.11	0.00	0.99
18–19	0.059	0.013	26	0.08	0.00	1.00
19–20	0.033	0.007	38	0.06	0.00	1.00
20–21	0.020	0.004	---[3]	0.00	0.00	1.00
21–22	0.003	0.001	---[3]	0.00	0.00	1.00
22–23	0.010	0.002	---[3]	0.00	0.00	1.00
23–24	0.003	0.001	---[3]	0.00	0.00	1.00
	$\sum Q_i$ =	0.996	$\sum C_i \times Q_i$ =	22.95		

1 ***Could not be assessed due to tank filling***

2 ***Estimated average***

3 ***No sample collected due to low/no outflow***

Table A.3. Data from Prototype Run FX050-3.

Time Interval [hr]	Level Drop [ft]	Flow Rate Q_i [cfs]	TSS C_i [mg/L]	$Mass_{OUT}$ $C_i \times Q_i$ [lb]	Mass Fraction $\frac{C_i \times Q_i}{\sum Ci \times Qi}$	Mass Fraction Cumulative
0–1	---[1]	0.050[2]	301	3.66	0.19	0.19
1–2	0.351	0.085	194	3.40	0.17	0.36
2–3	0.377	0.084	145	2.73	0.14	0.50
3–4	0.355	0.079	108	1.92	0.10	0.60
4–5	0.318	0.071	87	1.38	0.07	0.67
5–6	0.315	0.070	77	1.21	0.06	0.73
6–7	0.289	0.064	70	1.01	0.05	0.79
7–8	0.269	0.060	53	0.71	0.04	0.82
8–9	0.242	0.054	42	0.51	0.03	0.85
9–10	0.237	0.053	47	0.56	0.03	0.88
10–11	0.203	0.045	41	0.42	0.02	0.90
11–12	0.184	0.041	36	0.33	0.02	0.92
12–13	0.180	0.040	33	0.30	0.02	0.93
13–14	0.158	0.035	36	0.28	0.01	0.94
14–15	0.134	0.030	31	0.21	0.01	0.96
15–16	0.135	0.030	31	0.21	0.01	0.97
16–17	0.115	0.026	30	0.17	0.01	0.98
17–18	0.108	0.024	32	0.17	0.01	0.98
18–19	0.092	0.020	35	0.16	0.01	0.99
19–20	0.052	0.012	23	0.06	0.00	1.00
20–21	0.040	0.009	28	0.06	0.00	1.00
21–22	0.026	0.006	27	0.04	0.00	1.00
22–23	0.016	0.004	---[3]	0.00	0.00	1.00
23–24	0.003	0.001	---[3]	0.00	0.00	1.00
	$\sum Q_i$ =	0.990	$\sum C_i \times Q_i$ =	19.49		

[1] ***Could not be assessed due to tank filling***

[2] ***Estimated average***

[3] ***No sample collected due to low/no outflow***

Table A.4. Data from Prototype Run FX050-4.

Time Interval [hr]	Level Drop [ft]	Flow Rate Q_i [cfs]	TSS C_i [mg/L]	$Mass_{OUT}$ $C_i \times Q_i$ [lb]	Mass Fraction $\frac{C_i \times Q_i}{\sum Ci \times Qi}$	Mass Fraction Cumulative
0–1	---[1]	0.050[2]	265	3.28	0.17	0.17
1–2	0.364	0.090	185	3.36	0.18	0.35
2–3	0.384	0.085	150	2.88	0.15	0.50
3–4	0.354	0.079	116	2.05	0.11	0.61
4–5	0.328	0.073	92	1.51	0.08	0.68
5–6	0.315	0.070	71	1.12	0.06	0.74
6–7	0.289	0.064	66	0.95	0.05	0.79
7–8	0.256	0.057	49	0.63	0.03	0.83
8–9	0.249	0.055	45	0.56	0.03	0.86
9–10	0.223	0.050	43	0.48	0.03	0.88
10–11	0.207	0.046	40	0.41	0.02	0.90
11–12	0.187	0.042	35	0.33	0.02	0.92
12–13	0.180	0.040	33	0.30	0.02	0.93
13–14	0.158	0.035	31	0.24	0.01	0.95
14–15	0.138	0.031	30	0.21	0.01	0.96
15–16	0.134	0.030	30	0.20	0.01	0.97
16–17	0.121	0.027	29	0.18	0.01	0.98
17–18	0.102	0.023	32	0.16	0.01	0.99
18–19	0.095	0.021	26	0.12	0.01	0.99
19–20	0.063	0.014	27	0.08	0.00	1.00
20–21	0.032	0.007	30	0.05	0.00	1.00
21–22	0.023	0.005	---[3]	0.00	0.00	1.00
22–23	0.017	0.004	---[3]	0.00	0.00	1.00
23–24	0.003	0.001	---[3]	0.00	0.00	1.00
	$\sum Q_i$ =	0.997	$\sum C_i \times Q_i$ =	19.09		

1 ***Could not be assessed due to tank filling***

2 ***Estimated average***

3 ***No sample collected due to low/no outflow***

Table A.5. Data from Prototype Run FL025-1.

Time Interval [hr]	Level Drop [ft]	Flow Rate Q_i [cfs]	TSS C_i [mg/L]	$Mass_{OUT}$ $C_i \times Q_i$ [lb]	Mass Fraction $\frac{C_i \times Q_i}{\sum Ci \times Qi}$	Mass Fraction Cumulative
0–1	---[1]	0.038[2]	148	1.37	0.15	0.15
1–2	0.259	0.063	89	1.15	0.12	0.15
2–3	0.259	0.058	81	1.05	0.11	0.15
3–4	0.240	0.053	59	0.71	0.08	0.15
4–5	0.207	0.046	58	0.60	0.06	0.15
5–6	0.200	0.044	55	0.55	0.06	0.15
6–7	0.197	0.044	35	0.34	0.04	0.15
7–8	0.197	0.044	30	0.30	0.03	0.15
8–9	0.183	0.041	30	0.27	0.03	0.15
9–10	0.187	0.042	28	0.26	0.03	0.15
10–11	0.187	0.042	27	0.25	0.03	0.15
11–12	0.168	0.037	32	0.27	0.03	0.15
12–13	0.173	0.038	32	0.28	0.03	0.15
13–14	0.168	0.037	32	0.27	0.03	0.15
14–15	0.180	0.040	28	0.25	0.03	0.15
15–16	0.174	0.039	24	0.21	0.02	0.15
16–17	0.177	0.039	26	0.23	0.02	0.15
17–18	0.177	0.039	20	0.18	0.02	0.15
18–19	0.194	0.043	17	0.16	0.02	0.15
19–20	0.197	0.044	30	0.30	0.03	0.15
20–21	0.167	0.037	19	0.16	0.02	0.15
21–22	0.095	0.021	15	0.07	0.01	0.15
22–23	0.053	0.012	21	0.06	0.01	0.15
23–24	0.039	0.009	---[3]	0.00	0.00	0.15
	$\sum Q_i$ =	0.949	$\sum C_i \times Q_i$ =	9.27		

1 ***Could not be assessed due to tank filling***

2 ***Estimated average***

3 ***No sample collected due to low/no outflow***

Table A.6. Data from Prototype Run FL025-2.

Time Interval [hr]	Level Drop [ft]	Flow Rate Q_i [cfs]	TSS C_i [mg/L]	$Mass_{OUT}$ $C_i \times Q_i$ [lb]	Mass Fraction $\frac{C_i \times Q_i}{\sum Ci \times Qi}$	Mass Fraction Cumulative
0–1	---[1]	0.038[2]	143	1.32	0.15	0.15
1–2	0.272	0.066	77	1.05	0.12	0.28
2–3	0.292	0.065	59	0.86	0.10	0.38
3–4	0.250	0.056	42	0.52	0.06	0.44
4–5	0.246	0.055	36	0.44	0.05	0.49
5–6	0.196	0.044	29	0.28	0.03	0.52
6–7	0.210	0.047	28	0.29	0.03	0.56
7–8	0.210	0.047	30	0.31	0.04	0.59
8–9	0.191	0.042	33	0.31	0.04	0.63
9–10	0.197	0.044	30	0.30	0.03	0.67
10–11	0.193	0.043	29	0.28	0.03	0.70
11–12	0.187	0.042	25	0.23	0.03	0.73
12–13	0.184	0.041	30	0.28	0.03	0.76
13–14	0.184	0.041	30	0.28	0.03	0.79
14–15	0.177	0.039	32	0.28	0.03	0.82
15–16	0.180	0.040	26	0.23	0.03	0.85
16–17	0.177	0.039	25	0.22	0.03	0.88
17–18	0.191	0.042	20	0.19	0.02	0.90
18–19	0.206	0.046	30	0.31	0.04	0.93
19–20	0.187	0.042	27	0.25	0.03	0.96
20–21	0.109	0.024	23	0.13	0.01	0.98
21–22	0.072	0.016	25	0.09	0.01	0.99
22–23	0.046	0.010	23	0.05	0.01	1.00
23–24	0.026	0.006	29	0.04	0.00	1.00
	$\sum Q_i$ =	0.973	$\sum C_i \times Q_i$ =	8.55		

1 ***Could not be assessed due to tank filling***

2 ***Estimated average***

3 ***No sample collected due to low/no outflow***

Table A.7. Data from Prototype Run FL025-3.

Time Interval [hr]	Level Drop [ft]	Flow Rate Q_i [cfs]	TSS C_i [mg/L]	$Mass_{OUT}$ $C_i \times Q_i$ [lb]	Mass Fraction $\frac{C_i \times Q_i}{\sum Ci \times Qi}$	Mass Fraction Cumulative
0–1	---[1]	0.038[2]	129	1.15	0.16	0.16
1–2	0.243	0.057	62	0.75	0.11	0.27
2–3	0.223	0.050	53	0.59	0.08	0.35
3–4	0.207	0.046	41	0.42	0.06	0.41
4–5	0.210	0.047	41	0.43	0.06	0.47
5–6	0.170	0.038	39	0.33	0.05	0.52
6–7	0.177	0.039	34	0.30	0.04	0.56
7–8	0.168	0.037	38	0.32	0.05	0.61
8–9	0.177	0.039	33	0.29	0.04	0.65
9–10	0.138	0.031	32	0.22	0.03	0.68
10–11	0.170	0.038	31	0.26	0.04	0.72
11–12	0.161	0.036	27	0.22	0.03	0.75
12–13	0.161	0.036	24	0.19	0.03	0.78
13–14	0.157	0.035	25	0.20	0.03	0.81
14–15	0.154	0.034	27	0.21	0.03	0.83
15–16	0.158	0.035	25	0.20	0.03	0.86
16–17	0.167	0.037	27	0.23	0.03	0.89
17–18	0.158	0.035	24	0.19	0.03	0.92
18–19	0.147	0.033	25	0.18	0.03	0.95
19–20	0.151	0.034	23	0.17	0.02	0.97
20–21	0.158	0.035	25	0.20	0.03	1.00
21–22	0.170	0.038	24	0.20	0.00	1.00
22–23	0.171	0.038	21	0.18	0.00	1.00
23–24	0.151	0.034	21	0.16	0.00	1.00
	$\sum Q_i$ =	0.918	$\sum C_i \times Q_i$ =	7.60		

1 ***Could not be assessed due to tank filling***

2 ***Estimated average***

3 ***No sample collected due to low/no outflow***

Table A.8. Data from Prototype Run FL050-1.

Time Interval [hr]	Level Drop [ft]	Flow Rate Q_i [cfs]	TSS C_i [mg/L]	$Mass_{OUT}$ $C_i \times Q_i$ [lb]	Mass Fraction $\frac{C_i \times Q_i}{\sum Ci \times Qi}$	Mass Fraction Cumulative
0–1	---[1]	0.038[2]	290	2.63	0.17	0.17
1–2	0.342	0.081	127	2.17	0.14	0.31
2–3	0.334	0.074	102	1.70	0.11	0.42
3–4	0.256	0.057	87	1.11	0.07	0.50
4–5	0.246	0.055	74	0.91	0.06	0.55
5–6	0.207	0.046	63	0.65	0.04	0.60
6–7	0.213	0.047	62	0.66	0.04	0.64
7–8	0.194	0.043	60	0.58	0.04	0.68
8–9	0.197	0.044	57	0.56	0.04	0.71
9–10	0.180	0.040	54	0.49	0.03	0.75
10–11	0.180	0.040	53	0.48	0.03	0.78
11–12	0.181	0.040	48	0.43	0.03	0.81
12–13	0.171	0.038	47	0.40	0.03	0.83
13–14	0.170	0.038	42	0.36	0.02	0.85
14–15	0.181	0.040	45	0.41	0.03	0.88
15–16	0.160	0.036	37	0.30	0.02	0.90
16–17	0.181	0.040	37	0.33	0.02	0.92
17–18	0.243	0.054	37	0.45	0.03	0.95
18–19	0.239	0.053	29	0.35	0.02	0.97
19–20	0.144	0.032	31	0.22	0.01	0.99
20–21	0.076	0.017	28	0.11	0.01	1.00
21–22	0.056	0.012	27	0.08	0.00	1.00
22–23	0.026	0.006	---[3]	0.00	0.00	1.00
23–24	0.013	0.003	---[3]	0.00	0.00	1.00
	$\sum Q_i$ =	0.974	$\sum C_i \times Q_i$ =	15.37		

1 ***Could not be assessed due to tank filling***

2 ***Estimated average***

3 ***No sample collected due to low/no outflow***

Table A.9. Data from Prototype Run FL050-2.

Time Interval [hr]	Level Drop [ft]	Flow Rate Q_i [cfs]	TSS C_i [mg/L]	$Mass_{OUT}$ $C_i \times Q_i$ [lb]	Mass Fraction $\frac{C_i \times Q_i}{\sum Ci \times Qi}$	Mass Fraction Cumulative
0–1	---[1]	0.038[2]	254	2.27	0.16	0.16
1–2	0.263	0.062	117	1.54	0.11	0.27
2–3	0.262	0.058	111	1.45	0.10	0.38
3–4	0.224	0.050	90	1.01	0.07	0.45
4–5	0.229	0.051	75	0.86	0.06	0.51
5–6	0.177	0.039	69	0.61	0.04	0.56
6–7	0.204	0.045	65	0.66	0.05	0.60
7–8	0.180	0.040	60	0.54	0.04	0.64
8–9	0.184	0.041	58	0.53	0.04	0.68
9–10	0.177	0.039	52	0.46	0.03	0.71
10–11	0.171	0.038	51	0.44	0.03	0.74
11–12	0.190	0.042	44	0.42	0.03	0.77
12–13	0.141	0.031	43	0.30	0.02	0.80
13–14	0.190	0.042	43	0.41	0.03	0.83
14–15	0.171	0.038	41	0.35	0.03	0.85
15–16	0.190	0.042	38	0.36	0.03	0.88
16–17	0.191	0.042	37	0.35	0.03	0.90
17–18	0.259	0.058	34	0.44	0.03	0.93
18–19	0.220	0.049	34	0.37	0.03	0.96
19–20	0.183	0.041	31	0.28	0.02	0.98
20–21	0.112	0.025	26	0.15	0.01	0.99
21–22	0.059	0.013	26	0.08	0.01	1.00
22–23	0.039	0.009	17	0.03	0.00	1.00
23–24	0.020	0.004	22	0.02	0.00	1.00
	$\sum Q_i$ =	0.938	$\sum C_i \times Q_i$ =	13.93		

1 ***Could not be assessed due to tank filling***

2 ***Estimated average***

3 ***No sample collected due to low/no outflow***

Table A.10. Data from Prototype Run FL050-3.

Time Interval [hr]	Level Drop [ft]	Flow Rate Q_i [cfs]	TSS C_i [mg/L]	$Mass_{OUT}$ $C_i \times Q_i$ [lb]	Mass Fraction $\frac{C_i \times Q_i}{\sum Ci \times Qi}$	Mass Fraction Cumulative
0–1	---[1]	0.038[2]	223	2.12	0.15	0.15
1–2	0.266	0.067	92	1.22	0.09	0.24
2–3	0.259	0.058	87	1.13	0.08	0.33
3–4	0.276	0.061	79	1.09	0.08	0.41
4–5	0.203	0.045	73	0.74	0.05	0.46
5–6	0.220	0.049	67	0.74	0.05	0.51
6–7	0.180	0.040	64	0.58	0.04	0.56
7–8	0.204	0.045	61	0.62	0.05	0.60
8–9	0.203	0.045	56	0.57	0.04	0.64
9–10	0.138	0.031	54	0.37	0.03	0.67
10–11	0.181	0.040	54	0.49	0.04	0.71
11–12	0.206	0.046	50	0.51	0.04	0.74
12–13	0.145	0.032	46	0.33	0.02	0.77
13–14	0.177	0.039	44	0.39	0.03	0.80
14–15	0.144	0.032	46	0.33	0.02	0.82
15–16	0.164	0.036	40	0.33	0.02	0.84
16–17	0.161	0.036	44	0.35	0.03	0.87
17–18	0.203	0.045	39	0.40	0.03	0.90
18–19	0.210	0.047	37	0.39	0.03	0.93
19–20	0.250	0.056	35	0.44	0.03	0.96
20–21	0.177	0.039	34	0.30	0.02	0.98
21–22	0.101	0.022	31	0.16	0.01	0.99
22–23	0.056	0.012	30	0.08	0.01	1.00
23–24	0.010	0.003	27	0.02	0.00	1.00
	$\sum Q_i$ =	0.965	$\sum C_i \times Q_i$ =	13.69		

1 ***Could not be assessed due to tank filling***

2 ***Estimated average***

3 ***No sample collected due to low/no outflow***

Table A.11. Data from Prototype Run FL050-4.

Time Interval [hr]	Level Drop [ft]	Flow Rate Q_i [cfs]	TSS C_i [mg/L]	$Mass_{OUT}$ $C_i \times Q_i$ [lb]	Mass Fraction $\frac{C_i \times Q_i}{\sum Ci \times Qi}$	Mass Fraction Cumulative
0–1	---[1]	0.038[2]	316	2.87	0.20	0.20
1–2	0.325	0.077	135	2.19	0.15	0.35
2–3	0.308	0.068	86	1.32	0.09	0.44
3–4	0.204	0.045	71	0.72	0.05	0.49
4–5	0.242	0.054	65	0.79	0.05	0.55
5–6	0.191	0.042	58	0.55	0.04	0.58
6–7	0.183	0.041	55	0.50	0.03	0.62
7–8	0.204	0.045	55	0.56	0.04	0.66
8–9	0.161	0.036	51	0.41	0.03	0.69
9–10	0.193	0.043	52	0.50	0.03	0.72
10–11	0.151	0.034	48	0.36	0.03	0.75
11–12	0.184	0.041	45	0.41	0.03	0.78
12–13	0.151	0.034	46	0.35	0.02	0.80
13–14	0.157	0.035	42	0.33	0.02	0.82
14–15	0.181	0.040	41	0.37	0.03	0.85
15–16	0.167	0.037	36	0.30	0.02	0.87
16–17	0.180	0.040	38	0.34	0.02	0.89
17–18	0.178	0.040	38	0.34	0.02	0.92
18–19	0.229	0.051	36	0.41	0.03	0.94
19–20	0.227	0.050	30	0.34	0.02	0.97
20–21	0.144	0.032	31	0.22	0.02	0.98
21–22	0.098	0.022	29	0.14	0.01	0.99
22–23	0.037	0.008	29	0.05	0.00	1.00
23–24	0.036	0.008	27	0.05	0.00	1.00
	$\sum Q_i$ =	0.961	$\sum C_i \times Q_i$ =	14.44		

1 ***Could not be assessed due to tank filling***

2 ***Estimated average***

3 ***No sample collected due to low/no outflow***

Table A.12. Data from Prototype Run FL050-5.

Time Interval [hr]	Level Drop [ft]	Flow Rate Q_i [cfs]	TSS C_i [mg/L]	$Mass_{OUT}$ $C_i \times Q_i$ [lb]	Mass Fraction $\frac{C_i \times Q_i}{\sum Ci \times Qi}$	Mass Fraction Cumulative
0–1	---[1]	0.038[2]	320	2.91	0.21	0.21
1–2	0.289	0.069	163	2.35	0.17	0.38
2–3	0.325	0.072	69	1.12	0.08	0.46
3–4	0.220	0.049	62	0.68	0.05	0.51
4–5	0.226	0.050	51	0.58	0.04	0.55
5–6	0.243	0.054	43	0.52	0.04	0.59
6–7	0.203	0.045	35	0.35	0.03	0.62
7–8	0.210	0.047	36	0.38	0.03	0.64
8–9	0.207	0.046	45	0.47	0.03	0.68
9–10	0.171	0.038	45	0.38	0.03	0.71
10–11	0.180	0.040	51	0.46	0.03	0.74
11–12	0.194	0.043	49	0.47	0.03	0.77
12–13	0.160	0.036	45	0.36	0.03	0.80
13–14	0.174	0.039	43	0.37	0.03	0.83
14–15	0.158	0.035	39	0.31	0.02	0.85
15–16	0.157	0.035	39	0.31	0.02	0.87
16–17	0.194	0.043	37	0.36	0.03	0.90
17–18	0.216	0.048	41	0.44	0.03	0.93
18–19	0.200	0.044	32	0.32	0.02	0.95
19–20	0.191	0.042	33	0.31	0.02	0.97
20–21	0.082	0.018	31	0.13	0.01	0.98
21–22	0.078	0.017	30	0.12	0.01	0.99
22–23	0.043	0.010	29	0.06	0.00	1.00
23–24	0.023	0.005	35	0.04	0.00	1.00
	$\sum Q_i$ =	0.963	$\sum C_i \times Q_i$ =	13.80		

1 ***Could not be assessed due to tank filling***

2 ***Estimated average***

3 ***No sample collected due to low/no outflow***

Table A.13. Data from Prototype Run FL050-6.

Time Interval [hr]	Level Drop [ft]	Flow Rate Q_i [cfs]	TSS C_i [mg/L]	$Mass_{OUT}$ $C_i \times Q_i$ [lb]	Mass Fraction $\frac{C_i \times Q_i}{\sum Ci \times Qi}$	Mass Fraction Cumulative
0–1	---[1]	0.038[2]	334	2.94	0.18	0.18
1–2	0.308	0.071	155	2.38	0.14	0.32
2–3	0.295	0.066	105	1.55	0.09	0.41
3–4	0.250	0.056	95	1.19	0.07	0.48
4–5	0.226	0.050	81	0.91	0.05	0.54
5–6	0.190	0.042	74	0.70	0.04	0.58
6–7	0.194	0.043	71	0.69	0.04	0.62
7–8	0.180	0.040	68	0.61	0.04	0.66
8–9	0.161	0.036	63	0.51	0.03	0.69
9–10	0.161	0.036	62	0.50	0.03	0.72
10–11	0.174	0.039	58	0.50	0.03	0.75
11–12	0.157	0.035	56	0.44	0.03	0.78
12–13	0.174	0.039	52	0.45	0.03	0.80
13–14	0.164	0.036	54	0.44	0.03	0.83
14–15	0.158	0.035	46	0.36	0.02	0.85
15–16	0.167	0.037	45	0.38	0.02	0.87
16–17	0.174	0.039	46	0.40	0.02	0.90
17–18	0.187	0.042	42	0.39	0.02	0.92
18–19	0.223	0.050	41	0.46	0.03	0.95
19–20	0.200	0.044	36	0.36	0.02	0.97
20–21	0.141	0.031	35	0.25	0.01	0.98
21–22	0.069	0.015	36	0.12	0.01	0.99
22–23	0.039	0.009	33	0.06	0.00	1.00
23–24	0.046	0.010	29	0.07	0.00	1.00
	$\sum Q_i$ =	0.938	$\sum C_i \times Q_i$ =	16.66		

1 ***Could not be assessed due to tank filling***

2 ***Estimated average***

3 ***No sample collected due to low/no outflow***

Table A.14. Data from Prototype Run FL100-1.

Time Interval [hr]	Level Drop [ft]	Flow Rate Q_i [cfs]	TSS C_i [mg/L]	$Mass_{OUT}$ $C_i \times Q_i$ [lb]	Mass Fraction $\frac{C_i \times Q_i}{\sum Ci \times Qi}$	Mass Fraction Cumulative
0–1	---[1]	0.038[2]	469	4.39	0.19	0.19
1–2	0.259	0.064	246	3.18	0.14	0.33
2–3	0.279	0.062	129	1.80	0.08	0.41
3–4	0.239	0.053	101	1.21	0.05	0.46
4–5	0.214	0.048	86	0.92	0.04	0.50
5–6	0.219	0.049	78	0.85	0.04	0.54
6–7	0.187	0.042	89	0.83	0.04	0.57
7–8	0.204	0.045	72	0.73	0.03	0.60
8–9	0.187	0.042	82	0.77	0.03	0.64
9–10	0.193	0.043	84	0.81	0.04	0.67
10–11	0.191	0.042	85	0.81	0.04	0.71
11–12	0.170	0.038	89	0.76	0.03	0.74
12–13	0.168	0.037	86	0.72	0.03	0.77
13–14	0.180	0.040	78	0.70	0.03	0.80
14–15	0.171	0.038	75	0.64	0.03	0.83
15–16	0.203	0.045	72	0.73	0.03	0.86
16–17	0.158	0.035	67	0.53	0.02	0.88
17–18	0.216	0.048	68	0.73	0.03	0.92
18–19	0.210	0.047	63	0.66	0.03	0.94
19–20	0.194	0.043	62	0.60	0.03	0.97
20–21	0.115	0.026	52	0.30	0.01	0.98
21–22	0.068	0.015	56	0.19	0.01	0.99
22–23	0.050	0.011	49	0.12	0.01	1.00
23–24	0.029	0.006	44	0.06	0.00	1.00
	$\sum Q_i$ =	0.956	$\sum C_i \times Q_i$ =	23.05		

1 ***Could not be assessed due to tank filling***

2 ***Estimated average***

3 ***No sample collected due to low/no outflow***

Table A.15. Data from Prototype Run FL100-2.

Time Interval [hr]	Level Drop [ft]	Flow Rate Q_i [cfs]	TSS C_i [mg/L]	$Mass_{OUT}$ $C_i \times Q_i$ [lb]	Mass Fraction $\frac{C_i \times Q_i}{\sum Ci \times Qi}$	Mass Fraction Cumulative
0–1	---[1]	0.038[2]	504	4.43	0.17	0.17
1–2	0.236	0.054	267	3.15	0.12	0.29
2–3	0.220	0.049	180	1.98	0.08	0.37
3–4	0.236	0.052	143	1.69	0.06	0.43
4–5	0.197	0.044	127	1.25	0.05	0.48
5–6	0.197	0.044	115	1.13	0.04	0.52
6–7	0.194	0.043	112	1.09	0.04	0.56
7–8	0.187	0.042	107	1.00	0.04	0.60
8–9	0.196	0.044	100	0.98	0.04	0.64
9–10	0.161	0.036	102	0.82	0.03	0.67
10–11	0.174	0.039	101	0.88	0.03	0.71
11–12	0.171	0.038	97	0.83	0.03	0.74
12–13	0.170	0.038	93	0.79	0.03	0.77
13–14	0.168	0.037	89	0.75	0.03	0.80
14–15	0.157	0.035	82	0.64	0.02	0.82
15–16	0.154	0.034	76	0.58	0.02	0.84
16–17	0.181	0.040	73	0.66	0.03	0.87
17–18	0.154	0.034	74	0.57	0.02	0.89
18–19	0.167	0.037	71	0.59	0.02	0.91
19–20	0.187	0.042	69	0.64	0.02	0.94
20–21	0.200	0.044	62	0.62	0.02	0.96
21–22	0.181	0.040	61	0.55	0.02	0.98
22–23	0.098	0.022	54	0.26	0.01	0.99
23–24	0.063	0.014	52	0.16	0.01	1.00
	$\sum Q_i$ =	0.939	$\sum C_i \times Q_i$ =	26.05		

1 ***Could not be assessed due to tank filling***

2 ***Estimated average***

3 ***No sample collected due to low/no outflow***

Table A.16. Data from Prototype Run FL100-3.

Time Interval [hr]	Level Drop [ft]	Flow Rate Q_i [cfs]	TSS C_i [mg/L]	$Mass_{OUT}$ $C_i \times Q_i$ [lb]	Mass Fraction $\frac{C_i \times Q_i}{\sum Ci \times Qi}$	Mass Fraction Cumulative
0–1	---[1]	0.038[2]	528	4.79	0.18	0.18
1–2	0.259	0.062	274	2.30	0.13	0.31
2–3	0.239	0.053	193	1.64	0.09	0.39
3–4	0.220	0.049	149	1.35	0.06	0.45
4–5	0.210	0.047	129	1.17	0.05	0.50
5–6	0.200	0.044	117	1.11	0.04	0.55
6–7	0.201	0.045	111	1.01	0.04	0.59
7–8	0.196	0.044	103	0.93	0.04	0.62
8–9	0.187	0.042	100	0.94	0.03	0.66
9–10	0.197	0.044	96	0.79	0.03	0.69
10–11	0.171	0.038	93	0.77	0.03	0.72
11–12	0.174	0.039	89	0.73	0.03	0.75
12–13	0.167	0.037	87	0.77	0.03	0.78
13–14	0.177	0.039	87	0.65	0.03	0.81
14–15	0.161	0.036	81	0.64	0.02	0.83
15–16	0.161	0.036	80	0.64	0.02	0.86
16–17	0.167	0.037	77	0.63	0.02	0.88
17–18	0.167	0.037	76	0.63	0.02	0.90
18–19	0.174	0.039	72	0.64	0.02	0.93
19–20	0.191	0.042	67	0.60	0.02	0.95
20–21	0.187	0.042	64	0.41	0.02	0.97
21–22	0.134	0.030	62	0.23	0.02	0.99
22–23	0.079	0.018	59	0.13	0.01	1.00
23–24	0.049	0.011	55	22.29	0.00	1.00
	$\sum Q_i =$	0.946	$\sum C_i \times Q_i =$	27.08		

1 ***Could not be assessed due to tank filling***

2 ***Estimated average***

3 ***No sample collected due to low/no outflow***

APPENDIX B:
CONCEPTUAL MODEL PROGRAM IN MATLAB

The following is the MATLAB program developed for calculating particle removal efficiency of the rectangular detention basin by the conceptual model. Water level, outflow rate, and outflow SSC are also calculated in the program. The same kinds of calculation can be done for prototype by setting the flag scale to be 1.

```
%%%%%%%%%%%%%%%%%%%%%%%%%%%%%%%%%%%%%%%%%%%%%%%%%%%%%%%%
%%%%%%%%%%%%%%%%%%%%%%%%%%%%%%%%%%%%%%%%%%%%%%%%%%
%This is a MATLAB code to calculate Water level change, Outflow rate, outflow SSC, and SS removal ratio
%Author: Masatsugu Takamatsu
%%%%%%%%%%%%%%%%%%%%%%%%%%%%%%%%%%%%%%%%%%%%%%%%%%%%%%%%
%%%%%%%%%%%%%%%%%%%%%%%%%%%%%%%%%%%%%%%%%%%%%%%%%%

clear all

%<<Define flags>>
   flagScale=0;       %Model or Prototype (0 for model scale and 1 for scaled model)
   flagInflow=0;       %Inflow hydrograph type (0 for constant inflow, 1 for SCS triangular inflow)
   flagInput=1;       %Among eight data, A=1, B=2, C=3, D=4, E=5, F=6, G=7, H=8
   flagGraph=0;       %Graph options
                  %0 for no graph
                  %1 for water level change
                  %2 for flow rate
                  %3 for PDF of inflow PSD
                  %4 for CDF of inflow PSD
                  %5 for PDF of particle settling velocity of inflow
                  %6 for CDF of particle settling velocity of inflow
                  %7: dp-vp relationship
   flagSSC=1;         %0 for not calculating sedimentation process
                  %1 for calculating sedimentation process

%<<Define Variables>>
%%%%%%%%%%%%%%%%coeff for model%%%%%%%%%%
                    g=9.81;        % Gravity acceleration, g (m/s^2)
                    B=0.62;        % Width of the tank, B (m)

      if flagInflow==0 %parameter for constnat Qin
         if flagInput==1
            Ae=0.43*4;L=6.96;C0=202;Qconst=0.53;Ts=40*60;%runA
         elseif flagInput==2
            Ae=0.43;L=6.96;C0=267;Qconst=0.32;Ts=80*60;%runB
         elseif flagInput==3
            Ae=0.48;L=6.96;C0=246;Qconst=0.9;Ts=20*60;%runC
         elseif flagInput==4
            Ae=0.48;L=6.96;C0=258;Qconst=1.17;Ts=15*60;%runD
         elseif flagInput==5
            Ae=0.48;L=6.96;C0=212;Qconst=0.73;Ts=30*60;%runE
         elseif flagInput==6
            Ae=0.48;L=6.96*2/3;C0=192;Qconst=0.93;Ts=15*60;%runF
         elseif flagInput==7
            Ae=0.48;L=6.96*2/3;C0=255;Qconst=0.51;Ts=30*60;%runG
         elseif flagInput==8
            Ae=0.48;L=6.96*2/3;C0=277;Qconst=0.32;Ts=40*60;%runH
         end
         K2=(Ae/10000*(2*g)^0.5/2/B/L)^2; %K2 from (3.1.5)
      elseif flagInflow==1 %parameters for SCS triangular hydrograph
```

```
      Ae=0.43;        % Effective area of orifice
      L=6.96;        % Length of the tank, L=6.96 (m)
      C0=202;        %C0=constant inlet SSC (Suspended Solid Concentration)
      K2=(Ae/10000*(2*g)^0.5/2/B/L)^2; %K2 from (3.1.5)
      Qp=1.5/4;      %Peak flow rate (L/s)
                  Tp=20*4*60;   %Peak time (s)
    end


    %%%%%   Variables on particles  %%%%%%%%%%%%
              densP=2.65;    %density of silica particle (g/cm^3)
              densL=1.00;    %density of water (g/cm^3)
              viscs=1e-3;  %viscs (viscosity of water) (Pa*s)=0.1*viscosity of water(=0.01)(g/cm/s)
    rmdPsize=2.286; %mean of ln(particle size) (particle size (micron)) 2.252 from Ana's data and 2.651 for best
fit, 2.642 for manufacture data, (2.287, 0.906) is Jeff's data
    tyetaPsize=0.908;   %standard deviation of ln(particle size) 0.876 from Ana's data and 1.102 for best fit, and
0.588 for manufacture data
    k=g/18/viscs*(densP-densL)*3.6e-6; %(vs(m/hr)=k*dp(micron)^2)
              rmd=2*rmdPsize+log(k);%rmd is mean of ln(vp) and tyeta is std dev of ln(vp)
    tyeta=2*tyetaPsize;   %tyeta is std dev of ln(vp)


%%%%%%%%%%%%%%%%%%%%%%%Coeff for Scaled up model%%%%%%%%%%%%%%%%%
        if flagScale==1
              Lr=5;         %Length ratio
              Ae=Ae*Lr^1.5;   % Orifice area, Ap (cm^2)
              L=L*Lr;        % Length of the tank, L (m)
              B=B*Lr;        % Width of the tank, B (m)
    %parameters for SCS triangular hydrograph
    if flagInflow==0
      Qconst=Qconst*Lr^2;
      Ts=Ts*Lr;
    elseif flagInflow==1
      Qp=Qp*Lr^2;%Constant inflow rate, Qin (L/s), 0.53(L/s) and Ts=40 (min) is default value
                  Tp=Tp*Lr;% TS is the time when the runoff stops
    end
  end

%%%%%%%%%%%%%%%%%%%%%%%%%    Program for hydraulics   %%%%%
  i=1;
  dt=1;         %dt: time interval (min)
  WL=1e-4;       %Water level(m)

  %%%%%%%%%%%Constant Inflow%%%%%%%%%%%%%%%%%%%%%%

  if flagInflow==0     %Constant flow rate case
    QQ=0;
    tautau=0;
    while i<= 20*Ts/60/dt & WL>1e-5
      time(i)=i*dt;
      if i<(Ts/60+1)/dt
        WL=WL+60*dt/B/L*(Qconst/1000-Ae/10000*(2*g*WL)^0.5);    %WL (m)
        WLL(i)=WL;
        Qin(i)=Qconst;                             %Qinn (m^3/s)
        Q(i)=1000*Ae/10000*(2*g*WL)^0.5;        %Q (L/s)
        tau(i)=Q(i)*i*dt;
```

```
        else
            WL=WL+60*dt/B/L*(-Ae/10000*(2*g*WL)^0.5);
            WLL(i)=WL;
            Qin(i)=0;
            Q(i)=1000*Ae/10000*(2*g*WL)^0.5;
            tau(i)=Q(i)*i*dt;
        end
        QQ=QQ+Q(i);
        tautau=tautau+tau(i);
        i=i+1;
    end
    tmax=Ts/60/dt;
    detention=tautau/QQ-Ts/2/60
    WL_max=WLL(tmax);
    ni=Ts/60/dt;   %ni:Number of i

%%%%%%%%%%SCS Triangular inflow%%%%%%%%%%%%%%%%%%
elseif flagInflow==1     %SCS triangular hydrograph case
   while i<= 30*Tp/60/dt & WL>1e-5
        time(i)=i*dt;
        if i<(Tp/60+1)/dt
            WL=WL+60*dt/B/L*(i*dt/(Tp/60)*Qp/1000-Ae/10000*(2*g*WL)^0.5);
            WLL(i)=WL;
            Qin(i)=1000*i*dt/(Tp/60)*Qp/1000;
            Q(i)=1000*Ae/10000*(2*g*WL)^0.5;
        elseif i<(8/3*Tp/60+1)/dt
            WL=WL+60*dt/B/L*((1.6-0.6*i*dt/(Tp/60))*Qp/1000-Ae/10000*(2*g*WL)^0.5);
            WLL(i)=WL;
            Qin(i)=1000*(1.6-0.6*i*dt/(Tp/60))*Qp/1000;
            Q(i)=1000*Ae/10000*(2*g*WL)^0.5;
        else
            WL=WL+60*dt/B/L*(-Ae/10000*(2*g*WL)^0.5);
            WLL(i)=WL;
            Qin(i)=0;
            Q(i)=1000*Ae/10000*(2*g*WL)^0.5;
        end

        i=i+1;
    end
    ni=8/3*Tp/60/dt;   %ni:Number of iteration during runoff period
 end


 %Water level (m) change with time
 if flagGraph==1
    plot(time/60, WLL);
    hold on
    title('Water level change with time')
    xlabel('time(hr)');
    ylabel('Water Level (m)')
 elseif flagGraph==2
    plot(time/60, Q);
    hold on
    plot(time/60, Qin);
    title('In and outflow change')
    xlabel('time(hr)');
```

```
        ylabel('Flow Rate (L/s)')
    end


%%%%%%%%%%%%%%%%%%%%%%%%%%Program for calculating TSS outlet concentration
%%%%%%%%%%%%%%%%%
if flagSSC==1
   tic

    %%Calculating time to reach outlet zone
    for i=1:ni-1
        time=0;
        RHS=0;LHS=1;
        tDrain(i)=0;
        n=1;
        t0(i)=i*dt;
       while RHS<LHS %t0=TT*i and T=time(i)
          if i+n<ni
             iRange=[i:i+n];
          else
             iRange=[i:ni];
          end
          LHS=L;
          RHS=1/B/WLL(i+n)*trapz(iRange,Qin(iRange))*60/1000;
          RHSS(i)=RHS;
          tDrain(i)=i+n;
          tDetention(i)=n;
          n=n+1;
       end
    end
%        plot(t0, tDetention);
%        title('Figure2. Detention Time')
%        xlabel('Inflow time(min)');
%        ylabel('Detention time (min)')


      %%%%%%%%%%Timeseries TSS Concentration Calculation%%%%%%%%%%%%%%%
      for i=1:ni-1
          C00(i)=C0;
          vpMini=(densP-densL)*(100*g)*(1.5*1e-4).^2/18/(10*viscs)/100*3600; %vp(m/hr) for 1.5 micron particle
          vp=0;%vpMini;
                                %Calculating critical velocity
          time=[t0(i):tDrain(i)];
          vp=60*1./trapz(time,1./WLL(time));
          vpp(i)=vp;
          %Calculating critical particle size
          cpp(i)=10000*(vp/3600*100*10*viscs*18/((densP-densL)*100*g))^0.5;
          vp_interval=0.00001;
          if vp> vpMini
             criticalVP=vpMini:vp_interval:vp;%0.0073(m/hr) is settling velocity for dp=1.5(micron)
              %P_Conc is the ratio of particles smaller than critical particle size, which means 1-P_Conc is the portion
all of which settles down
              P_Conc(i)=1/(tyeta*(2*pi)^0.5)*trapz(criticalVP, exp(-0.5*((log(criticalVP)-rmd)./tyeta).^2)./criticalVP);
              %E2_out is the portion that settles down among whole PSD
              E2_out(i)=60*trapz(time,1./WLL(time))*1/(tyeta*(2*pi)^0.5)*trapz(criticalVP, 1/3600*exp(-
(log(criticalVP)-rmd).^2/(2*tyeta^2)));
```

```
            E_out(i)=P_Conc(i)-E2_out(i);
            C(i)=C0*E_out(i);
        else
            C(i)=0;
        end

    end
    plot(tDrain/60, C);
    hold on
    title('Figure2. Timeseries TSS concentration')
    xlabel('Time (hr)');
    ylabel('Concentration (mg/L)')

     %%%%%%%%%%%%5%Total removal ratio calculation%%%%%%%%%%%
     timeIn=[1:ni-1];
     totalMassIn=C0/1000*60*trapz(timeIn,Qin(timeIn));
     totalMassOut=60/1000*trapz(timeIn,Qin(timeIn).*C(timeIn));
     RemovalRatio=1-totalMassOut/totalMassIn
end


%%%%%%%%%%%%%%%%%%%%%% PSD graphs %%%%%%%%%%%%%%%%%%%%%%%%
lndp=[-5:0.1:4];
x_dp=exp(lndp);
lnvp=[-8:0.1:2];
x_vp=exp(lnvp);
if flagGraph==3 | flagGraph==4
    pPDF=1./((2*pi)^0.5*tyetaPsize.*exp(lndp)).*exp(-0.5*((lndp-rmdPsize)/tyetaPsize).^2);
    pCDF=cumtrapz(exp(lndp),pPDF);
    if flagGraph==3
        plot(x_dp,pPDF);
        title('PDF of Particle Size Distribution')
        xlabel('Particle Size (micron)');
        ylabel('PDF')
    else
        plot(x_dp,pCDF);
        title('CDF of Particle Size Distribution')
        xlabel('Particle Size (micron)');
        ylabel('CDF')
    end
end

if flagGraph==7
    vp=(densP-densL)*(100*g)*(exp(lndp)*1e-4).^2/18/(10*viscs)/100*3600; %vp(m/hr)
    plot(x_dp,vp)
    title('Relationship between particle size and settlign velocity')
    xlabel('Particle Size (micron)');
    ylabel('Particle Settling velocity (m/hr)')
end

if flagGraph==5 | flagGraph==6
    pPDF=1./((2*pi)^0.5*tyeta.*exp(lnvp)).*exp(-0.5*((lnvp-rmd)/tyeta).^2);
    pCDF=cumtrapz(exp(lnvp),pPDF);
    if flagGraph==5
        plot(x_vp,pPDF);
        title('PDF of Particle Settling Velocity')
```

```
        xlabel('Particle settling velocity (m/hr)');
        ylabel('PDF')
    else
        plot(x_vp,pCDF);
        title('CDF of Particle Settling Velocity')
        xlabel('Particle settling velocity (m/hr)');
        ylabel('CDF')
    end
end
```

Symbols	Descriptions
A_0	Actual orifice area
A_e	Effective area of an orifice
B	Width of the sedimentation basin
C	Concentration
C_D	Drag coefficient
Cd	Orifice coefficient
C_{in}	Inflow SSC
C_{out}	Outflow SSC
CU	Uniformity coefficient
d_p	Diameter of a particle
$d_{p,c}$	Critical particle diameter
EMC	Event Mean Concentration of particles
F	Force (in Chapter 2)
F	Potential settling function (except Chapter2)
F_b	Body force
F_d	Drag force
F_g	Gravitational force
F_r	Froude number
g	Gravitational acceleration
h	Water level
H_a	Hazen number
L	Length of the sedimentation basin
L_R	Length ratio of prototype to model
M	Mass
M_{in}	Total mass of inflow particles
M_{out}	Total mass of outflow particles
Q	Flow rate
Q_{in}	Inflow rate
Q_{out}	Outflow rate
Q_p	Peak flow of a triangular hydrograph
R	Removal efficiency
R_e	Reynolds number
R_{out} (t_{in})	Removal ratio of particles which flows into the basin at t_{in}
t	Time
tin	Time when a particle flows into the basin

t_{out}	Time when a particle flows out of the basin
T_p	Peak time of a triangular hydrograph
T_s	Duration of a runoff
u	Longitudinal fluid velocity
u_p	Longitudinal particle velocity
v	Velocity
v	Vertical fluid velocity
V_{in}	Total inflow volume
v_{or}	Overlflow velocity
V_{out}	Total outflow volume
v_p	Vertical particle velocity
v_s	Particle settling velocity
$v_{s,c}$	Critical particle settling velocity
x	Longitudinal position
x_p	Longitudinal position of a particle
x_w	Longitudinal position of water molecules
ζ	Lognormal standard deviation
ζ_p	Lognormal standard deviation of particle diameter
ζ_v	Lognormal standard deviation of particle settling velocity
λ	Lognormal mean
λ_p	Lognormal mean of particle diameter
λ_v	Lognormal mean of particle settling velocity
μ	Viscosity of a fluid
ν	Kinematic viscosity of a fluid
ρ	Density
ρ_f	Density of a fluid
t_d	Drainage time
ρ_p	Density of a particle
Superscript	
M	Model
P	Prototype
*	Nondimensionalized
k	Time step
Subscript	
E	Emptying period
F	Filling period

APPENDIX C:
CONCEPTUAL MODEL APPLICATION

C.1 First Application Example: Constant Inflow Case

Assume that there is a constant inflow of Q_{in}=0.53 L/s for the duration of T_s=40 min, and the inflow SSC is C_{in}=202 mg/L. Outflow is governed by a small orifice installed at the bottom of the end wall. The effective area of the orifice is $A_e = C_d \cdot A_p(cm^2) = 0.43 cm^2$, the multiplication of the orifice coefficient and the area of orifice. Assume the particle size distribution of inflow suspended solid can be properly described by lognormal distribution and the mean of ln(dp); λ_p, is 2.286 [dp (μm)] and the standard deviation of ln(dp), ζ_p, is 0.908 [dp (μm)]. Several articles (e.g., Campbell, 1985; Buchan, 1989) suggested that soil particle size distribution can be well described by lognormal distribution. Table C.1 summarizes the input parameter values used in the example.

Table C.1. Input Parameters, their Units, and Values for the Model Application.

Parameters	Unit	Value
Ae	cm^2	0.43
L	m	6.96
B	m	0.62
Q_{in}	L/s	0.53
T_s	min	40
C_{in}	mg/L	202
λ_p		0.908
ζ_p		2.286
ρ_p	g/cm^3	2.65
ρ_w	g/cm^3	1
μ	g/cm-s	0.01

Inflow Suspended Solid Particles

Stokes law, shown in Equation C.1, was applied to calculate particle settling velocity, v_s m/hr, from the diameter of a particle, d_p μm.

$$
\begin{aligned}
v_s &= \frac{g\cdot(\rho_p-\rho_w)}{18\mu}\cdot\left(d_p*10^{-4}\left[\frac{cm}{\mu m}\right]\right)^2 * \frac{3600}{100}\left[\frac{s}{hr}\right] \\
&= \frac{g\cdot(\rho_p-\rho_w)}{18\mu}\cdot\left(3.6*10^{-7}\right)\cdot {d_p}^2 \\
&= 3.24*10^{-3}\cdot {d_p}^2
\end{aligned}
\qquad (C.1)
$$

For the parameter values in this equation, gravitational acceleration, g, is 981cm/s^2; density of particles, ρ_p, is 2.65 g/cm^3; density of water, ρ_w, is 1.00 g/cm^3; and viscosity of water is 10^{-2} g/cm-s, which are shown in Table C.1. Figure C.1 shows the relationship between diameter of the silica particles and their settling velocity using Stokes law.

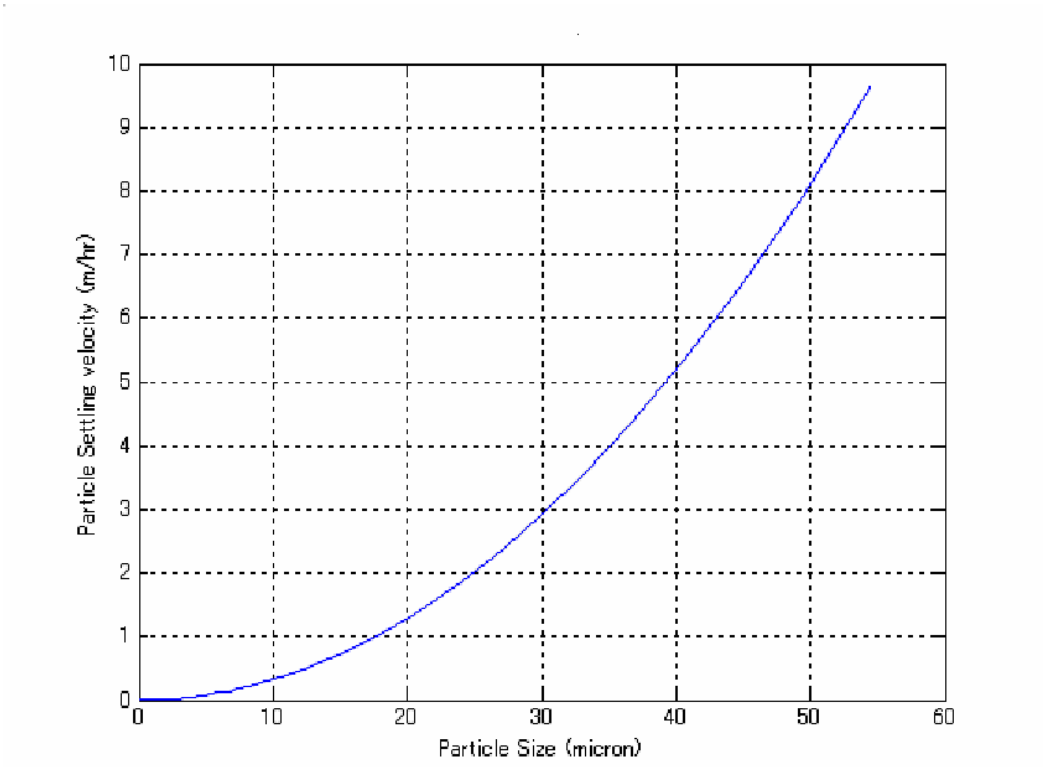

Figure C.1. Relationship between Particle Diameter and Settling Velocity.

Equation C.1 implies suspensions settling velocities will have a lognormal distribution (v_s=LN(λ_v,ζ_v)) if particle size assumes to have a lognormal distribution (d_p=LN(λ_p,ζ_p)) with the random variable transformation. The validity of the assumption is shown in Figure C.2. The relationship of lognormal mean and lognormal standard deviation of particle diameter and settling velocity is as follows using the relationship (C.1):

$$\lambda_v = 2 \cdot \lambda_p + \ln\left(3.24 * 10^{-3}\right)$$
$$\zeta_v = 2 \cdot \zeta_p \qquad \text{(C.2)}$$

Then, the mean of lognormal settling velocity, λ_v, is -1.186 [v_s (m/hr)], and the standard deviation of lognormal settling velocity, ζ_v, is 1.816 (v_s (m/hr)) from the calculation of Equation C.2. Figure C.3 shows particle size distribution (PSD) and settling velocity distribution of inflow runoff in the forms of a probability density function (PDF) and cumulative density function (CDF).

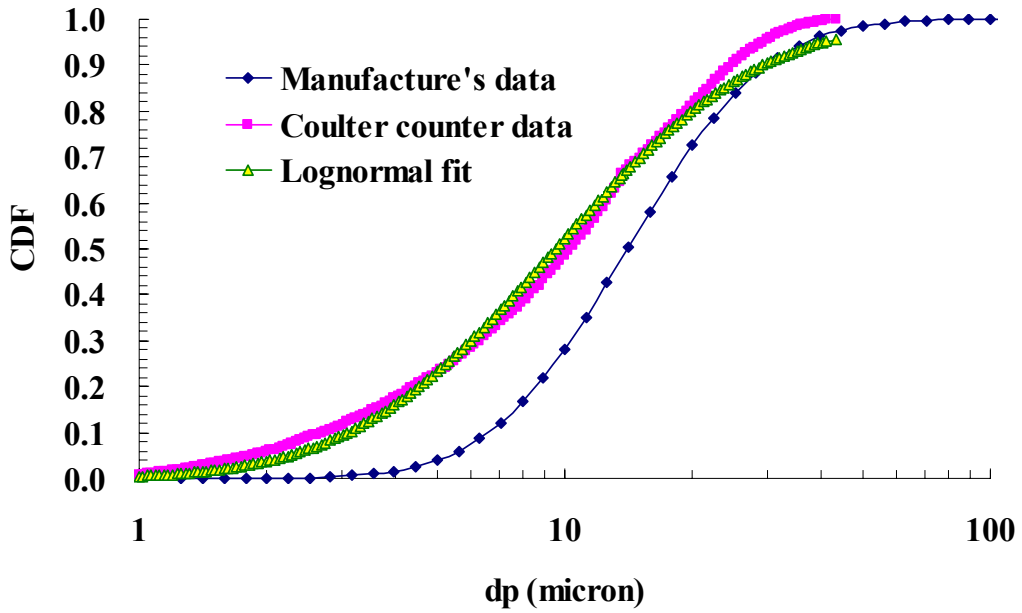

Figure C.2. Particle Size Distribution of SIL-CO-SIL®49 (Manufacturer Provided), Inflow Sample Measured by Coulter Counter, and the Best Fit Lognormal Distribution.

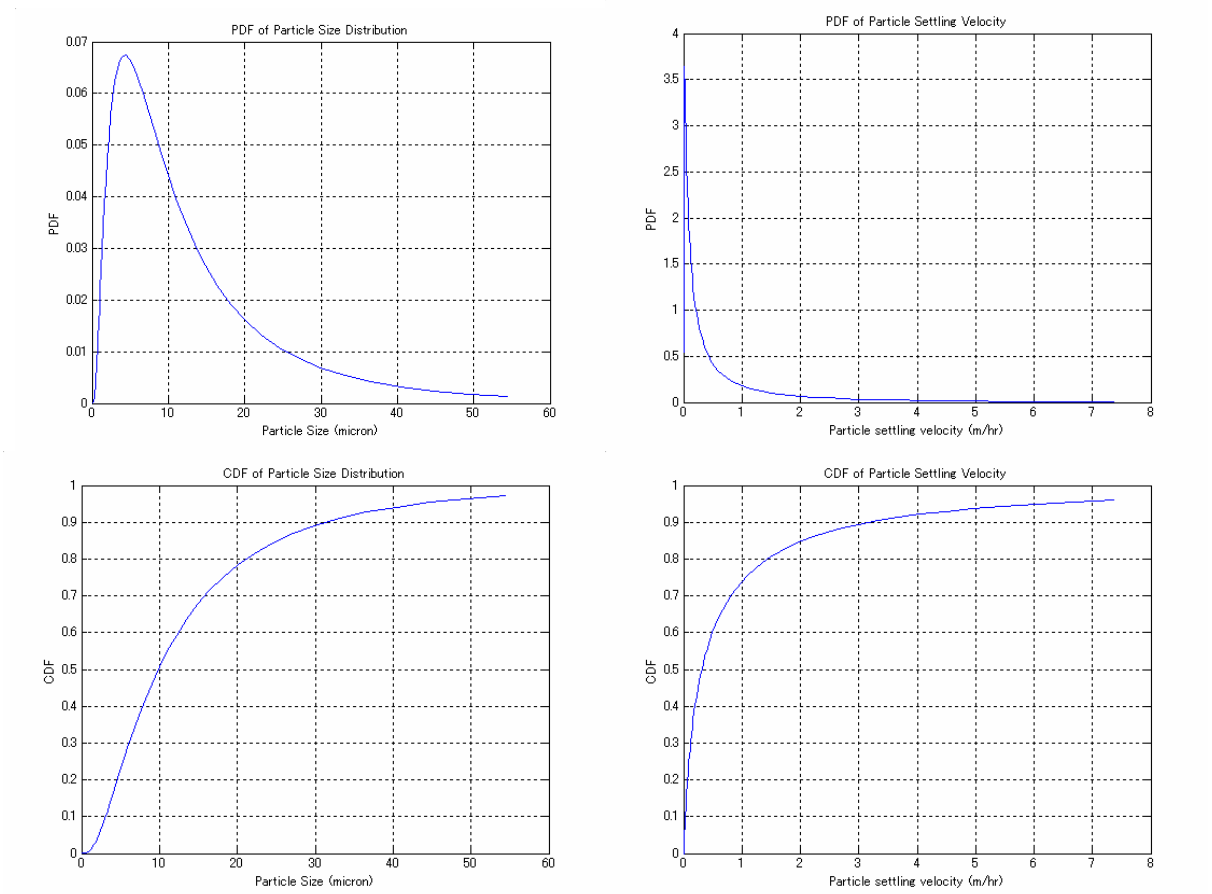

Figure C.3. PDF of Mass Base Particle Size Distribution (Top-Left), CDF of Mass Base Particle Size Distribution (Bottom-Left), PDF of Theoretical Settling Velocity (Top-Right), and CDF of Theoretical Settling Velocity (Bottom-Right).

The PDF of the particle size distribution graph shows the majority of the particle sizes are less than 20 μm, and the PDF of the particle settling velocity graph shows the majority of the particle settling velocities are less than 1 m/hr. That observation can be confirmed in the graphs of CDFs with actual numbers. The CDF of the particle size distribution graph shows that about 50 percent of particles on the mass base are smaller than 10 μm, which correspond to the settling velocity smaller than 0.32 m/hr; 80 percent of particles are smaller than 20 μm, which correspond to the settling velocity smaller than 1.3 m/hr. The CDF of the settling velocity distribution graph shows that more than 70 percent of the particles have settling velocities less than 1m/hr.

Model Application

The example problem was solved by writing a code in MATLAB. The creation of the MATLAB code is shown in this section.

1) Water Level and Flow Rate Calculation

The mass balance equation (3.1) was rewritten by substituting an orifice equation for outflow rate.

$$\frac{dh(t)}{dt} = \frac{1}{B \cdot L}\left(Q_{in}(t) - A_e\sqrt{2gh(t)}\right) \qquad \text{(C.3)}$$

This nonlinear differential equation about mass balance was solved numerically. Equation (C.3) was discretized as Equation C.4, and water level was solved explicitly by using previous time step water level values with an initial condition of water level (H^0=0).

$$\frac{h^{n+1} - h^n}{dt} = \frac{1}{B \cdot L}\left({Q_{in}}^n - {Q_{out}}^n\right)$$
$$h^{n+1} = h^n + \frac{dt}{B \cdot L}\left({Q_{in}}^n - {Q_{out}}^n\right) \qquad \text{(C.4)}$$

Where

$${Q_{in}}^n = Q_{in} \qquad \text{for } 0 < n \le \frac{T_s}{dt}$$
$${Q_{in}}^n = 0 \qquad \text{for } \frac{T_s}{dt} < n$$
$${Q_{out}}^n = A_e\sqrt{2gH^n} \quad \text{for any } n$$

Calculated water level change, given inflow rate, and calculated outflow rate are shown in Figure C.4. As the graph shows, it takes about 6 hours to drain all of the water after runoff stops, and the drainage time is about 9 times as long as the 40 minute runoff period.

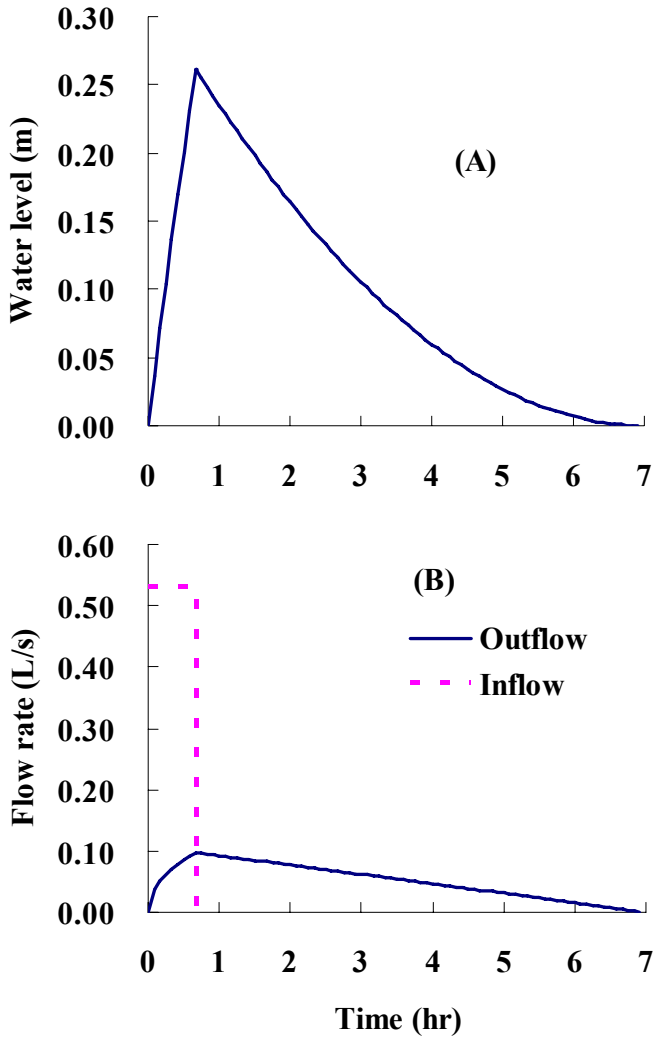

Figure C.4. (A) Calculated Water Level Change in the Sedimentation Basin and (B) Inflow and Outflow Rate.

2) Critical Settling Velocity Calculation

An imaginary water column was released from the inlet every time step, *dt*, from the beginning to the end of the runoff. The water column travels through the sedimentation basin and eventually reaches the outlet. Time to reach outlet, t_{out}^{n}, corresponding to each inflow time, t_{in}^{n}, was calculated by substituting $x_p(t_{out};t_{in})=L$ in Equation 3.10.

$$L = \frac{1}{B \cdot h(t_{out}^{\,n})} \int_{tin,n}^{tout,n} Q_{in}\,dt = \frac{\left(t_{out}^{\,n} - t_{in}^{\,n}\right) \cdot Q_{in}}{B \cdot h(t_{out}^{\,n})} \qquad \text{(C.5)}$$

End of the travel time, $t_{out}^{\,n}$, of a water column, which started traveling at $t_{in}^{\,n}$, can be calculated iteratively from Equation C.5. Figure C.5 shows the calculated detention time, $t_{out}^{\,n}$-$t_{in}^{\,n}$ of water columns released at $t_{in}^{\,n}$. In the graph, traveling time, or detention time, of the first quarter (0 to 10 minutes) is less than an hour while detention time of the last quarter (30-40 minutes) is around 4 hours. Therefore, the initial part of a runoff, which is sometimes the dirtiest, will not stay in the basin longer compared to the latter part of the runoff.

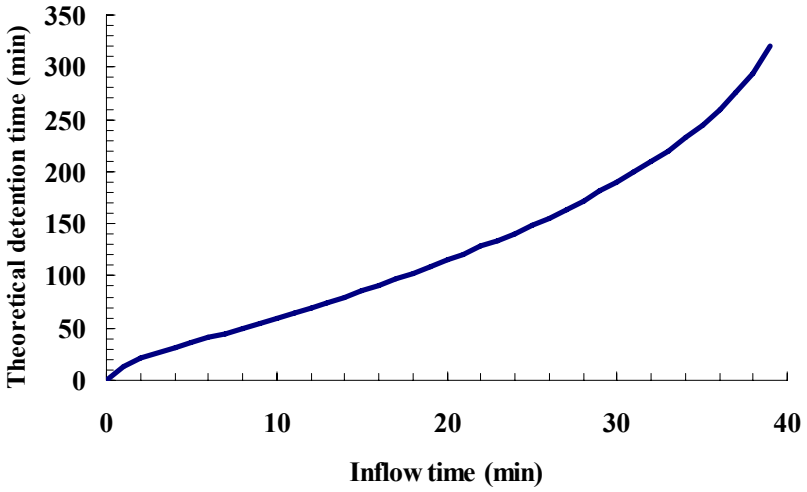

Figure C.5. Theoretical Detention Time of Water Columns with Respect to their Inflow Time.

Critical settling velocity, $v_{p,c}(t_{in})$, was calculated from Equation 3.14. The integral, in the denominator of Equation 3.14, was calculated using the MATLAB function "trapz," which conducts a trapezoidal numerical integration. Figure C.6 shows the critical particle size change with respect to the inflow time, t_{in}. This implies that particles larger than 8 μm would all settle throughout the runoff-drainage process.

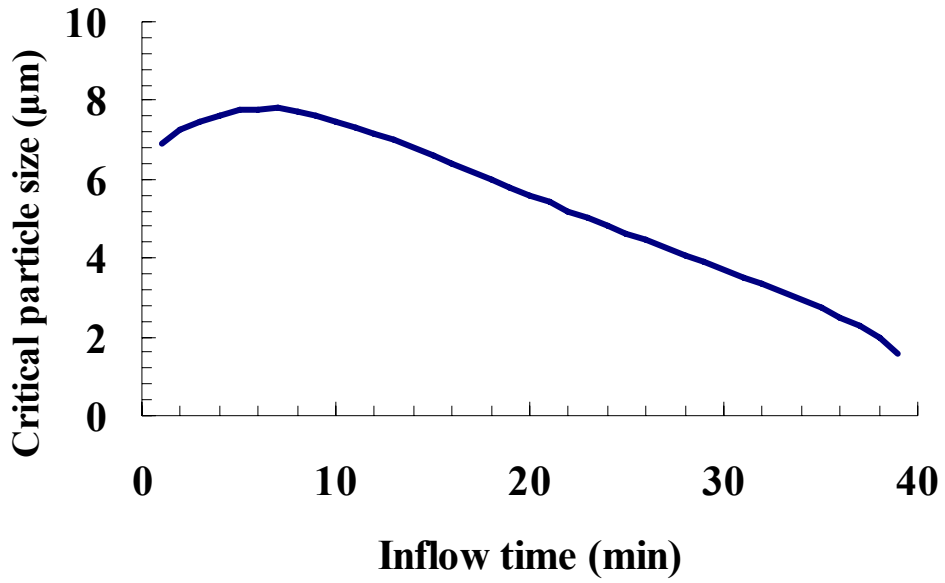

Figure C.6. Critical Particle Size Change with Respect to Inflow Time.

3) Overall Particle Removal Ratio Calculation

As shown in Equation 3.17, PDF of settling velocity, e(v), and potential settling function, F(v), should be known to calculate the overall particle removal ratio. PDF of settling velocity, e(v), shown in the top-right graph in Figure C.3 can be described as follows using the calculated mean and standard deviation value of natural logarithm of particle diameter, $\ln(d_p)$:

$$e(v_s) = \frac{1}{v_s \cdot \zeta_v \sqrt{2\pi}} e^{\frac{-1}{2}\left(\frac{\ln(v_s)-\lambda_v}{\zeta_v}\right)^2} \qquad \text{(C.6)}$$

Settling potential function, $F(v_s)$, can be calculated from the calculated critical particle velocity. For this application case, Stokes velocity, equation (C.1), can be put into (3.16) and can be further transformed as follows:

$$F(v_s) = \begin{cases} 1 \text{ for } v_s > v_{s,c} \\ \dfrac{v_s}{v_{s,c}} = \left(\dfrac{d_p}{d_{p,c}}\right)^2 \text{ for } v_s < v_{s,c} \end{cases} \qquad \text{(C.7)}$$

This settling potential function varies depending on inflow time. This function can be visually understood by Figure C.7. This graph shows the particle size distribution of inflow and the fraction removed in the form of PDF. The group of particles shown in the graph flowed into the detention basin at t_{in}=5 min and flowed out at t_{out}=40 min. Calculated critical particle settling

velocity, $v_{s,c}$, is 0.195 m/hr, and the corresponding critical particle size, $d_{p,c}$, is 7.8 μm. The area surrounded by the solid and dotted lines corresponds to the fraction flowing out, and the area under the dotted line is the fraction settled out.

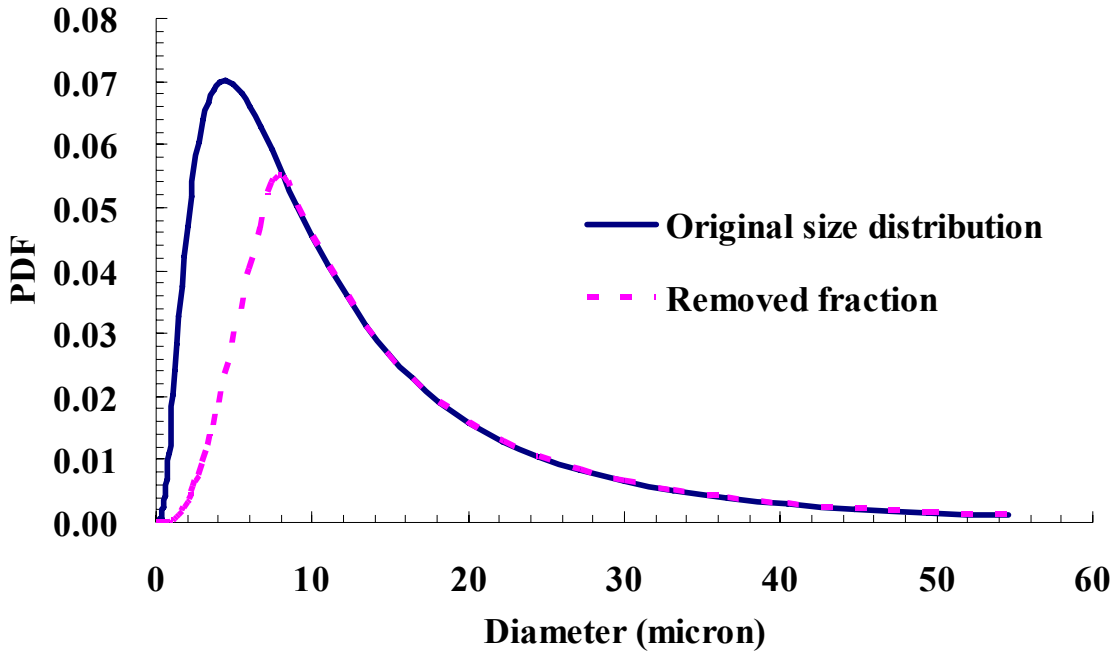

Figure C.7. Particle Size Distribution of Inflow Suspended Solid and the Fraction Removed.

Given the particle size distribution, (Equation C.6), and calculated reactor potential settling function, (Equation C.7), these can be plugged into Equation 3.17. The first term, called $R_1(t_{in})$, of the right-hand side of Equation (3.17) is the ratio of particles larger than the critical particle size. The second term, $R_2(t_{in})$, is the amount of captured particles smaller than critical particle size. Each term was transformed as follows and calculated separately using the numerical integration function "trapz" in MATLAB. Figure C.8 shows the calculation results of $R_1(t_{in})$ and $R_2(t_{in})$. The graph shows that $R_1(t_{in})$ is much greater than the $R_2(t_{in})$, the scale of which is between the $R_1(t_{in})$ lines and $R_1(t_{in})+ R_2(t_{in})$ lines. This implies that most of inflow particles will be removed because the particle size is just larger than the critical particle size.

$$R_1(t_{in}) = \int_{vs,c(tin)}^{\infty} 1 \cdot e(v_s) dv_s = \int_{vs,c(tin)}^{\infty} \frac{1}{v_s \cdot \zeta_v \sqrt{2\pi}} e^{\frac{-1}{2}\left(\frac{\ln(v_s)-\lambda_v}{\zeta_v}\right)^2} dv_s$$

$$= 1 - \int_{0}^{vs,c(tin)} \frac{1}{v_s \cdot \zeta_v \sqrt{2\pi}} e^{\frac{-1}{2}\left(\frac{\ln(v_s)-\lambda_v}{\zeta_v}\right)^2} dv_s \qquad \text{(C.8)}$$

$$R_2(t_{in}) = \int_{0}^{vs,c(tin)} \frac{v_s}{v_{s,c}(t_{in})} \cdot e(v_s) dv_s$$

$$= \frac{1}{v_{s,c}(t_{in})} \int_{0}^{vs,c(tin)} \frac{1}{\zeta_v \sqrt{2\pi}} e^{\frac{-1}{2}\left(\frac{\ln(v_s)-\lambda_v}{\zeta_v}\right)^2} dv_s$$

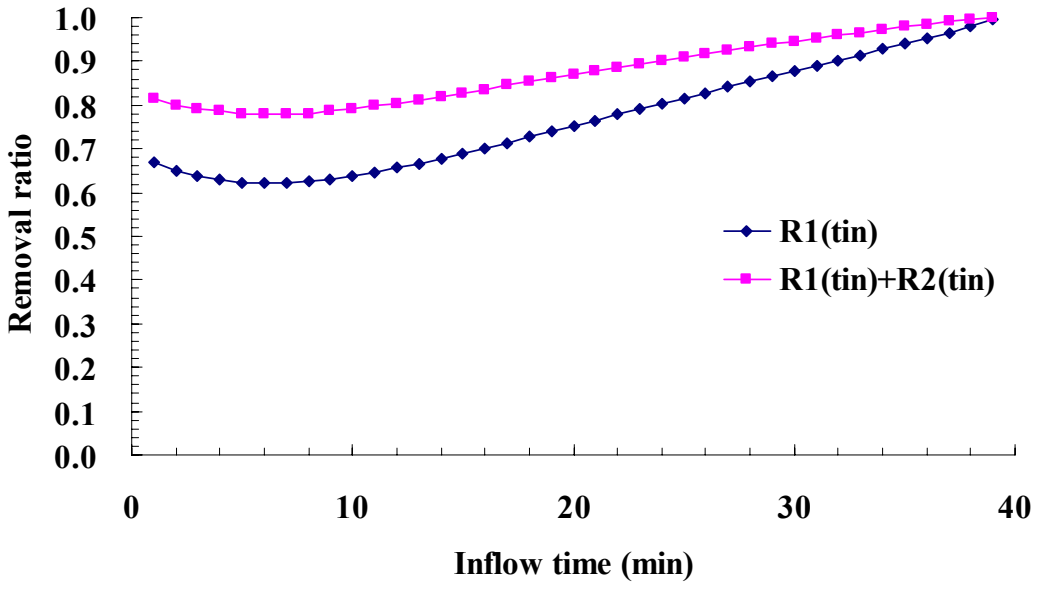

Figure C.8. Time Series Removal Ratio of Particles.

Finally, the total removal ratio of suspended solid and the time series outlet SSC were calculated by substituting the calculated Equation 3.17 for Equations 3.18 and 3.19. Figure C.9 shows the calculated time series outflow SSC. This graph shows that the outflow SSC gradually increased until approximately 50 min, which is 10 minutes after runoff stopped. Subsequently,

the concentration dropped steadily with increasing time until the water was completely drained. The calculated total particle removal ratio was 0.875.

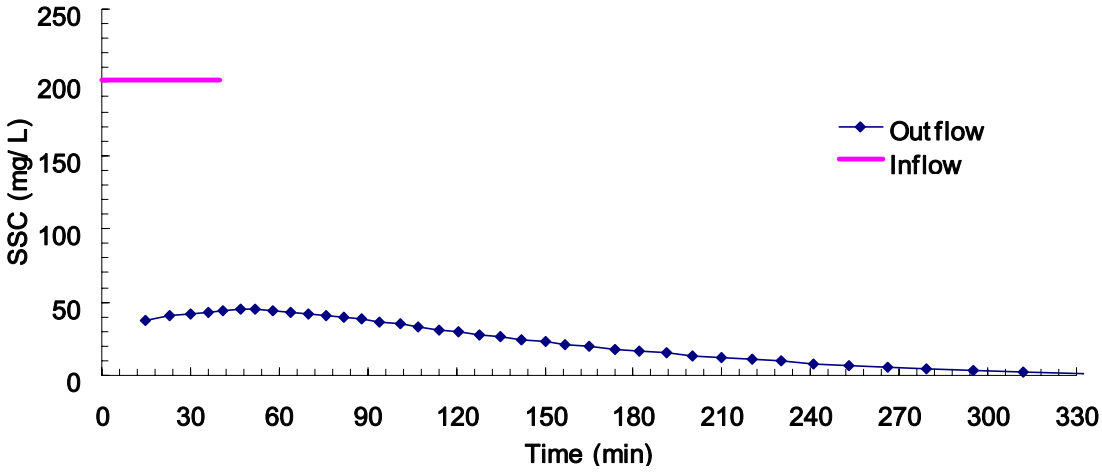

Figure C.9. Time Series Inflow SSC and Calculated Outflow SSC.

Timeseries outflow SSC from the outlet may not be necessary to be estimated for stormwater management purposes since the total particle removal ratio is more important in the general case. However, this model can determine the particle size distribution change in the outflow. This information implies that this study could be extended for estimating removal ratio of other important pollutants in stormwater such as nutrients, heavy metals, and organic materials in particulate form since hydrophobic pollutants are likely to attach to the surface of suspended solids. Absorption is usually highly dependent on the surface area of sediment, which can be estimated from the particle size distribution.

C.2 An Example with Triangular Hydrograph Inflow

The conceptual model was applied to deal with the Soil Conservation Service (SCS) triangular hydrograph as an inflow rate. The SCS triangular hydrograph is a synthetic unit hydrograph, which relates direct runoff to a unit depth of excess rainfall. The benefit of applying a synthetic hydrograph, such as this triangular hydrograph, is that it is more realistic than a constant runoff (inflow) rate since a hydrograph tends to have a skewed bell shape rather than a rectangular shape. One drawback, on the other hand, is that these bell-shaped hydrographs are

very difficult to reproduce experimentally. The triangular hydrograph can be determined by specifying the peak flow rate, Q_p, and peak time, T_p, as shown in Figure C.10.

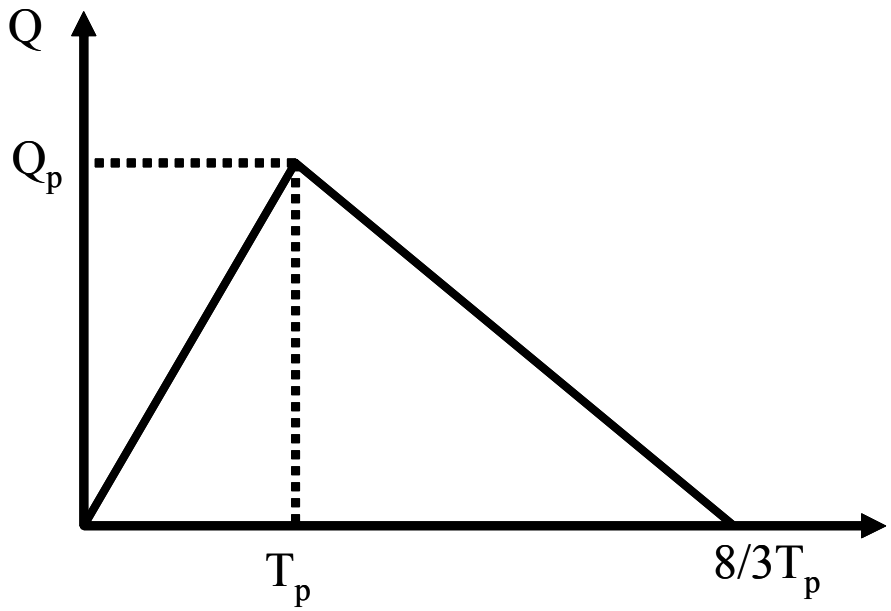

Figure C.10. SCS Triangular Hydrograph.

An Example Problem

The MATLAB program was modified to have an unsteady state inflow and run with a triangular hydrograph. As an example, the inflow condition was set with Q_p=1 L/s and T_p= 30 minutes at the model scale. Figure C.11 shows inflow and outflow rate, and Figure C.12 shows time series SSC. The calculated removal ratio was 84.1 percent. The outflow peak occurred at 70 minutes, and the outlet SSC peak was at 77 minutes.

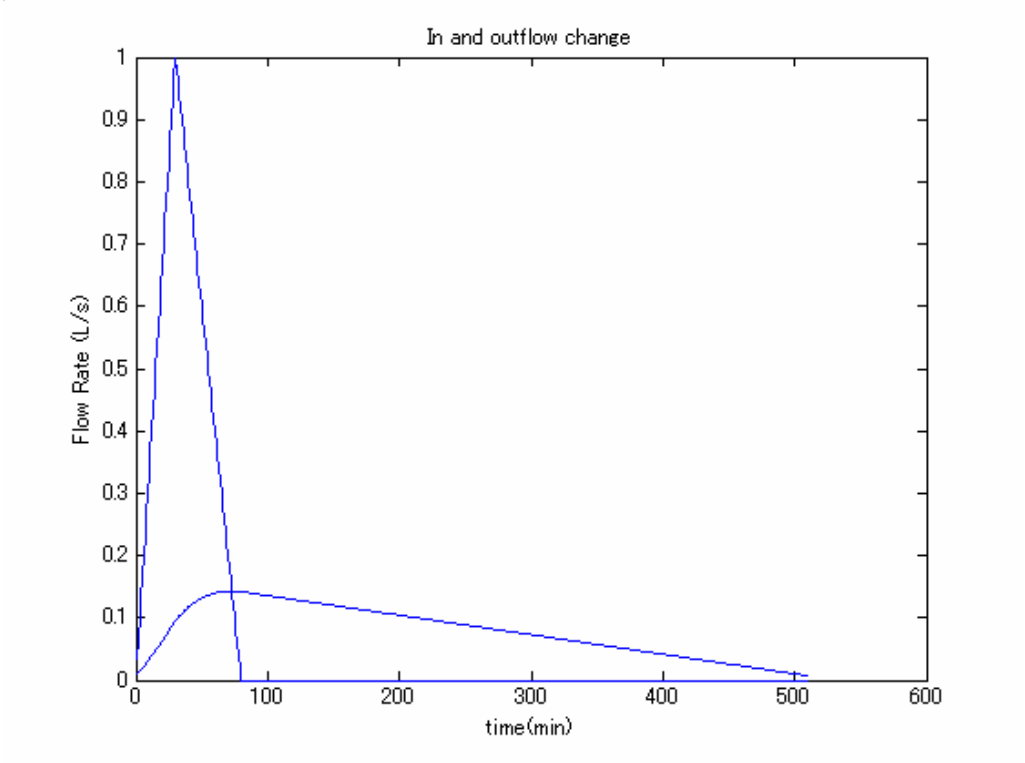

Figure C.11. Calculated Inflow and Outflow Rate Change.

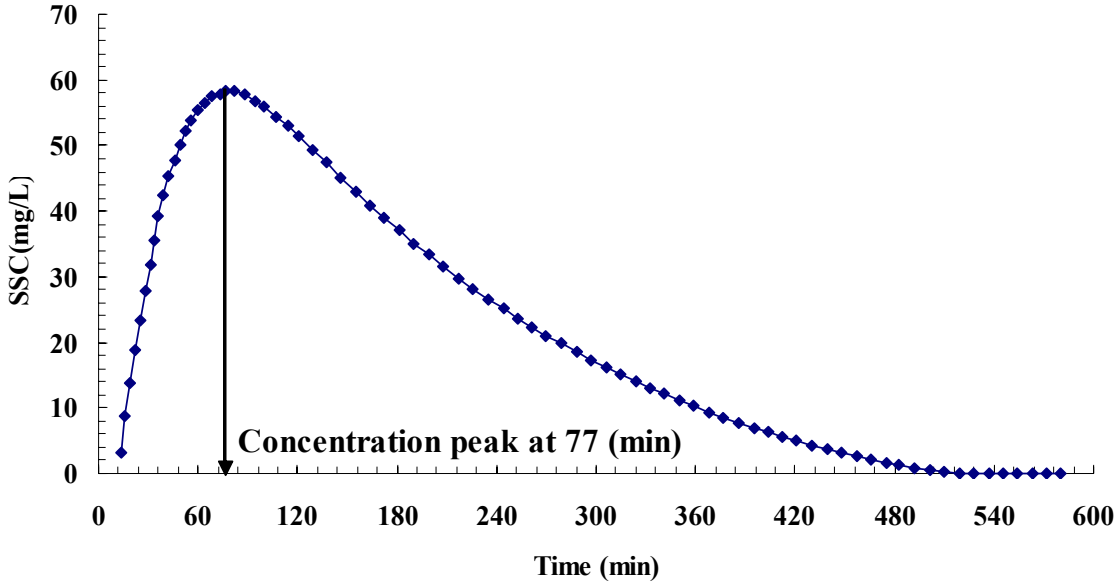

Figure C.12. Calculated Time Series Outflow SSC.

Application and Comparison

A) Three Different Triangular Hydrographs

Water level in the detention basin and the corresponding outflow rate were calculated numerically in an explicit method based on the mass balance (Equation 3.1) with the defined triangular inflow rate. The conceptual model was run in the model scale with three different triangular hydrographs (Figure C.13) and the same runoff volume of 2400 L to see how the removal ratio would be different for different runoff intensity. Table C.2 shows the inflow conditions and resulting particle removal ratio. This table clearly shows that the removal ratio for slower runoff is better than that for rapid runoff. Figure C.14 shows outflow SSC change for runs A, B, and C. According to the graph, the peak SSC in a short and intense storm is higher than that in a slower storm.

Table C.2. Inflow Condition and Calculated Removal Ratio.

Run	Peak time (min)	Duration (min)	Peak flow rate (L/s)	Runoff Volume (L)	Removal ratio
A	20	53	1.5	2400	0.828
B	40	107	0.75	2400	0.852
C	80	213	0.375	2400	0.879

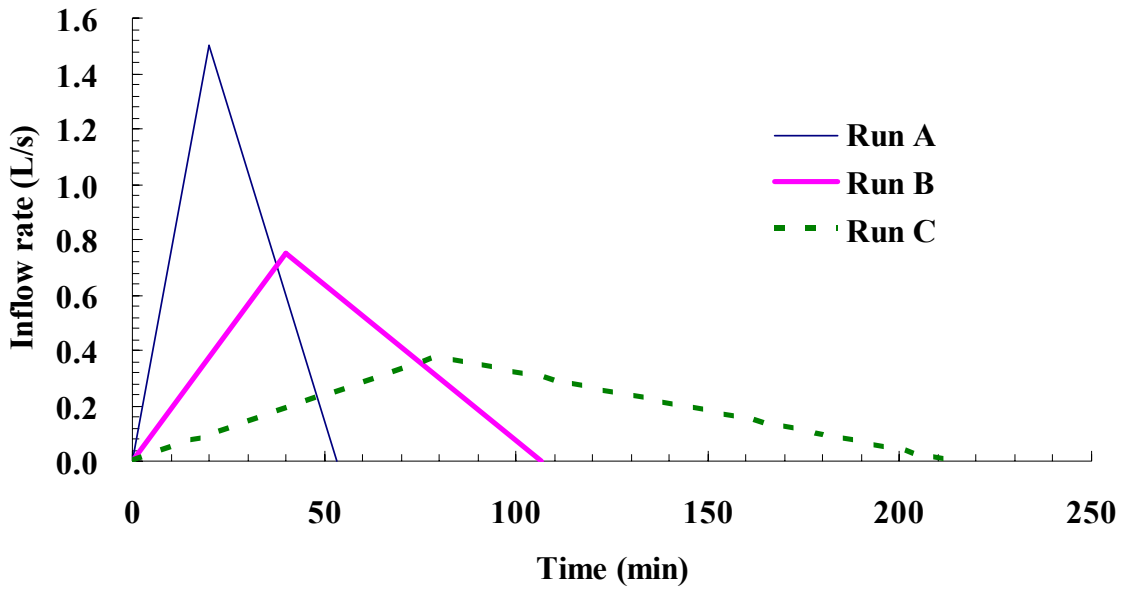

Figure C.13. Inflow Hydrographs of Three Tested Examples.

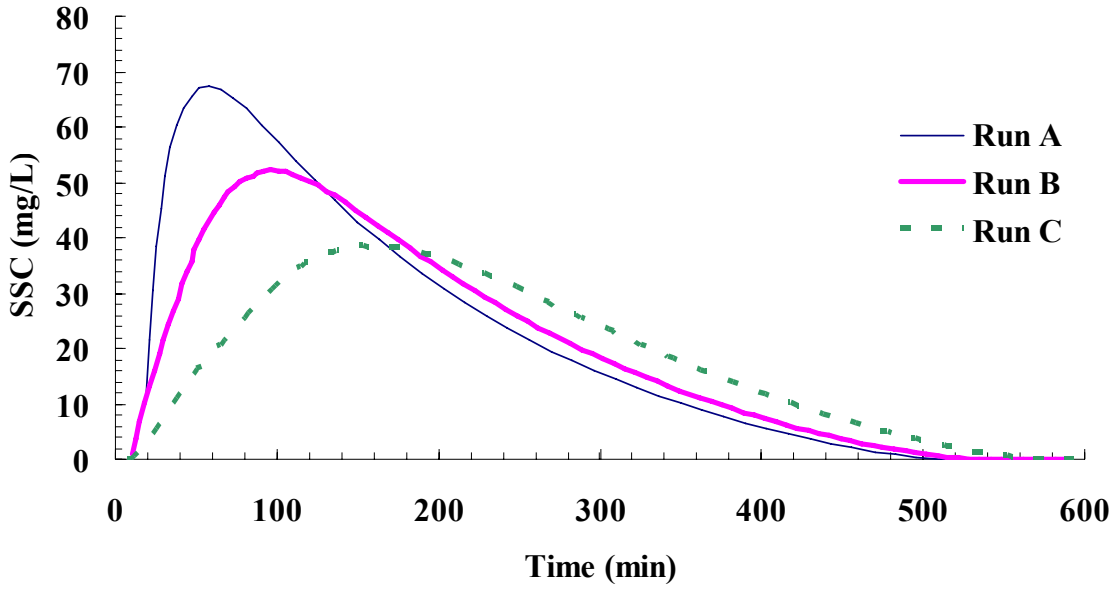

Figure C.14. Timeseries Outlet Concentrations for the Three Different Hydrographs.

B) Triangular Hydrograph versus Flat Hydrograph

Performance differences between a triangular hydrograph and a flat hydrograph are also of interest. Three runoff values with flat hydrographs, each of which corresponds to the triangular hydrograph shown in Table C.2, were tested to compare their removal ratios. These three flat hydrographs were made to have the same durations and runoff volumes from their corresponding triangular hydrographs. Table C.3 shows the inflow conditions, and Figure C.15 shows the tested inflow hydrographs of both the triangular and flat hydrographs.

Table C.3. Inflow Conditions and Resulting Particle Removal Ratios for Flat Hydrographs (A', B', and C') and Particle Removal Ratio of Corresponding Triangular Hydrograph (A, B, and C).

Run	Duration (min)	Inflow rate (L/s)	Runoff Volume (L)	Removal ratio	Removal ratio of corresponding triangular hydrograph (A, B, and C)
A'	53	0.750	2400	0.837	0.828
B'	107	0.375	2400	0.863	0.852
C'	213	0.188	2400	0.893	0.879

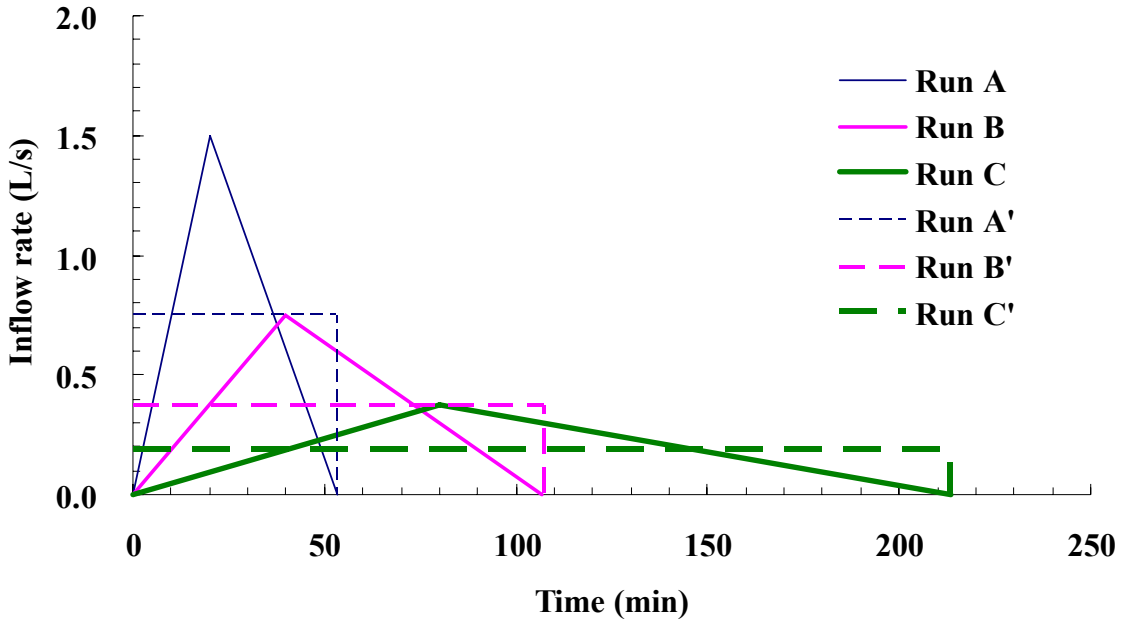

Figure C.15. Triangular and Flat Inflow Hydrograph.

Table C.3 also displays the results of the removal ratio calculation for both triangular and flat hydrographs. The removal ratio results from corresponding hydrographs are very close (around 1 percent difference), while the removal ratio of the triangular hydrograph is always a little less than that of flat hydrograph. However, the peak SSCs is different. Figure C.16 shows the calculated SSC change of runoff B for both triangular and flat hydrographs. According to the graph, the peak SSC of the triangular hydrograph is much higher than that of the flat hydrograph. These simulation results imply that particle removal efficiency results from physical models with constant inflow which would not differ much from the results with the corresponding actual stormwater runoffs such as bell-shaped inflows.

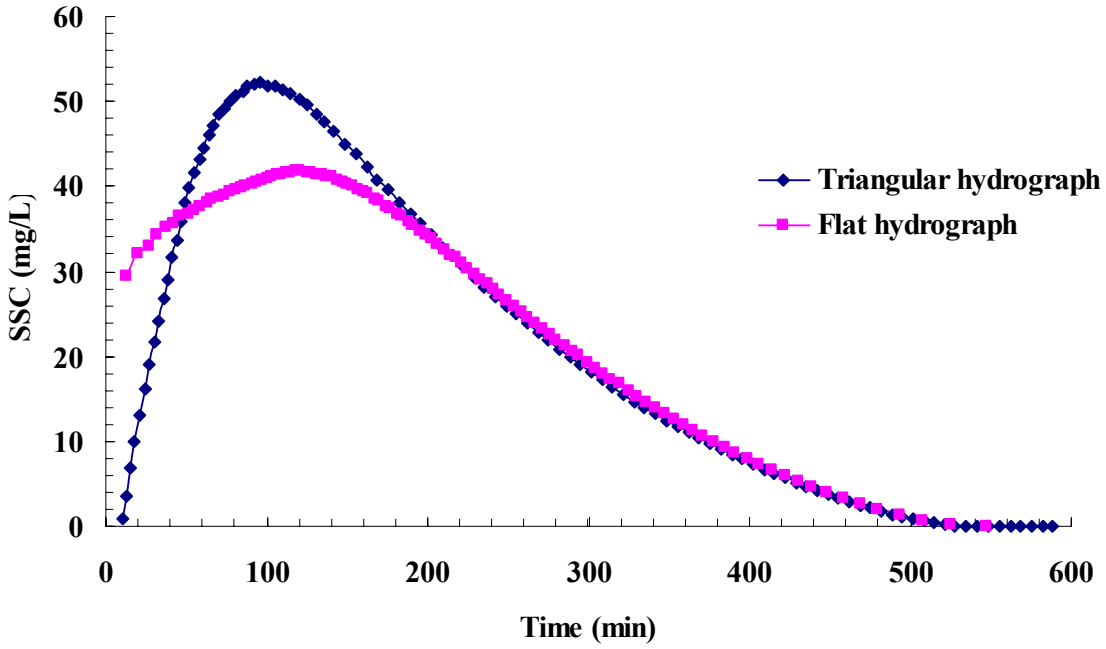

Figure C.16. Outflow SSC for Triangular and Flat Hydrograph.